Wireless data communication for autonomous farming & precision agriculture applications: Harnessing ISM band radio for real-time data connectivity & monitoring to enhance data analysis and logistic operations

by

Ketan Shende

B.S., University of Mumbai, 2015
M.S., Texas Tech University, 2019

AN ABSTRACT OF A DISSERTATION

submitted in partial fulfillment of the requirements for the degree

DOCTOR OF PHILOSOPHY

Carl and Melinda Helwig Department of Biological & Agricultural Engineering
Carl R. Ice College of Engineering

KANSAS STATE UNIVERSITY
Manhattan, Kansas

2024

Abstract

Recent advancements in autonomous farming and precision agriculture have significantly enhanced machinery and systems, enabling large-scale automation and upgrades for growers. Efficiently managing real-time information is vital for these dynamic systems due to their significant variabilities. The adoption of wireless data communication facilitates instantaneous information handling, ensuring seamless data transfer. Amongst the demand for efficient wireless data communication solutions continues to rise, the utilization of license-free spectrum band radios, particularly Industrial, Scientific, and Medical (ISM) band, has expanded. This research aims to leverage these radios to establish a data communication platform for transferring information independently or when integrated with an autonomous liquid application system. Additionally, these radios communicate RTK correction signals to improve image triggering and geotagging accuracy in UAV remote sensing.

To demonstrate an end-to-end wireless data communication link, a platform referred as Pico Radio Interface Microcontroller Electronics (PRIME) board, was designed using a PICO 900 radio, a Teensy 4.1 microcontroller and power electronics component. The radio with a link rate of 276 kbps, 40 miles (60 km) LOS, and power of 1 Watt was utilized to build a network of 4 remotes, 2 repeaters, and a master. The remotes were configured to continuously transfer simulated information to the master at the central hub with repeaters which are in secondary configuration are used to expand the scope of the network. The data communication system was deployed in outdoor environment consisting of undulating terrain and dense crop canopy and was tested for its transmission efficacy for 15-, 25-, and 30-minutes experiment. A packet delivery ratio of greater than 0.98 was observed meaning a successful packet transmission of more than 98% for per second data transfer and close to 100 % for per 30 second data transfer in both the field conditions and for

all the experimental runs. Also, a power consumption of less than 0.42 watts was attained proving the power efficiency of the PRIME boards.

Further, to gauge the data communication ability of the license free spectrum band radio operating in 2.4 GHz frequency, a combination of 2X2 Multiple Input Multiple Output (MIMO) radio modules is configured for setting up a wireless data link between an autonomous rover platform and a central hub for real-time data accumulation. The radio with extensive speed of 25 Mbps and low power consumption is integrated with autonomous platform using ROS2 middleware. The data packets consist of system-level details, including location information, signal status, and operational metrics like target detection, nozzle pressure, and tank level. These are gathered from three onboarded subsystems: navigation, computer vision, and site-specific liquid application. Two out of three configuration were able to achieve a packet delivery ratio of more than 98% and collective loss of less than 2 % for a timed experiments of 5 minutes each in two different environments. Data packet latency was also calculated between the transmission where a range between 0.1 to 0.4 seconds was observed for both the environments. This proved the ability of the MIMO radios operating in license free spectrum to be deployed in autonomous farming application and collect information from mobile platforms.

A wireless data communication radio setup is used to improve the image triggering and image geotagging accuracy for a UAV based remote sensing application. A Real-Time Kinematics (RTK)-enabled GNSS solution was designed to achieve a cm-level accuracy for a UAV based imagery data collection for consumer-grade RGB cameras as well as Thermal Infrared Cameras (TIR). This consisted of a base station setup that generated RTK correction signals which are serially sent to a transmitting radio operating in 900 MHz license free spectrum band. The receiving radio which is onboard with the GNSS solution collects the RTK-signals and feeds them to the GNSS module which rectifies the location information. For the flights conducted to test the image triggering mechanism, the radio was able to communicate 80 % of RTK signals for both the 20 m and 30 m flight. The RTK-enabled data points were in the range of 0.36 to 3.48 m for the 20 m flight whereas 0.37 to 3.6 m for the 30 m flight. Whereas to assess the image geotagging accuracy, the radio was able to communicate 86% of the time during 50 m flights and 93% of the time during 80 m. RTK-enabled flight data points were in the range of 0.7 meters to less than 3 m for 50 meters flight and 0.6 meters to 2.75 meters for the 80 m flight. This proved the ability of the radios to communicate information in real-time for a dynamic UAV remote sensing application improving the image triggering & geotagging accuracy.

In conclusion, this research underlined the ability of radio communication operating in license free spectrum band to effectively communicate information for end-to-end data transfer and improving the ability of image triggering and geotagging for remote sensing applications by communicating RTK correction signals.

Wireless data communication for autonomous farming & precision agriculture applications: Harnessing ISM band radio for real-time data connectivity & monitoring to enhance data analysis and logistic operations.

by

Ketan Shende

B.S., University of Mumbai, 2015
M.S., Texas Tech University, 2019

A DISSERTATION

submitted in partial fulfillment of the requirements for the degree

DOCTOR OF PHILOSOPHY

Carl and Melinda Helwig Department of Biological and Agricultural Engineering
Carl R. Ice College of Engineering

KANSAS STATE UNIVERSITY
Manhattan, Kansas

2024

Approved by:

Major Professor
Dr. Ajay Sharda

Copyright

Abstract

Recent advancements in autonomous farming and precision agriculture have significantly enhanced machinery and systems, enabling large-scale automation and upgrades for growers. Efficiently managing real-time information is vital for these dynamic systems due to their significant variabilities. The adoption of wireless data communication facilitates instantaneous information handling, ensuring seamless data transfer. Amongst the demand for efficient wireless data communication solutions continues to rise, the utilization of license-free spectrum band radios, particularly Industrial, Scientific, and Medical (ISM) band, has expanded. This research aims to leverage these radios to establish a data communication platform for transferring information independently or when integrated with an autonomous liquid application system. Additionally, these radios communicate RTK correction signals to improve image triggering and geotagging accuracy in UAV remote sensing.

To demonstrate an end-to-end wireless data communication link, a platform referred as Pico Radio Interface Microcontroller Electronics (PRIME) board, was designed using a PICO 900 radio, a Teensy 4.1 microcontroller and power electronics component. The radio with a link rate of 276 kbps, 40 miles (60 km) LOS, and power of 1 Watt was utilized to build a network of 4 remotes, 2 repeaters, and a master. The remotes were configured to continuously transfer simulated information to the master at the central hub with repeaters which are in secondary configuration are used to expand the scope of the network. The data communication system was deployed in outdoor environment consisting of undulating terrain and dense crop canopy and was tested for its transmission efficacy for 15-, 25-, and 30-minutes experiment. A packet delivery ratio of greater than 0.98 was observed meaning a successful packet transmission of more than 98% for per second data transfer and close to 100 % for per 30 second data transfer in both the field conditions and for

all the experimental runs. Also, a power consumption of less than 0.42 watts was attained proving the power efficiency of the PRIME boards.

Further, to gauge the data communication ability of the license free spectrum band radio operating in 2.4 GHz frequency, a combination of 2X2 Multiple Input Multiple Output (MIMO) radio modules is configured for setting up a wireless data link between an autonomous rover platform and a central hub for real-time data accumulation. The radio with extensive speed of 25 Mbps and low power consumption is integrated with autonomous platform using ROS2 middleware. The data packets consist of system-level details, including location information, signal status, and operational metrics like target detection, nozzle pressure, and tank level. These are gathered from three onboarded subsystems: navigation, computer vision, and site-specific liquid application. Two out of three configuration were able to achieve a packet delivery ratio of more than 98% and collective loss of less than 2 % for a timed experiments of 5 minutes each in two different environments. Data packet latency was also calculated between the transmission where a range between 0.1 to 0.4 seconds was observed for both the environments. This proved the ability of the MIMO radios operating in license free spectrum to be deployed in autonomous farming application and collect information from mobile platforms.

A wireless data communication radio setup is used to improve the image triggering and image geotagging accuracy for a UAV based remote sensing application. A Real-Time Kinematics (RTK)-enabled GNSS solution was designed to achieve a cm-level accuracy for a UAV based imagery data collection for consumer-grade RGB cameras as well as Thermal Infrared Cameras (TIR). This consisted of a base station setup that generated RTK correction signals which are serially sent to a transmitting radio operating in 900 MHz license free spectrum band. The receiving radio which is onboard with the GNSS solution collects the RTK-signals and feeds them to the GNSS module which rectifies the location information. For the flights conducted to test the image triggering mechanism, the radio was able to communicate 80 % of RTK signals for both the 20 m and 30 m flight. The RTK-enabled data points were in the range of 0.36 to 3.48 m for the 20 m flight whereas 0.37 to 3.6 m for the 30 m flight. Whereas to assess the image geotagging accuracy, the radio was able to communicate 86% of the time during 50 m flights and 93% of the time during 80 m. RTK-enabled flight data points were in the range of 0.7 meters to less than 3 m for 50 meters flight and 0.6 meters to 2.75 meters for the 80 m flight. This proved the ability of the radios to communicate information in real-time for a dynamic UAV remote sensing application improving the image triggering & geotagging accuracy.

In conclusion, this research underlined the ability of radio communication operating in license free spectrum band to effectively communicate information for end-to-end data transfer and improving the ability of image triggering and geotagging for remote sensing applications by communicating RTK correction signals.

Table of Contents

List of Figures ... xiv
List of Tables ... xvii
Acknowledgements ... xviii
Dedication ... xix
Chapter 1 - Introduction ... 1
1.1 Wireless data communication for agriculture sensing ... 1
1.2 On-board data handling of existing farm machineries ... 3
1.3 Data handling on autonomous farming platforms ... 4
1.4 Data communication using license free spectrum radios in ISM band ... 6
1.5 Use of RTK-enabled GNSS for remote sensing applications ... 7
1.6 Research Objective ... 9
Chapter 2 - Hardware design & preliminary evaluation of wireless data communication for autonomous farming applications ... 11
2.1 Abstract ... 11
2.2 Introduction ... 13
2.3 Materials & Methods ... 16
2.3.1 Application System ... 16
2.3.1.1 Pico Radio Interface µController Electronics (PRIME) Board ... 18
2.3.1.1.1 PICO 900 Mesh Radio ... 19
2.3.1.1.2 Antenna ... 20
2.3.1.1.3 Teensy Microcontroller ... 21
2.3.2 Data Packet Characteristics ... 21
2.3.3 Experimental Sites ... 22
2.3.4 Data Collection and Experimentation ... 24
2.3.4.1 Packet Delivery Ratio and Power Consumption ... 25
2.4 Results and discussion ... 26
2.4.1 ASF Site ... 27
2.4.2 CC Site ... 28
2.5 Conclusion & Future Work ... 29

Chapter 3 - Integration & testing of wireless data communication system with autonomous site-specific liquid application platform 31
3.1 Abstract 31
3.2 Introduction 32
3.3 Materials & Methods 35
3.3.1 Rover Platform 35
3.3.1.1 Subsystem Description 36
3.3.1.1.1 Navigation System 37
3.3.1.1.2 Computer Vision System 37
3.3.1.1.3 Liquid Application System 38
3.3.2 2x2 MIMO Wireless Digital Link 38
3.3.2.1 Ping Test 39
3.3.2.2 File Transfer Test 41
3.3.2.3 Radio Configurations 42
3.3.3 Robot Operation System 2 (ROS2) Middleware 43
3.3.3.1 Node 44
3.3.3.2 Topic 45
3.3.3.5 ROS2 Bag 45
3.3.4 Radio & Platform Integration using ROS2 46
3.3.5 Data packet characteristics 47
3.3.6 System Testing 47
3.3.6.1 Simulation using ROS2 Bags and RQT graph 47
3.3.6.2 On-ground Testing 49
3.3.6.3 Experimental Setup 49
3.4 Results & Discussion 52
3.4.1 Evaluation Metrics 52
3.4.1.1 Packet Delivery Ratio 52
3.4.1.2 Packet Loss 52
3.4.1.3 Latency 53
3.4.2 Experimental Output 53
3.4.2.1 Football Stadium Experiment 53

3.4.2.2 For the Agricultural Field experiment ... 56
3.5 Conclusion & Future Work ... 59
Chapter 4 - Improving the image triggering and geotagging accuracy using RTK-enabled GNSS solution for UAV remote- sensing applications ... 62
4.1 Abstract ... 62
4.2 Introduction ... 64
4.3 Materials & Methods ... 67
4.3.1 System Design ... 67
4.3.1.1 Topcon B110 GNSS Receiver module ... 68
4.3.1.2 Microhard P900 miniature wireless radio ... 69
4.3.1.3 Teensy Microcontroller ... 70
4.3.1.4 RTK Setup ... 71
4.3.1.4.1 Radio Configuration ... 72
4.3.1.5 NMEA Strings ... 72
4.3.2 UAV Platform ... 73
4.3.3 Image Triggering for RGB Camera ... 74
4.3.3.1 Image Triggering Unit ... 74
4.3.3.1.1 Distance based image triggering algorithm ... 75
4.3.3.3 System Integration ... 76
4.3.3.4 Experimental Site & Setup ... 77
4.3.4 Image Geotagging for Thermal Imaging system ... 80
4.3.3.2 System Integration ... 80
4.3.3.3 Experimental Site and Setup ... 81
4.4 Results and Discussion ... 83
4.4.1 Image Triggering ... 83
4.4.2 Image Geotagging ... 91
4.5 Conclusion and Future Work ... 97
4.5.1 Image Triggering ... 97
4.5.2 Image Geotagging ... 98
Chapter 5 - Conclusion and Future Work ... 100
5.1 Conclusion ... 100

5.2 Future work and recommendations 104
References 106
Appendix A - Data Communication, GNSS and Development Platform 112

List of Figures

Figure 1.1. Comparing different wireless data communication technologies (Feng, X. et al., 2019) ... 2
Figure 2.1. System Data Flow for Autonomous Liquid Application Platform ... 16
Figure 2.2. Multiagent Wireless Data Communication Schematic ... 17
Figure 2.3. Block Diagram and Printed Circuit Board (PCB) for PRIME Board ... 18
Figure 2.4. Microhard PICO 900 Mesh Radio module ... 19
Figure 2.5. ½-wave dipole omnidirectional antennas product dimension (ANT-916-OC-LG-RPS Datasheet) ... 20
Figure 2.6. Teensy 4.1 Microcontroller module ... 21
Figure 2.7. Data Packet Characterization ... 21
Figure 2.8. Wireless radio installation of remote (a) and primary (central hub) at the edge of the field (b) ... 23
Figure 2.9. Radio placement for ASF site (a) and CC site (b) ... 24
Figure 2.10. Power consumption for 30-minute experiment at ASF (a) and CC (b) sites ... 27
Figure 3.1. Rover Platform ... 36
Figure 3.2. Operational flow and event-based system data logging ... 36
Figure 3.3. Representation of April Tag (https://april.eecs.umich.edu/software/apriltag) ... 37
Figure 3.4. pMDDL 2450 module and development board ... 39
Figure 3.5. Wireless configuration for the master radio ... 40
Figure 3.6. Diagnostic testing of master & slave ... 41
Figure 3.7. Test setup for the file transfer test ... 42
Figure 3.8. ROS node illustration communicating messages through topics (https://docs.ros.org/en/humble/Tutorials/) ... 44
Figure 3.9. Multiple nodes communicating with each other (https://docs.ros.org/en/humble/Tutorials/) ... 45
Figure 3.10. Radio communication and peripheral connection ... 46
Figure 3.11. Example of data packet containing information from spraying system ... 47
Figure 3.12. Example of data packet containing information from the navigation system ... 47

Figure 3.13. Representation of ROS2 node dedicated for serial communication subscribing to a ROS2 bag 48
Figure 3.14. MIMO radio installed on the Rover Platform 49
Figure 3.15. Central Hub setup & rover maneuvering in the field 50
Figure 3.16. Rover maneuvering on track of the football stadium 51
Figure 3.17. Latency Plots for liquid application and computer vision data collection in various configurations 54
Figure 3.18. Latency plots for navigation system data collection in various configurations 55
Figure 3.19. Latency Plots for Computer vision and Liquid application system data collection in various configurations 57
Figure 3.20. Latency plots for Navigation system data collection in various configurations 58
Figure 4.1. Major components present on GNSS solution contributing to serve image triggering and image geotagging mechanism 67
Figure 4.2. GNSS Solution Printed Circuit Board 68
Figure 4.3. Topcon B110 GNSS Module 69
Figure 4.4. Pico 900 Radio 70
Figure 4.5. Teensy 4.1 Microcontroller 70
Figure 4.6. Base Station & Radio setup for RTK 71
Figure 4.7. Matrice 100 Quad-Rotor Platform 74
Figure 4.8. Schematic representation of the image trigger mechanism 75
Figure 4.9. Pseudo code for calculating the distance between two points 76
Figure 4.10. Integration of Sony camera, GNSS solution with the UAV platform 77
Figure 4.11. Recording geolocation of the GCP and measuring distance between each GCP 78
Figure 4.12. Status of GNSS module during the a) RTK-enabled flight b) Standalone flight 79
Figure 4.13. Representation of NMEA Strings 80
Figure 4.14. GNSS Solution integrated with UAV Platform 81
Figure 4.15. GCP co-ordinates collection and UAV flight setup 82
Figure 4.16. Status of GNSS module before a) RTK enabled and b) Standalone 83
Figure 4.17. (a) Perfectly aligned, (b) Angled shot during turns, (c) Indistinct, (d) Dis-oriented84
Figure 4.18. Distance trigger for Standalone and RTK-enabled flight using location information for 20 m altitude 86

Figure 4.19. Variation in haversine distance for standalone and RTK-enabled flight 87
Figure 4.20. Distance trigger for Standalone and RTK-enabled flight using location information for 30 m altitude 89
Figure 4.21. Variation of haversine distance for standalone and RTK-enabled flight 90
Figure 4.22. Comparing difference of Standalone and RTK-enabled flight points with GCP's for 50 m flight 92
Figure 4.23. Visual representation of (a) Standalone and (b) RTK-enabled points compared with GCP's geolocation for 50 m flight 94
Figure 4.24. Comparing difference of Standalone and RTK-enabled flight points with GCP's for 80 m flight 95
Figure 4.25. Visual representation of (a) Standalone and (b) RTK-enabled points compared with GCP's geolocation for 80 m flight 96

List of Tables

Table 2.1. Comparison of wireless technologies and their characteristics (Ojha T., et al., 2015). 15
Table 2.2. Data packet description........ 22
Table 2.3. Distance of each remote from Primary........ 24
Table 2.4. Packet Delivery Statistics for ASF Site........ 26
Table 2.5. Packet Delivery Statistics for CC Site........ 26
Table 3.1. Radio configuration for outdoor testing........ 42
Table 3.2. Packet Statistics for liquid application and computer vision system experiment....... 53
Table 3.3. Packet Statistics for Navigation System experiment........ 55
Table 3.4. Packet Statistics for the Computer Vision and Spraying System experiment........ 56
Table 3.5. Packet Statistics for the Navigation System experiment........ 58
Table 4.1. Description of NMEA Strings........ 73
Table 4.2. UAV flight details for image triggering experiment........ 79
Table 4.3. Characteristics of UAV flight for image geotagging........ 82
Table 4.4. Comparison of imagery data flight log in standalone mode with ground control points for 20 m altitude........ 85
Table 4.5. Comparison of imagery data flight log in RTK-enabled mode with ground control points for 20 m altitude........ 86
Table 4.6. Comparison of imagery data flight log in standalone mode with ground control points for 30 m altitude........ 88
Table 4.7. Comparison of imagery data flight log in RTK-enabled mode with ground control points for 30 m flight........ 89
Table 4.8. Geolocation comparison of Standalone and RTK-enabled GNSS data with GCP’s for 50 m Flight........ 92
Table 4.9. Geolocation comparison of Standalone and RTK-enabled GNSS data with GCP’s for 80 m Flight........ 94

Acknowledgements

I would like to express my deepest appreciation to my major professor, Dr. Ajay Sharda, for his unwavering support and aiding me with the opportunity to undertake my Ph.D. research under his guidance. I am grateful for his motivation throughout the program which has been instrumental in determining my professional growth, concluding into achieving a significant academic advancement.

I want to extend my sincere gratitude to my supervisory committee members, Dr. Daniel Flippo, Dr. Naiquain Zhang, and Dr. Bala Natarajan for their time, suggestions, and valuable feedback throughout my PhD journey. Also, the support that I have received from all the faculty and the staff representatives at the Department of Biological & Agricultural Engineering, especially Arlene, Jamie, and Tawnie, helped me to conduct my obligations towards my degree.

I am thankful to Manoj, Rahul Singh, Rahul Harsha, Mateus, Nirajan, John, EDL team and all the FARMS (Fusing Automation & Robotics in Ag Machine Systems) lab members for their assistance throughout conducting my research and contributing their efforts especially during the field experiments.

My sincere and heartfelt thanks to my mother and my elder sister in supporting my decision to pursue a PhD and for all the constant motivation. Their unconditional backing and immeasurable sacrifices have led me to where I currently stand in my professional and personal pursuits. I am blessed to have them as most important pillars of my life.

Lastly, I express my deep appreciation to all who have played a key role in my achievements, recognizing the divine blessings that have paved the way for this journey.

Dedication

Dedicated to my mother, my sister, & almighty

whose support played a key role in my higher education journey.

Chapter 1 - Introduction

1.1 Wireless data communication for agriculture sensing

Wireless data communication plays a crucial role in modern agriculture as it assists in monitoring different environmental factors such as soil, water, climate pertaining to agricultural operations in order to make farming viable and sustainable. By providing wireless access to the information, it helps and facilitates growers in managing their resources such as land, water, soil as well as their time and efforts compared to manually collecting all this information. Technological advancements have revolutionized the global crop and livestock production whether it’s in terms of quality of the product, considering environmental impacts, and the safety and security of the growers and the livestock.

Sensor integration and Internet of Things (IoT) has been a widespread concept specifically used for farming and agricultural industry (Ray, P.P., 2017). A plethora of sensor network monitoring use cases are available to meet the diverse application requirements of sustainable smart agriculture operations. Environmental entities such as soil moisture, temperature, soil nutrient is examined based on weather and the soil properties (Zhang, X. et al., 2017). Edge computing has emerged as a transformative tool, bringing the capabilities of on-demand platforms like cloud computing directly to the field. This is to have better control over decision making prior to pushing any information to an on-demand platform (Kalyani, Y. et al., 2021).

Diverse wireless data communication technologies are available for a wide variety of applications depending upon the need and the requirements. As field agriculture is characterized by its complex terrain and wide geographical area, determining the most suitable protocol for different environments poses a significant challenge. There are numerous technologies which are upfront in providing the facility to wirelessly transfer information based on the different characteristics that they offer (Feng, X. et al., 2019).

Figure 1.1. Comparing different wireless data communication technologies (Feng, X. et al., 2019)

Parameters/technologies	Bluetooth	ZigBee	Wi-Fi	LoRa	NB-IoT
Standard	IEEE802.15.1	IEEE802.15.4	IEEE802.11	IEEE802.15.4g	3GPP release 13
Frequency	2.4 GHz (unlicensed)	868/915 MHz and 2.4 GHz(unlicensed)	2.4 GHz (unlicensed)	869/915 MHz (unlicensed)	LTE frequency (licensed)
Modulation	GMSK	BPSK/OQPSK	BPSK/OQPSK	GFSK	SC-FDMA(UL) OFDMA(DL)
Data rate	1 Mbps	20, 40, and 250 kbps	11–54 and 150 Mbps	50kbps	160–200kbps(UL) 160–250 kbps(DL)
Power consumption (Tx)	10 mw	36.9mw	835mw	100 mw	106 mw
Range	indoor: 20 m out-door:100 m	100m	100m	Urban: 2–5 km suburban: 15 km	Urban: 1–8 km suburban: 25 km

Protocols such as Bluetooth, RFID, WIFI, Zigbee, CDMA and GPRS are further categorized by short distance, medium distance, and long distance according to their reach. GPRS and CDMA has higher accuracy over other options, but their power consumption rate is also high. LoRa and NB-IOT wireless protocol is considered for low power consumption and long range and they can communicate with a cloud server with 90% power efficiency (Feng, X. et al., 2019). While implementing NB-IOT, there is a need to connect every sensor to a specific gateway whereas in LoRa you can connect a module to any gateway. LoRa and NB-IOT offers more than a 15km range with acceptable throughput and less power consumption.

Along with sensing the key elements in the farming environment, the nodes or the point of data generation are also becoming more capable of handling the data at a priliminary stage. This includes processing of the information at the node itself and then sending the required information to the destination. For example, the cameras that are setup on the field continuously monitor and collect information and send it to the headland for further processing (Garcia-Sanchez, A. J. et al., 2011). There are other unique applications such as using wireless data communication for sensing underground entities such as soil parameters, water content, and electrical conductivity (Vuran, M. C., et al., 2018) making sure the information is first broken down at the source using capabilities and processing power of the nodes.

1.2 On-board data handling of existing farm machineries

The on-board data management system is an essential component of all the commercially available agricultural machinery. The central computing system oversees all the information generated from various field operations conducted by the machinery. It consists of information from different subsystems that are embedded on the machinery and the operation for which it is used. Information sources represents GPS, equipment performance, machinery functionalities & control, area covered, and operational information depending upon whether it is used for planting, spraying, harvesting, etc. This information is made available using a standard ISOBUS protocol which is a common protocol used by the manufacturers as a standard procedure. This information is gathered and made accessible to the operator inside the cabin to get an overview and if there are any failures that needs to be addressed (Fountas, S., et al., 2015).

These on-board systems are built from a perspective where the grower would be able to access all the information at a single place. As these systems started to advance in terms of their feature set, they were made efficient in terms of interfacing with any external systems or a peripheral. For farmers and the manufacturers, this has become a means of accessing the on-board computing platform for tasks ranging from troubleshooting to transferring operational data. Subsequently, this information gathered could be uploaded to an online or offline software for conducting further analysis. This provides growers with detailed machinery performance evaluations to optimize their operations, and aiding manufacturers in enhancing their products (Sørensen, C. G., et al., 2011).

In the recent times, with advancements in machinery development, their ability to handle the information has also increased in folds. Data collected on-board can now be seamlessly transmitted to on-demand remote platforms like the cloud, facilitated by cellular networks (Köksal, Ö., & Tekinerdogan, B., 2019). There are commercially available platforms such as John Deere Operation Center, New holland MyPLM™ Connect, and CLASS DataConnect that can save the transferred information for up to 2 machines. This is applicable given they are executed for similar operations and at the same location. Also, they are dependent on cellular connection where end-user is provided with visualization of the machine performance. On the other hand, apart from visualizing the constant movement of the machinery, there is a lack of real-time diagnostics and prognostics during the in-field operations.

1.3 Data handling on autonomous farming platforms

A shift from the traditional and conventional agriculture machinery to a more robust autonomous and semi-autonomous vehicles is currently been witnessed since more than a decade (De Alwis, S., et al., 2022). With advancements in various subsystems employed on conventional tractors and implements, these vehicles are increasingly gaining independence in their overall control. Also, due to the reduction in the workforce, the time and efforts invested has increased leading to less people for more farming activities (Schimmelpfennig, D. 2016). Consequently, there is a gradual automation of routine tasks such as guidance, equipment attachment and detachment, and logistical operations, freeing up growers to focus on more critical and important activities. Also, the labor cost has increased leading to a slow shift of the farmers towards adapting precision agriculture practices at some scale (Miller, N. J., et al., 2017).

Moreover, the broader advancements in autonomous technologies have led to the creation of tailored solutions for enabling a specific farming operation to be autonomously conducted.

These include implementing advanced systems for planting (Tylek, P., et al., 2023), for identifying weeds for spraying (Bakker, T., et al., 2010), phenotyping using autonomous platforms (Atefi, A., et al., 2021), and harvesting (Maja, J. M., et al., 2021). The more these systems become autonomous, they subsequently rely on the data generated in order to gauge their performance while operating in real time. This leads to building an intensive data management platform that will be able to accommodate a stream of information originating from diverse autonomous subsystems as well as able to unload it safely making sure the information is not lost and the data management platform is not under stress.

In order to handle the influx of information streams, data driven agriculture systems and practices are been adopted lately. By merging the benefits of telematics and data management with established precision agriculture technologies, the overall accuracy of operations can be significantly enhanced (Saiz-Rubio, V., et al., 2020). Internet of Things (Khan, A., et al., 2020) and Big-Data (Kamilaris, A., et al., 2017) are the two most upcoming domains after robotics automation and artificial intelligence that will assist in advancing the data management platforms for autonomous systems. This will lead to involvement of human interaction at a minimum scale restricted for supervision purposes only. A direct adoption of existing data management systems available for conventional machinery into autonomous systems is not feasible at various levels. Since autonomous platforms have most of their actions and operations conducted without human interventions, the existing data management platforms will not be able to cope up with large streams of information. Also, the new data handling protocols which are adopted for making the autonomous systems robust will not be suitable and easily integrated with the existing conventional systems. Hence a shift from the traditional data handling platforms to new robust management platforms would be viable.

Middleware's like Robot Operating Systems 2 (ROS2) are becoming a norm in the development process of the autonomous platforms. Various components of autonomous platforms such as navigation, localization, sensing, etc. could be implemented with the stack provided by ROS2 platform. Using the building blocks of the ROS2 middleware such as nodes, topics, services, actions, etc. it is possible to efficiently handle the incoming information and seamlessly offload to a stationary location, a remote platform or any connected peripheral system.

1.4 Data communication using license free spectrum radios in ISM band

As agricultural systems increasingly automate, managing on-board data for immediate or subsequent processing becomes pivotal. To fulfill this requirement, wireless radio data communication is one of the sought-after options given its wide range of availability and application strength. The licensed and unlicensed bands are two ways to access the wireless spectrum as denoted by the Federal Communication Commission (FCC) for the United States. Licensed bands incur a cost and comes with many advantages such as private network, can control the operating ability of the channel, as well as have hold on the outages. In case of license-free bands, there is no cost incurred thereby not giving us the total control but could be used for generic applications where data to be sent is not sensitive.

Unlicensed band offers a reserved radio spectrum for Industrial, Scientific, and Medical (ISM) purposes internationally, where the frequency range is between 902MHz to 928 MHz. The modules can be utilized along with frequency hopping for sending the information using Frequency Hopping Spread Spectrum (FHSS) technique where the algorithm creates hopping sequence from one frequency to another within a given frequency range (King, C. 2013, April). Also, the radio modules equipped with 2.4 GHz range frequency range are being used for various telecommunication applications (Lloret, J., et al, 2012). These can offer higher data rates in Mbps providing the ability to transfer more information at once.

The use of license-free spectrum bands ranges from environment and proximal sensors, IoT applications, and now being utilized as a subsystem of autonomous platforms for offloading the information to an edge platform which can be further routed to a remote location. This can assist in establishing a connection between diverse nodes which are both mobile and stationary, serving as a primary source of information thereby creating a network comprising of the participating nodes in the given application context.

1.5 Use of RTK-enabled GNSS for remote sensing applications

Unmanned Aerial Systems (UAS) are being used for diverse applications such as military, surveying, environment, forestry, agriculture, etc. As the sensing elements such as optical sensors, IMU's, localization sensors started becoming more and more prevalent, the UAS platform became more equipped for diverse applications in crop health and monitoring use case scenarios. Also, due to high maneuvering ability, compact size, and ability to carry diverse payloads has contributed to its expansion (Nevalainen, O., et al., 2017).

Use of Real-Time Kinematics (RTK) enabled Global Navigation Satellite System (GNSS) systems has found its applications in robot navigation, automobile systems, and UAS. The GNSS systems provide an improved positioning accuracy especially when enabled by RTK corrections. By doing so, the GNSS receiver can rectify its location information which is often affected by the atmospheric layers while it communicates with different constellation of satellites (Fan, P., et al., 2019). This accurate localization helps in pinpointing to the exact location of interest and improving the overall corrections of the location information. GPS on the other hand is often used to provide the location co-ordinate but it is prone to errors such as satellite positioning, noise in signals, and provides the accuracy in the range of a few meters which is highly unreliable (Eissfeller, B., et al., 2007).

The GNSS receiver in order to calculate its own position, it requires exposure to at least 4 satellites provided it is not interrupted leading to decrease in the accuracy (Klimánek, M., 2010). When GNSS is used in a dense environment, it can lead to multipath interruption, which affects the positional accuracy to be achieved. To avoid these issues, there are various mathematical models which are used in order to compensate for any specific type of error caused.

Utilizing RTK correction for adjusting the positioning accuracy has been practiced for compensating the errors caused due to atmospheric interference that affects when the GNSS receiver trying to localize itself. In order to send the RTK correction signals to the GNSS receiver, a base station is installed at a known position which calculates the error values required to produces the correction signals (Gumilar, I., et al., 2019). These signals are then sent to the GNSS receiver so that it allows to adjust the ambiguities while it calculates its own position. In order to send these signals, a radio communication medium could be established between the base station and the GNSS receiver where the base station sends out these RTK correction errors and the GNSS receiver accepts these to rectify its positioning information. Depending upon the environment in which this setup is deployed, the radios can be chosen accordingly making sure the signal does not disperse during the wireless transmission. The entire setup could be achieved using a plug-and-play mechanism thereby making it easy for the deploying and achieving the required positional accuracy. Also, in order to receive a constant source of RTK correction signals, it is important that the base station is in constant exposure to the satellites. Therefore, the GNSS receiver installed on the UAV will be able to generate the accurate location information for different purpose such as geotagging, image triggering, data logging, feeding forward to the navigation control, etc.

1.6 Research Objective

The objective of this research can be divided into two parts, A) To establish a wireless communication platform for an autonomous farming application. This includes developing a data communication system that could be integrated with the autonomous liquid application system to seamlessly relay all its information to a single location called central hub in real time. B) To develop RTK-enabled GNSS solution for remote sensing platform, UAV, in order to improve the positional accuracy of the imagery data collected. This could improve the remote sensing studies that requires zone-level and plant-level control further assisting in producing precise irrigation or nutrient management strategies. Therefore, the study aims to:

1) Developing and testing of a wireless data communication platform
    a) Hardware design and testing of wireless data communication platform using a license-free spectrum band radio along with a micro-controller unit integrated together on a single PCB.
    b) Field testing of these units by random deployment with simulated dataset and evaluating for its end-to-end data transmission accuracy
2) Integration of radio communication platform with autonomous liquid application system using ROS2 interface
    a) Configuring license free spectrum band radio providing link rate of Mbps and integrating it with the autonomous liquid application platform using ROS2 middleware for transmitting the system-level information
    b) Deployment and field testing of the setup in diverse field environment to ensure end-to-end connectivity and packet delivery efficiency for different configurations.

3) Improving the positioning accuracy of imagery data using RTK-enabled GNSS solution for UAV applications involving
    a) Development and testing of an optocoupler based distance trigger mechanism for RGB imagery collection.
    b) Redefining image geotagging workflow Thermal-Infrared (TIR) imagery for improving the geotagging accuracy.

Overall, the research conducted in this study aims to develop solution solving the need of instantaneous data handling which is a challenge especially for the autonomous farming systems. As the traditional methods of accessing information results in extensive lead time for the data to reach to its destination, the wireless data communication system proposed in this research contributes to the expedited trans-reception using the license free wireless spectrum band. The system developed can be implemented independently & integrated with autonomous platform operating in ROS2 environment. This ability of the system to readily integrate with existing platforms makes it suitable for rapid application development. Currently available data handling systems for the existing platforms includes traditional practices of accessing information which might not suit the modern autonomous farming solutions. As most of them would be built upon robotic system infrastructure, the data communication system developed in this research would seamlessly integrate. Lastly, the challenge of obtaining a precise geolocation is widely experienced in many remote sensing applications for agriculture. Thus, by using wireless data communication, a GNSS solution onboard an unmanned aerial system was fed with real-time kinematic correction signals. These help in eradicating error and assists precise geolocation capture.

Chapter 2 - Hardware design & preliminary evaluation of wireless data communication for autonomous farming applications

2.1 Abstract

Autonomous farm robotic solutions involve multi-agents co-managing farming operations. These systems enable granular data collection of dynamic entities such as operational vehicle health, position, and diverse multi-dimensional data gathered from multiple control and actuation sensor suites. Real-time and continuous data acquisition from multiple agents to a single location, a critical logistic requirement, is often found missing in existing farm management information systems (FMIS). Therefore, this study was designed to develop a continuous data communication system for autonomous robotic agricultural vehicles. The objective of this study was to realize a continuous wireless data communication for autonomous farm robots (AFR) to seamlessly transmit data to central datahub during the field operation. The wireless data communication platform collectively referred to as the Pico-Radio Interface Microcontroller Electronics (PRIME) board was designed which incorporated a radio with different topologies, a range of 40 miles (60 km) in line of sight (LOS) and a maximum wireless link rate of 276 kbps, ensuring reliable and robust trans-reception of information. Additionally, the PRIME consisted of a microcontroller that controls the overall operations and continuously feeds information to the radios, along with power conditioning electronics. Seven PRIME systems were programmed to function as remote (four), repeaters (two) and primary (central hub) respectively & were deployed at distinct locations to function independently and tested in a dynamic farming environment encompassing variable undulating terrain and a dense crop canopy. To evaluate the effectiveness of wireless radio communication system, simulated data packets were transmitted from four remote systems to primary for time periods of 15, 25, and 30 minutes. For each remote, Packet Delivery Ratio (PDR),

quantifying packet transmission and reception accuracy, was calculated. The obtained PDR exceeded 0.98, signifying an accuracy rate of over 98% across all three experimental runs. Furthermore, every PRIME system exhibited low power consumption, averaging less than 0.42 W throughout all experiments, attesting to its energy efficiency. Overall, the designed PRIME system, which is a plug-and-play unit, has the potential to be integrated with diverse AFR connectivity applications in varying real-world conditions to co-manage the operations in a multi-agent setting.

2.2 Introduction

The agricultural industry is preparing for the predicted increase in global population to 9.7 billion by 2050 (UN,2019), which requires a significant 50% increase in global food production (FAO, 2017). To meet these demands, advancements in farming systems are being made, with a focus on creating robust platforms that involve human intervention only for the purpose of supervising and implementing the systems (Rahmadian, R. et.al., 2020). Several developments are being made in farming system components such as platform, sensor, and control system development (Bawden et.al., 2014, Sowjanya, K. D. et.al., 2017) to meet future efficiency and productivity demands of existing machine systems. Precision agriculture technology adoptions (N. J. Miller et.al., 2019, Griffin et.al., 2017) are generating and accumulating high-volume data from various farming activities to understand both machine system performance and agronomic decision-making. Current FMIS solutions such as John Deere Operations Center, DataConnect (CLAAS), Granular (Corteva), MyPLMTM Connect (CNH) saves information about machine status reports, operational efficiency & performance. At times, this information is for limited number of machines from a single location & transfers data using cellular connectivity which is an overarching issue in the rural environment where majority of farming lands exist. This data is available on mobile platform and outside farm environment in the form of on-field visualization and post processing correlation analysis. A few systems with continuous high-volume data accumulation are available (Xu, R., et.al., 2022, Pak, J., et.al., 2022) but it creates a burden on the platform for which data needs to be offloaded periodically. Two-way communication, data prognostic & diagnostics are some of the features that are currently lacking on the existing platforms which are essential for AFR's to work collaboratively.

Various autonomous farming system concepts are being developed to meet labor challenges within agricultural landscape, address environmental concerns and tackle increasing machine size, compaction, scalability, and safety challenges (Srivastava, V., et.al., 2022, R Shamshiri et.al., 2018). A large proportion of such efforts includes developing a fleet of small autonomous rovers to replace single machine operation within a single field. To enable effective operation of the autonomous rovers, it is necessary to communicate, analyze, and visualize machine operational data from multiple autonomous rovers instantaneously. Real-time data access is very critical for safe rover maneuverability, operational health monitoring (orientation and battery), and meeting the needs of different application systems (such as seed, fertilizer, and chemicals). Traditional data collection and communication techniques involving human intervention are inadequate for successful autonomous system operation. Therefore, robust, and resilient distribution system is required that can provide a seamless data communication between multiple autonomous rovers and central hub in real-time.

Wireless data communication is a promising solution for instantaneous data transfer due to its high speed, ubiquity, affordability, and use in diverse IoT and sensor networks, including farming applications (Khan, N., et. al., 2021, Atmaja, A. P., et.al., 2021). Outdoor farming activities require specific characteristics such as good range, power efficiency, high data rate, low error rate, and durability in extreme environments. From the characteristics of different wireless data communication standardized techniques mentioned in Table 2.1, Bluetooth provides a data rate in Mbps but is not suitable for long-distance communication needed on large-scale agricultural farms. Zigbee, while suitable for short-range communication applications, has limited data rate. WIFI is power consuming and suits medium-range communication up to 100 m, while GPRS/3G/4G is a cellular-based connection that is useful for indoor but is heavily dependent on cellular connectivity which can often be challenging at agricultural farms. WIFI and Cellular communication also incur high cost of infrastructure and setup.

Table 2.1. Comparison of wireless technologies and their characteristics (Ojha T., et al., 2015).

Parameter	ZigBee	WiFi	Bluetooth	GPRS/3G/4G	WiMAX
Standard	IEEE 802.15.4	IEEE 802.11 a, b, g, n	IEEE 802.15.1	–	IEEE 802.16 a, e
Frequency band	868/915 MHz, 2.4 GHz	2.4 GHz	2.4 GHz	865 MHz, 2.4 GHz	2–66 GHz
Data rate	20–250 kbps	2–54 Mbps	1–24 Mbps	50–100 kbps/200 kbps/0.1–1 Gbps	0.4–1 Gbps (stationary), 50–100 mbps (mobile)
Transmission range	10–20 m	20–100 m	8–10 m	Entire GSM coverage area	⩽50 km
Energy consumption	Low	High	Medium	Medium	Medium
Cost	Low	High	Low	Medium	High

Radios with MESH capability operating in a license-free (ISM) spectrum band (900 MHz, 2.4 GHz, and 5.8 GHz) have gained popularity in long-distance communication by reducing packet loss (M. Bogdanoff et.al., 2020). Excellent link rate, a wide range of line-of-sight distance metrics, and error correction and detection techniques, make them suitable for applications like autonomous farming systems. Additionally, frequency hopping spread spectrum (FHSS) technique used in wireless communication systems avoids interference from other wireless devices by periodically changing the frequency in use (Motlagh et.al., 2010). Therefore, the objective of this study was 1) To build a wireless data communication system for an autonomous farm robot (AFR), and 2) Evaluate the system in different environmental conditions by quantifying packet delivery performance and power consumption for robust data communication.

2.3 Materials & Methods

2.3.1 Application System

An AFR platform for site-specific liquid application system has been built at Fusing Automation & Robotics in Machine Systems Lab (FARMS) Lab, Kansas State University.

The platform has a computer vision system to capture plant images and detect insect incidence using onboard convolutional neural network (CNN) model (Grijalva et.al.,2023). Based on computer vision system feedback, the AFR conducts site specific applications using controller area network (CAN) based liquid application system. The on-board computing system (ORIN, NVIDIA, Santa Clara, CA, USA) collects and records operational data as shown in Figure 2.1 from AFR platform (geo-location, robot orientation, speed, battery voltage, current usage on four electric motors), computer vision system (pest geo-location and severity derived from CNN model), and liquid application system (tank liquid level, liquid amount sprayed, application pressure) integrated using robot operating system (ROS2, Open Robotics). The geo-location data is collected using an on-board dual frequency (B110, Topcon, Tokyo, Japan) global navigation satellite system (GNSS) receiver.

Figure 2.1. System Data Flow for Autonomous Liquid Application Platform

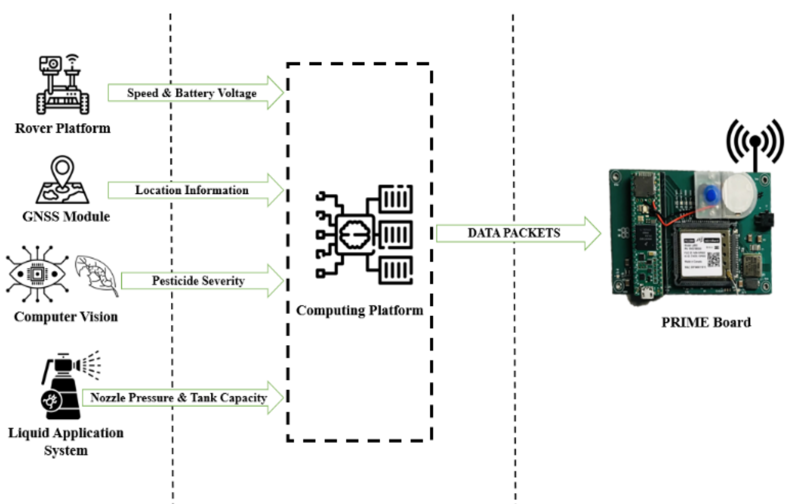

The data collected is packed in small data packets with two classifications, time-critical and system operational data. Each data packet is time stamped and contains metadata to indicate date, time, type of operation and AFR identification. The time critical data packets are designed to be captured and transferred every second while system operational data packets are captured every second and sent every 30 seconds. The time critical data packet includes geo-location information of the AFR so that real-time movement of AFR can be tracked. This information is useful to gauge safe and seamless navigation of AFRs through the crop rows at a desired speed without affecting the crop. The system operational data packet consists of event driven information from all the subsystems mentioned above. During field operation, multiple AFR working in unison would be tasked to traverse crop rows in a pre-defined boundary of the field and perform desired action of pest detection and control through liquid application. All the operations right from detecting the pest, spraying at the pest, accumulation of data and transferring data are done in real-time as shown in Figure 2.2.

Figure 2.2. Multiagent Wireless Data Communication Schematic

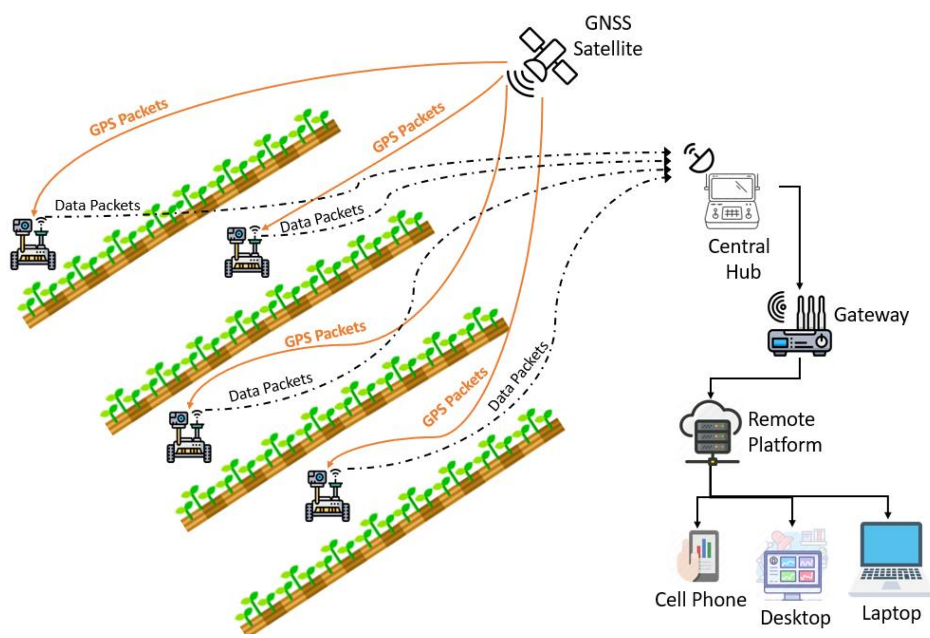

2.3.1.1 Pico Radio Interface µController Electronics (PRIME) Board

A custom-made Pico Radio Interface Microcontroller Electronics (PRIME) board was designed and developed which hosts a radio, a microcontroller and on-board power electronics component that provides controlled power to the components as show in Figure 2.3. The input voltage requirement of the radio is in the range of 9-30 VDC and the board was operated using a 11. 1V battery pack to function longer durations. The PRIME board was programmed for three configurations namely remote, primary, and repeaters. The AFR would be hosting these remotes to enable them reading the data packets over serial communication. The repeaters were installed in a stationary position to improve the scope of the network and increase coverage. The primary acted as the ‘central hub’ where all the data transferred by remotes was collected for packet delivery statistics. While beyond the scope of this study, future research could develop a system to stream data from the primary to the on-demand platforms like cloud. This would facilitate the generation and visualization of analytical insights accessible through user interfaces.

Figure 2.3. Block Diagram and Printed Circuit Board (PCB) for PRIME Board

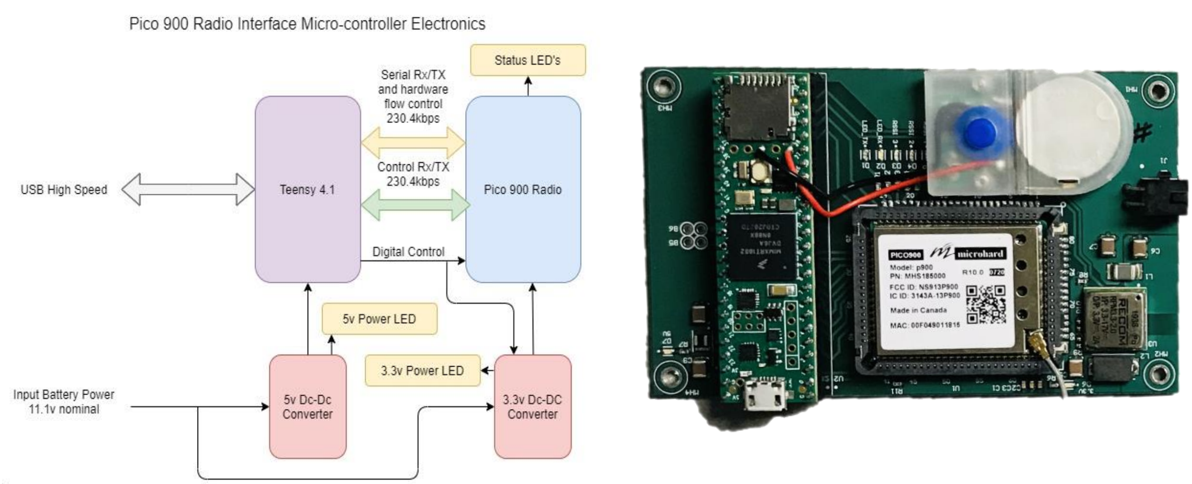

2.3.1.1.1 *PICO 900 Mesh Radio*

A miniature radio (PICO 900, Microhard Corp, Calgary, Alberta, Canada) modem shown in Figure 2.4 was selected for PRIME board that has capability to deliver point-to-point, point-to-multipoint, and mesh functionality.

Figure 2.4. Microhard PICO 900 Mesh Radio module

The radio utilized Frequency Hopping Spread Spectrum (FHSS) and operates in license free 900 MHz spectrum band, which resulted in low power consumption for its functioning. The radio characteristics also included 1-W power consumption, 3.3V logic level compatibility, 902-928 MHz operational frequency, and offers a good range of 60 km line of sight (LOS). The radio had capabilities such as auto-routing which helps to navigate data packets seamlessly, and self-healing assisting in minimizing data loss with a compact footprint. The radio supported maximum serial baud rate of 230 kbps asynchronous and link rate of 276 kbps, making it suitable for autonomous platform applications which requires a constant data transfer in continuous operation use case scenarios. The radio was configured with the help of an initialization file consisting of all the Attention (AT) Commands required to perform functional actions. On the startup of PRIME board, the radio proceeded to command mode, and it configured itself using the AT commands placed in the initialization file which resides in the SD card situated on Teensy Microcontroller.

To implement wireless transmissions and minimize the network congestion, the radios in remote configuration were programmed in channel access mode wherein data packets were divided into data frames and further into slots using Additive Links On-line Hawaii Area (ALOHA) technique. This was accomplished where every particular modem can access the channel for transmission at every assigned frame slot. It also offers packet retransmission, and ALOHA slot synchronization for optimum channel access to each contributing radio node.

2.3.1.1.2 Antenna

The ANT-916-OC-LG-RPS whip antenna (Linx Technologies, Orlando, Florida, USA) shown in Figure 2.5 was used as per the specification provided by the radio manufacturer. The antenna ranges in 895-935 MHz with a center frequency of 916MHz. An omnidirectional & compact antenna provided the operating frequency range within the radio specifications with impedance of 50 ohms. Also, tilt and the rotation provided with the antenna helps in steady alignment with the PRIME board. RP-SMA type connector was available with the antenna which coupled perfectly with the radio connector.

Figure 2.5. ½-wave dipole omnidirectional antennas product dimension (ANT-916-OC-LG-RPS Datasheet)

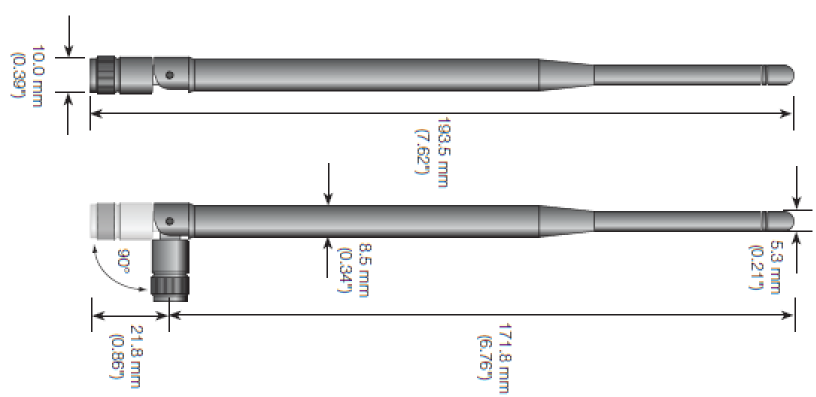

2.3.1.1.3 Teensy Microcontroller

The Teensy 4.1 microcontroller (PJRC, Sherwood, Portland, Oregon, USA) is a simple & compact USB development board having Arm Cortex-M7 processor with 600 MHz & multiple I/O. Figure 2.6 displays different components onboard the Teensy 4.1.

Figure 2.6. Teensy 4.1 Microcontroller module

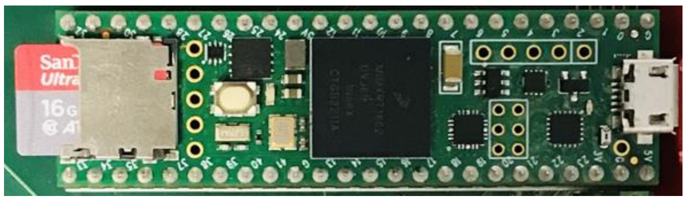

This microcontroller matched the computing needs of the PRIME board operations & provided features such as standard power requirements, SD card slot availability, multiple I/O and small footprint. The SD card slot helped in storing the data collected throughout experiments which was useful in backtracking any missing data packet and extracting more information.

2.3.2 Data Packet Characteristics

The data packet comprised of information from various subsystems such as AFR platform, computer vision system, and liquid application system. On the AFR, the data from these individual subsystems was collected on a common platform with the help of an on-board computer NVIDIA ORIN. The illustration in Figure 2.7 shows an example data packet & its description in Table 2.2.

Figure 2.7. Data Packet Characterization

```
R1
$GPGGA,155938.10,3911.4201813,N,09634.9626850,W,1,05,3.00,284.1718,M,0.0000,M,,*72;-0.07 0.90 0.42 -0.06
60%, 1mph
0.547 -0.059 -0.059 0.234 0.12 0.05, 0.1 GPM, 12 gal, d: 0.1 0.5 0.3 0.2 0.2 0.1, SolTD: 0.9 0.8 0.9 0.6 0.5 0.8
39.07,-95.768,317.369
```

Table 2.2. Data packet description

Line	Placeholder	Placeholder description
1	Unique identifier	AFR identification
2	NMEA string from GNSS module	Geo-location Information
3	Health and operational AFR data	Orientation, battery voltage & speed of autonomous platform
4	Liquid application system data	Nozzle spray rate, liquid level of the tank, nozzle pressure and solenoid timing information
5	Computer vision system data	Pest geo-location, and severity

The size of the data packet, approximately 256 bytes, complimented the maximum individual packet buffer capacity of the selected radio before character timeout timer. Since the data packets are simulated, they were kept in ASCII format for the purpose of simplicity. This enhances human readability, avoids additional conversion mechanism and is easier to debug since the purpose was to examine the performance of the radio used to send data without losing any information. The radio was also configured for retransmission as a default setting to avoid loss in noisy environment. To keep track of data coming from various subsystems during the different phases of the experiments, it was timestamped in order to perform any diagnosis or back tracing any errors. During the system development, a continuous geo-location feed of the AFR is desired facilitating visualization of where and how the AFRs are operating. Continuous geo-location feed addressed concerns regarding proper operation of AFR's within crop rows, interference between units, and potential boundary breaches or over-extension.

After initiating wireless data transfer, it was important to ensure that the information was accurately acquired on the receiving end. The primary radio on the receiving end was attached to a laptop for real time data visualization using an open-source serial terminal program Tera Term.

2.3.3 Experimental Sites

For the outdoor experiment, two locations were selected: 1) Animal Science Farm (ASF) at Kansas State University and 2) Clay Center (CC), Kansas. The experiment involved four remotes (henceforth referred to as R1, R2, R3 and R4), one primary as a central hub, and two repeaters' in secondary configurations. All the radios were installed with the help of a stationary pole and were at a height of 8-10 feet above ground as shown in Figure 2.8.

All installation sites underwent surveying with a GNSS receiver to capture geolocation of all the installed radios ensuring ground data collection as shown in Table 2.3. They were transferred to ArcMap software (ESRI, California, USA) for plotting with the help of distance tool and generating maps of the experimental sites. This geo-location information allowed to visualize the distance between each of the remotes and the central hub and get a range of distances covered.

Figure 2.8. Wireless radio installation of remote (a) and primary (central hub) at the edge of the field (b)

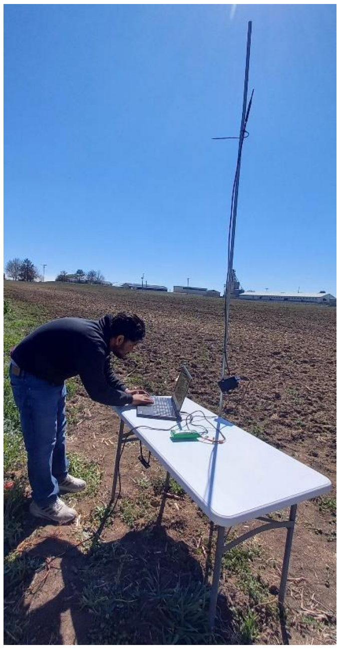

(a) (b)

The ASF site shown in Figure 2.9 was a fallow agricultural field with varying terrain that allowed for testing the line-of-sight communication abilities of the radios, whereas the CC site had corn crop with a canopy height of approximately 8-9 feet which provided dense canopy to assess the signal propagation quality and impact on the packet delivery ratio. Studies have shown that the climatic conditions affect the propagation of the signal in vegetative environment (Goense et.al., 2005). The installation of the PRIME boards was arbitrarily done, distances were measured and later calculated during the analysis. The distances measured from the central hub to each of the remotes for ASF site was in the range of 20 to 150 m whereas for CC site it was in between 100 to 500 m.

Table 2.3. Distance of each remote from Primary

Units	Distance from Primary	
	Animal Science Farm	Clay Center
R1	23.14 m	99.07 m
R2	125.42 m	300.88 m
R3	146.08 m	417.98 m
R4	128.85 m	417 m

Figure 2.9. Radio placement for ASF site (a) and CC site (b)

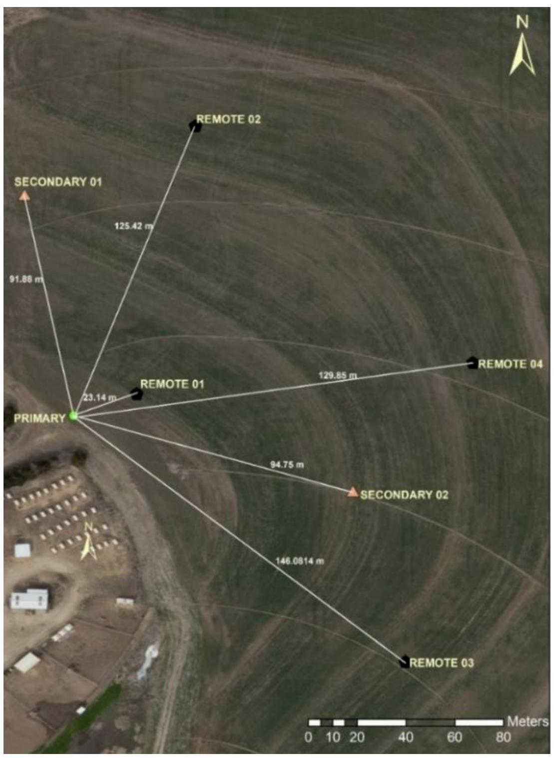

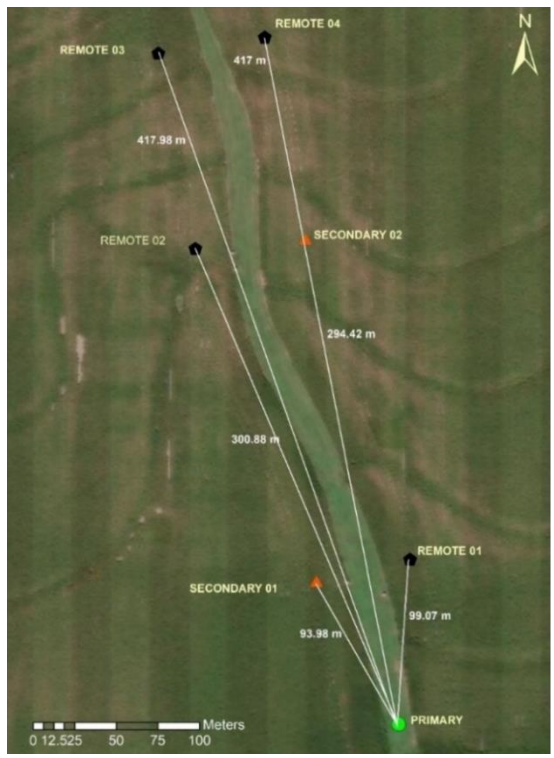

(a) (b)

2.3.4 Data Collection and Experimentation

To evaluate the efficacy of the wireless data communication network, outdoor experiments were conducted in actual farming fields. The radios were randomly installed in the agricultural field to continuously transmit and receive simulated data packets to the central hub. These data packets were generated as an example of how the sub-system level data would appear and were stored in the SD card of the PRIME board. This approach facilitated and simulated real-time monitoring of the AFR’s instantaneous positions. Each experimental run at both sites was 15, 25, and 30 minutes long to send both time critical and operation data packets to the central hub. These time periods were considered assuming enough duration was provided for the PRIME board to carry out the data transfer which can be changed as per the requirement. The analysis of the per second data and the per 30 second data packets received was carried out separately to observe any packet loss, given the data packets differ in terms of what they consist and their size. After powering up all the modules, the central hub sends an initiate command, after which the data transmission begins which establishes a two-way communication. The collected data, which included the count of transmitted and received packets, was used to calculate packet delivery ratio. Additionally, instantaneous power consumption was also gathered throughout the experiment leveraging the onboard power electronics.

2.3.4.1 Packet Delivery Ratio and Power Consumption

The packet delivery ratio is a critical metric used to assess the wireless network's performance. It is calculated based on the number of data packets received versus the number of data packets transmitted. This metric allowed to evaluate the efficiency of packet transmission, radio hardware capabilities, and link characteristics. The packet delivery ratio is calculated as shown in Equation 2.1

Equation 2.1. Packet Delivery Ratio

$$*\,Packet\ Delivery\ Ratio = \frac{Number\ of\ packets\ received}{Number\ of\ packets\ transmitted}$$

While radios were active, the power consumption was continuously monitored per second with the help of onboard power management circuitry and the average was calculated every 30 seconds and sent along with the operational data packet. At the conclusion of every experimental run, a final summary data packet is transferred by all the remotes to the central hub consisting of packet delivery ratio for every radio and its corresponding power consumption information.

2.4 Results and discussion

The packet delivery ratio calculated for each of the PRIME boards for the 15, 25- and 30-minute experimental run are shown in Table 2.4 for the ASF site and Table 2.5 for CC site. Also, to depict the power consumption of the PRIME boards, an example of average power consumed for 30 minutes experimental run for both the sites is shown in Figure 2.10.

Table 2.4. Packet Delivery Statistics for ASF Site

Units / Duration Information	R1				R2				R3				R4			
	Packets Received		Packet Delivery %		Packets Received		Packet Delivery %		Packets Received		Packet Delivery %		Packets Received		Packet Delivery %	
	1 Sec	30 Sec	1 Sec	30 Sec	1 Sec	30 Sec	1 Sec	30 Sec	1 Sec	30 Sec	1 Sec	30 Sec	1 Sec	30 Sec	1 Sec	30 Sec
15 Minutes # 1 sec packets = 870 # 30 sec packets = 30	867	30	99.6	100	868	30	99.7	100	867	30	99.6	100	868	30	99.7	100
25 Minutes # 1 sec packets = 1450 # 30 sec packets = 50	1448	49	99.8	98.0	1446	50	99.7	100	1446	50	99.7	100	1447	50	99.7	100
30 Minutes # 1 sec packets = 1740 # 30 sec packets = 60	1729	59	99.3	98.3	1733	60	99.5	100	1736	60	99.7	100	1736	59	99.7	98.3

***Packet Delivery % = Number of Packets received/Number of Packets sent**

Table 2.5. Packet Delivery Statistics for CC Site

Units / Duration Information	R1				R2				R3				R4			
	Packets Received		Packet Delivery %		Packets Received		Packet Delivery %		Packets Received		Packet Delivery %		Packets Received		Packet Delivery %	
	1 Sec	30 Sec	1 Sec	30 Sec	1 Sec	30 Sec	1 Sec	30 Sec	1 Sec	30 Sec	1 Sec	30 Sec	1 Sec	30 Sec	1 Sec	30 Sec
15 Minutes # 1 sec packets = 870 # 30 sec packets = 30	867	30	99.6	100	868	30	99.7	100	867	30	99.6	100	868	30	99.7	100
25 Minutes # 1 sec packets = 1450 # 30 sec packets = 50	1448	50	99.8	100	1447	49	99.7	98	1444	50	99.5	100	1443	50	99.5	100
30 Minutes # 1 sec packets = 1740 # 30 sec packets = 60	1733	60	99.5	100	1737	60	99.8	100	1738	60	99.8	100	1731	60	99.4	100

*Packet Delivery % = Number of Packets received/Number of Packets sent

Figure 2.10. Power consumption for 30-minute experiment at ASF (a) and CC (b) sites

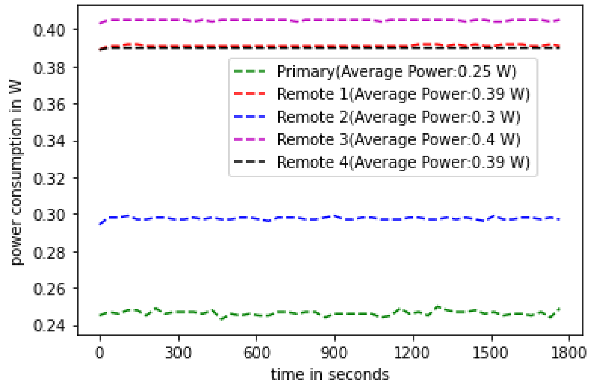

(a)

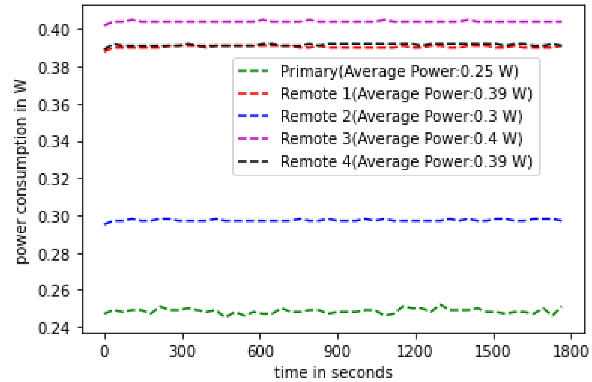

(b)

If one has to imitate a continuous moment of the AFR to implement the system, it will require the user to implement the same system frequently which would thereby cause some amount of redundancy. For a continuous data communication with real-time movement of the AFR, a mobile platform would be required which can be integrated with PRIME boards and then deployed in real-time. This would require deploying multiple AFR which are standardized in terms of their functionality and operation. The PRIME board has the functionality to be able to seamlessly integrate with the AFR using a simple USB interface.

2.4.1 ASF Site

As mentioned, the ASF site was a fallow land providing undulating terrain, thereby testing the line-of-sight ability of the PRIME boards installed. All the PRIME boards for the 15- and 25-minute run provided a packet delivery of 99% for per second data transfer and 100 % for per 30 second data transfer. For the 30-minute experimental run, the PRIME boards lost some data ranging from 4-10 data packets for per-second data transfer and provided an overall packet delivery of 98 % for both the data transfer schemes. Also, the power consumption of all the PRIME board were less than 0.42 W for all the experimental runs. Therefore, it can be concluded that the network of PRIME boards installed at the ASF site performed well in providing a close to perfect data transfer ability with low power consumption in an undulating terrain environment.

2.4.2 CC Site

The CC site consisted of a dense crop canopy that tested the signal strength of PRIME boards seamlessly transferring information to the central hub. For the 15- and 25- minute experimental run, all the PRIME boards performed excellent by losing only a couple of data packets and provided a packet delivery of 99 % for per second data transfer and 100 % for per 30 second data transfer. For the 30-minute experimental run, it lost some data within the range of 3-9 data packets for per second data transfer but provided a decent packet delivery of 99 %. Whereas in the case of per 30 second data transfer, all the PRIME boards provided 100 % packet delivery. Despite the dense crop canopy potentially necessitating increased power consumption from all participating PRIME boards to maintain signal strength, measurements revealed power consumption remained below 0.4 W. This proves the ability of PRIME boards to perform well in a dense canopy environment by providing a seamless end-to-end information delivery.

Given the test environment considered in which the experiments were conducted, the PRIME board network can be implemented for farming operations in croplands that encompass varying land undulation and dense vegetative environments, thereby fulfilling functional requirements for various pre- and post-planting farming tasks. These test runs conducted in the experimental phase provided a packet delivery of 98% and above for per second data transfer and close to 100 % in almost all the cases of 30 second data transfer for both the sites. Also, the PRIME boards consumed less than 0.5 W power for all their experimental runs at both the selected locations.

It will be noteworthy to examine when the PRIME board network operates for a continuous duration of several hours and if it will be able to maintain the packet delivery performance as obtained during the experimental phase. Also, when installed on mobile AFR's, the continuous movement of the platform would test the ability of the PRIME boards to maintain a seamless channel for continuously sending the information to the central hub.

2.5 Conclusion & Future Work

The study describes the development and practical implementation of a continuous wireless data communication platform for autonomous farming operations. The overall outcomes were

- To design the PRIME boards incorporating a Teensy microcontroller and Microhard Pico 900 radio for wirelessly transmitting the information to the central hub within real-world field conditions of varying terrain and dense crop canopy conditions.
- The experiments showed an overall packet delivery of 98% for per second packet transfer, whereas 100% for almost all scenarios for per 30-second packet transfer.
- Due to the low power consumption ability of the radio, all the remotes and the primary could complete the task utilizing less than 0.42 watts for all the experimental runs.

In a nutshell, the communication system can be implemented in diverse applications requiring a need to transfer data wirelessly from multiple locations to a central hub in real time.

As the system is currently tested for independent functioning, future research will integrate the PRIME boards with the AFR's using ROS2 to access instantaneous data for communicating with the central hub. The performance could be tested for real-time field data gathered from different subsystems that are onboarded on an AFR. In order to handle data remotely, further research can be conducted to develop interpretation and to extract meaningful insights from data directed towards cloud platforms. This will open a wide range of applications for diverse farming operations implemented using AFR. It will provide the required autonomy as farming operations are multifold in nature whether its planting, spraying, harvesting etc. An FMIS for autonomous farming system can be developed for the farmers where they can remotely monitor the AFR operations on their field. Timely notification can be provided which can offer the current status of the operation thereby updating the farmer about the whereabout of every single AFR. If required, the farmer can engage themselves in making sure the requirements are met and stay in the supervisory mode by letting the system accomplish the designated task.

Chapter 3 - Integration & testing of wireless data communication system with autonomous site-specific liquid application platform

3.1 Abstract

Autonomous ground vehicles have gained widespread adoption and are steadily being practiced for various farming operations like scouting, weeding, planting, spraying, etc. The instantaneous data collection from these autonomous ground vehicles holds prime importance for multiple reasons such as continuous update of their locations, ensuring the health & safety of the vehicles, and especially acquiring the operational information from different subsystems while they interact with the dynamic field conditions. Transferring the captured information in real-time is one of the features that is deficient in many such readily available systems which leads to losing track of the vehicle, the status of the subsystems, and the vehicle prognostics for avoiding any malfunctions. To address this, a real-time wireless data communication system is devised and integrated with an autonomous rover platform designed for carrying a site-specific liquid application system. 2x2 Multiple Input Multiple Output (MIMO) radios are configured for setting up an end-to-end wireless digital data link between an autonomous rover platform and a central hub for data accumulation. The radio serves an extensive speed of up to 25 Mbps with other capabilities such as Low-Density Parity Check (LPDC) and low power consumption. ROS2 (Robot Operating System 2), which is the foundational software stack for overall system development, was utilized in integrating the MIMO radio with an autonomous rover platform. The data packets comprised of information from all the subsystems such as autonomous platform, computer vision, and liquid application system. The evaluation of the Packet Delivery Ratio (PDR), Packet Loss, and Latency under diverse field conditions becomes imperative, serving as a metric to determine the responsiveness and reliability of the wireless data communication platform. The radio

communication was tested for three different configurations at two different experimental locations to gauge the line-of-sight ability and long-range communication. Two sets of configurations produced more than 98% of packet delivery with a data loss of less than 2%. Also, the latency between the transmission was observed between 0.1 to 0.4 seconds throughout all the configurations and field tests. Overall performance by the data communication system proved to be suitable for real-time data collection tasks within the autonomous farming application.

3.2 Introduction

The advent of autonomous farming technology has emerged as a preeminent practice for enhancing agricultural productivity, mitigating waste, and fostering sustainable operations (McGlynn, S. et al., 2019). This paradigm shift involves the substitution of traditional single-unit machinery with a fleet of collaborative autonomous platforms, adept at multifarious tasks such as weeding, spraying, harvesting, and planting (Gonzalez-de-Santos, P. et al., 2017; Zangina, U. et al., 2021). These autonomous platforms are equipped with diverse sensing elements that make them accustomed and actionable in the dynamic variations of the farming environment. The amount of information collected by these systems includes data from cameras, sensors, actuating systems, platforms, etc. (Santhi, P. V., et al., 2017). To instantly utilize the information collected, there is a need to communicate this information in near real-time, facilitating data analysis for enhanced decision-making (Steward, B. L., et al., 2015). However, the challenge lies in the limited connectivity available at the farms, necessitating the extraction of information post-operation when the platforms are within adequate network coverage. This procedural delay leads to a substantial loss of crucial data since the dynamic environmental conditions captured by the sensing elements are not catered to right away. The need for incorporating wireless data communication with autonomous farming robots includes:

- Expedite human-machine interaction for autonomous farming platforms,
- Supervising and controlling for safe functioning of autonomous platforms,
- To facilitate data exchange and co-ordinate operations with the central hub

Wireless data communication emerges as one of the top priority options for remotely transferring data from the edge nodes such as sensors and actuators which capture dynamic attributes within the agricultural field (Conesa-Muñoz, J., et al., 2015). Contemporary machinery, equipped with a diverse sensor suite, accumulates extensive data comprising both system-level information and environmental variables indicative of on-field conditions. These machineries often store information on the platform which is later collected by the grower once the operation is completed. Extensive research explores various aspects of how autonomous platforms are being used for farming operations, yet there is a notable gap in discussing how the data collected can be communicated in real-time to the desired location. The currently available findings discuss the hardware and software implementation with respect to the development of the platform, and installation of diverse sensor suites (Cheng, C., et al., 2023) but seldom mentions how the data collected could be managed and efficiently transferred in real time. Also, existing wireless data communication technologies often struggle to cope with the demanding, extreme and dynamic nature of farming environments. Therefore, a need to manage and communicate the information instantaneously arises to emphasize the importance of real-time data gathering and prompt decision-making.

Currently available Farm Management Information Systems (FMIS) on existing precision agriculture machinery collects information such as status reports, operational efficiency, and performance. The recent advancements include integration of on-demand cloud computing strategies that provide an extension to these information systems and allow remote access

(Hewage, P., et al., 2017). Also, some of them integrate new technologies for making spatiotemporal patterns and assessments based on publicly available data assets (Liao, W. T., et al., 2015) whereas some provide an end-to-end decision support system using diverse modelling techniques (Kukar, M., et al., 2019). As these technologies are helping in managing information for big unit machineries, they are unable to readily support the data management ecosystem on autonomous platforms that have most of their operations in a self-governing paradigm. Hence, there is a need to develop a data management platform that would provide the features of the existing frameworks available as well as give a near real-time overview of all the operational activities for autonomous platforms. Since, the currently available FMIS infrastructure requires a continuous network coverage, which is often an issue as majority of farmlands are geographically in the outskirts, a radical change is required to develop well connected autonomous farming network going ahead.

To overcome this challenge, a study was conducted by realizing a wireless data communication system for autonomous site-specific liquid application platform. The overarching goal was to route the operational and system information from distinct subsystems such as computer vision, liquid application system, and autonomous platform instantaneously to the central hub located on the headlands. This is pivotal from a systematic and prognostic point of view to avoid any foreseeable failures and for the safety of the entire platform maneuvering inside the crop rows without harming the plants. The efficiency of the data communication is calculated in terms of packet delivery ratio, packet loss and the latency in the system.

3.3 Materials & Methods

3.3.1 Rover Platform

The autonomous rover platform containing a site-specific liquid application system developed consists of an onboard Nvidia's Jetson AGX ORIN GPU (Nvidia, Santa Clara, CA) as shown in Figure 3.1. The GPU runs a pest identification algorithm powered by the deep learning neural network model (Grijalva, I., et al., 2023) to accurately identify the pest infestation using high-resolution cameras. Upon pest identification, a prompt response triggers the liquid application system to spray precisely at the detected pest location, determined by the camera's observations. This event creates multiple data points such as the location of the pest detected (latitude, longitude), the amount of pest severity, the amount of liquid sprayed, etc. Also, some system-level information is continuously generated such as the constant location, speed, battery voltage of the platform, the liquid level in the spraying tank, and pressure at the spray nozzles which is important to verify whether the overall platform is in good health as shown in Figure 3.2. Routing all this information to a location like a central hub would require a robust and seamless wireless data communication link. The ROS2 middleware is used to manage the operations, control the motion, navigate through crop rows and onboard communication between different subsystems. This capability of ROS2 was extended further to integrate the radio with the onboard computing system. The node and topic structure of the ROS2 framework is utilized to communicate and obtain the required information whether it is system-level information or information that is generated based on the occurrence of the events.

Figure 3.1. Rover Platform

Figure 3.2. Operational flow and event-based system data logging

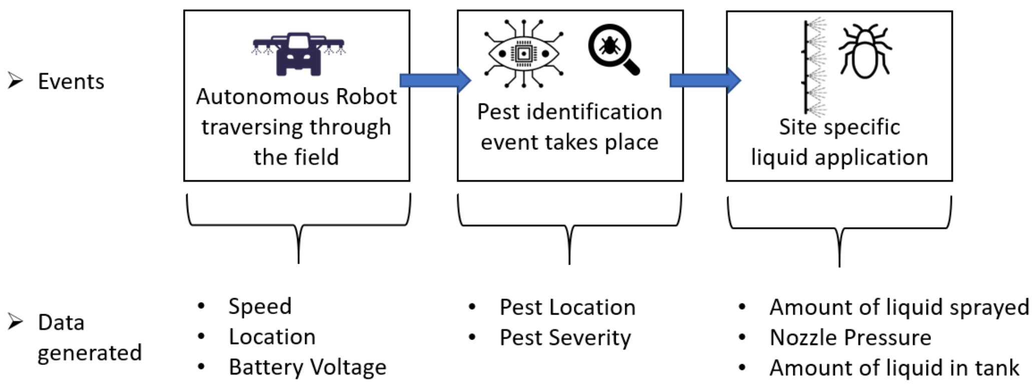

3.3.1.1 Subsystem Description

Each of the subsystems (Navigation, Computer Vision, Liquid Application) mounted on the autonomous rover platform was tested for its functionality and durability. The experiments included operating each of the subsystem to gauge its overall behavior in diverse environments and covering corner cases for identifying any failures that occurred during the experiments. The overall behavior of each subsystem is captured and sent to the central hub in the form of data packets.

3.3.1.1.1 Navigation System

The autonomous rover platform consists of a skid-steer navigation system that can turn inside the row crops without damaging the plants. The platform runs on the navigation2 ROS stack that enables it to traverse point-to-point in the dynamic field environment. Conditions can be challenging when the platform travels inside the field and at times can be devoid of getting strong positioning signals. Hence, to get a good estimate of the robot's current location a combination of GNSS module, camera, and IMU is utilized for seamless navigation through the dense crop rows.

3.3.1.1.2 Computer Vision System

The computer vision system was operated to detect the April tags as ‘aphids’ were not present while the experiment was conducted. April tags are visual representation identifiers used for various tasks like identification, robotics, and camera calibration. They are small and visually appear to be miniature versions of the QR codes used for various applications (Wang, J., & Olson, E. 2016). An example of April tags is shown below in Figure 3.3.

Figure 3.3. Representation of April Tag (https://april.eecs.umich.edu/software/apriltag)

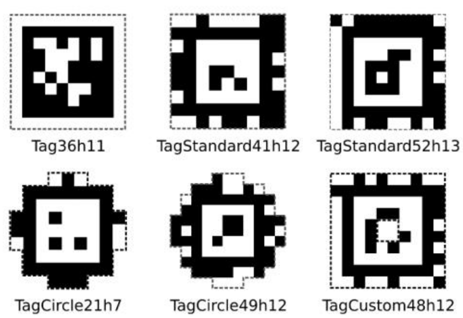

The two cameras were mounted on either side of the rover at the front of the autonomous platform at an angle to be able to view the maximum area of the plant. The ORIN served as the main computing platform for running the computer vision-based detection algorithm (https://github.com/NVIDIA-ISAAC-ROS/isaac_ros_apriltag). Since this system was tested when there were no plants available, the computing platform generated the random April Tag IDs as if it is actually detecting them in real-time. This was done to make sure the data generated will be a part of the data packets sent to the central hub.

3.3.1.1.3 Liquid Application System

The autonomous rover platform consists of a liquid application system to apply pesticide upon detecting pests called ‘aphids’ utilizing the response from the computer vision subsystem. The system consists of a 20-gallon tank with a pump and solenoid system used to transport the pesticide to the nozzles that spray at the pests. The liquid application system was controlled using an Electronic Control Unit (ECU) and driver along with an STM32 Microcontroller. The liquid application system also consists of booms that directly interact with the plants to spray at them.

The experiment conducted for collecting the data observed the pressure variations at different duty cycles as pressure variations impact the spray pattern. As the liquid application system is controlled using an ECU, the routing was established using Micro-ROS implemented on STM32 Microcontroller. The Pulse Width Modulation (PWM) signals were generated by the central computing unit ORIN and the information was logged also available in the form of ROS2 bags.

3.3.2 2x2 MIMO Wireless Digital Link

The 2x2 MIMO radio (pMDDL 2450, Microhard Corp, Calgary, Alberta, Canada) used in this experiment is a feature-rich digital data link with high-performance wireless capabilities in a rugged and compact module as shown in Figure 3.4. It operates in 2.4 GHz ISM band and provides capabilities such as high-speed wireless data communication of up to 25Mbps with adjustable high transmission power of up to 1W total. The unit can operate as a master, slave, or mesh node to establish robust long-range wireless links. The serial port is robust providing a baud rate of 230 kbps which enhances seamless integration with any subsystem and ensures flow of information using 128-bit AES encryption. The MIMO radio is mounted on the development board used to test and evaluate the operations. It provides multiple interfaces such as USB port, RS232 Serial Port, and Ethernet LAN and WAN port. It provides an easy interface for factory default settings and firmware recovery.

Figure 3.4. pMDDL 2450 module and development board

3.3.2.1 Ping Test

To assess the master and slave configuration intended for testing communication in between the autonomous platform and the central hub, both units were set up with the default settings provided by the manufacturer. Wireless RF configuration settings for a master is shown below in Figure 3.5.

Figure 3.5. Wireless configuration for the master radio

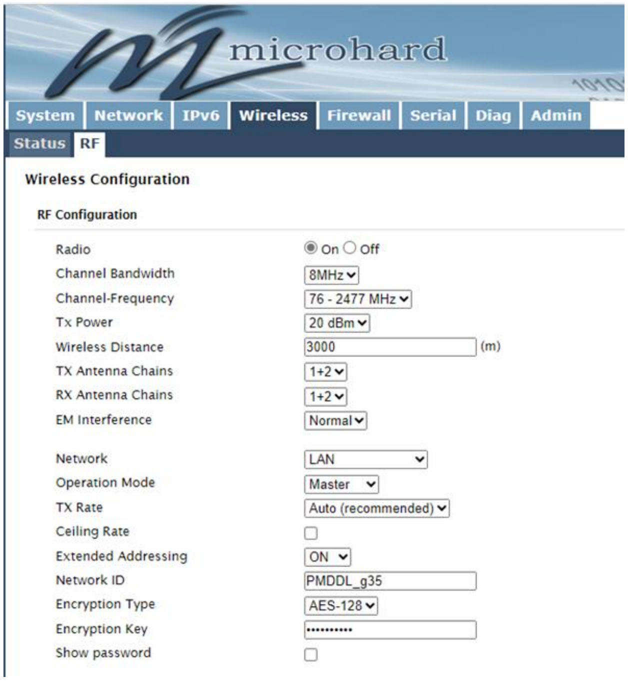

The radios were tested for end-to-end connectivity using the network tools ping feature provided by the manufacturer's web user interface. The following shows the data transmission and reception on both slave and master respectively. The master IP address for the master is 192.168.168.1 and for the slave is 192.168.169.12. Figure 3.6 illustrates the diagnostic test showing the communication between the slave and the master exchanging a specific number of pings and ping size.

Figure 3.6. Diagnostic testing of master & slave

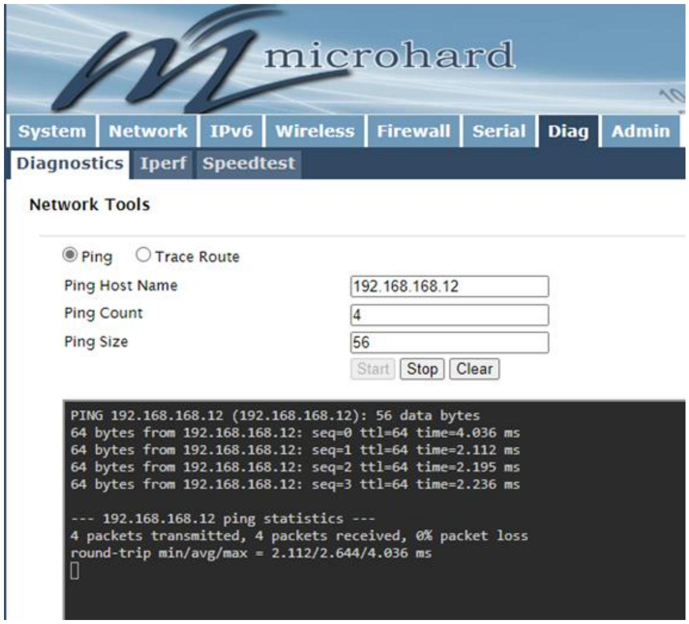

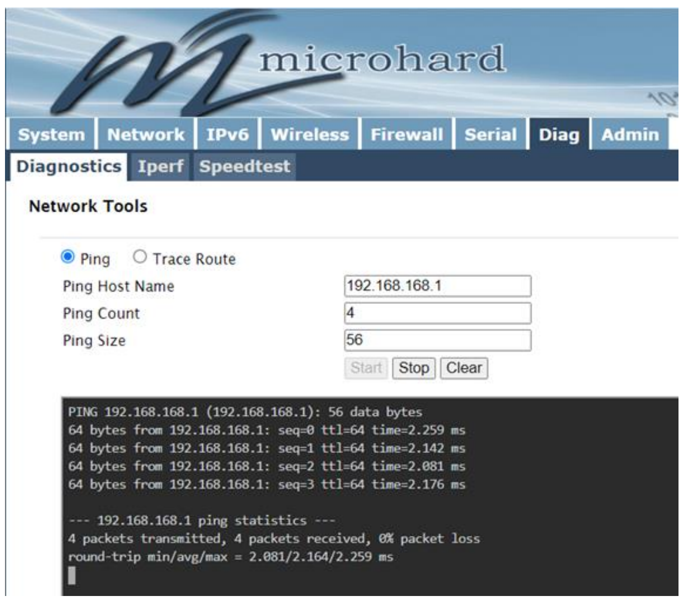

3.3.2.2 File Transfer Test

Figure 3.7 displays another way of communication between the Master and the Slave that was established by writing a simple Python program for serial communication. The Master was connected to a desktop to display the received file sent by the Slave connected to a laptop. On both ends, a simple Python script was utilized to send and receive a text file containing simulated information. This was to test whether the radios could transfer information in the form of text files other than using tools such as ping test.

Figure 3.7. Test setup for the file transfer test

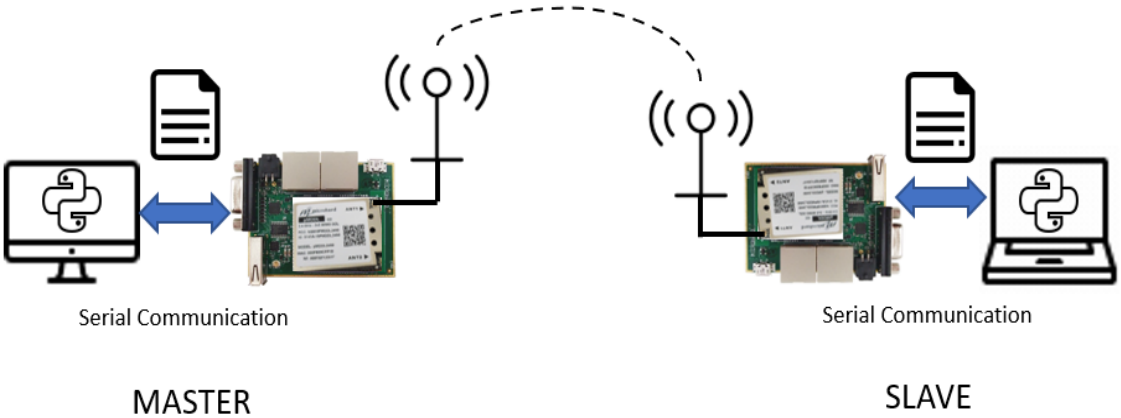

3.3.2.3 Radio Configurations

For the initial ping and file transfer test, the radios were operating in default configuration. For the on-ground experiment to be conducted for real-time system testing, there were three configurations tested to gauge the end-to-end data transfer. Following Table 3.1 consists of the description for various RF parameters in different configuration.

Table 3.1. Radio configuration for outdoor testing

Configuration	Feature	Value
Default	Channel Bandwidth	8 MHz
	Channel Frequency	2472 MHz
	Tx Power	20 dBm
	Wireless Distance	3000 m
	Tx Rate	Auto*
Config 2	Channel Bandwidth	4 MHz
	Channel Frequency	2410 MHz
	Tx Power	10 dBm
	Wireless Distance	1000 m
	Tx Rate	64-QAM 3/4
Config 3	Channel Bandwidth	8 MHz
	Channel Frequency	2443 MHz
	Tx Power	15 dBm
	Wireless Distance	2000 m
	Tx Rate	16-QAM 3/4

* When in 'Auto' the unit will transfer data at the highest possible rate in consideration of the receive signal strength (RSSI).

3.3.3 Robot Operation System 2 (ROS2) Middleware

As collaborative robotics platforms are becoming a norm for building intelligent systems, they differ in terms of their functionality from traditional methods since the challenges that they face are multifold in nature. The Robot Operating System (ROS), used as a platform to build intelligent robotics systems, provides various tools and operational capabilities, making these intelligent systems robust and cross-functional (Kapetanović, N., et al., 2021). The Robot Operating System (ROS) is a middleware that is installed on top of an actual operating system (usually Linux) for implementing complex robotic systems and applications (Macenski, S., et al., 2022). At a foundational level of the ROS2 framework, there are different independent nodes which are a piece of software program that communicates with each other using a publish-subscribe messaging platform as shown in Figure 3.8. For example, a GPS sensor node that is constantly updating the positioning information is publishing the latitude and longitude data for a particular topic. Another node which can be a simple data logger program can subscribe to this topic and record all the information. ROS is a middleware installed on top of an operating system, that abstracts all the hardware features of the host thus making it suitable to communicate with the other hardware environment.

Figure 3.8. ROS node illustration communicating messages through topics (https://docs.ros.org/en/humble/Tutorials/)

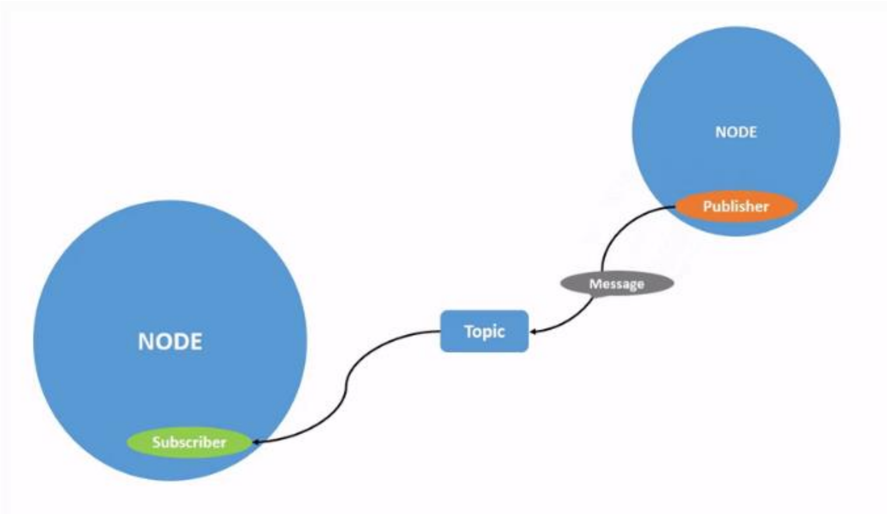

ROS2 is one of the most widely used ROS frameworks for its enhanced efficiency and reliability, low latency, and scalability. This is provided by Data Distribution Service (DDS) which is beneficial for implementing real-time systems where deterministic and low-latency communication is needed. In a ROS2 environment, data is stored in the rosbag format, offering enhanced flexibility for information serialization. A few basic building blocks of ROS middleware are discussed briefly.

3.3.3.1 Node

A node is an independent piece of code that helps in processing computations as well as subscribes to the topics to obtain information and publishes to the topics to provide information. The robotic system can have multiple nodes communicating with one another and collaborating to initiate multiple tasks. The nodes are communicating through topics as they do not interact with each other directly. Nodes can be written in C++ (roscpp) or Python (rclpy) programming languages depending on the library used. The node written in Python can communicate with a node written in C++, making it language agnostic.

3.3.3.2 Topic

Topics act as a communication medium between two nodes that are exchanging information. The topics make the nodes communicate using the publish and subscribe model. The publisher node sends information, and the subscriber node receives this information. The list of topics to which the node publishes can be obtained and then the subscriber node can choose from those topics to subscribe thereby acting as a bridge. The node may publish data to any number of topics as well as subscribe to any number of topics. At a time, multiple such nodes can interact with multiple other nodes through ROS topics as shown in following Figure 3.9.

Figure 3.9. Multiple nodes communicating with each other (https://docs.ros.org/en/humble/Tutorials/)

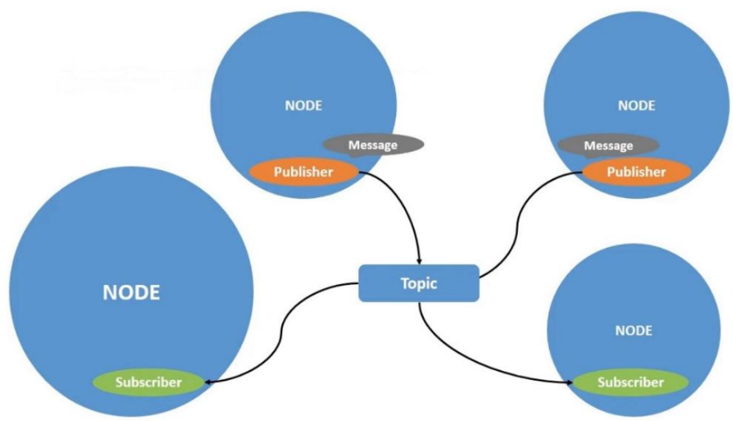

3.3.3.5 ROS2 Bag

ROS2 bag is a tool for recording the data published on different topics on the ROS2 system. It gathers the data passed on the topics and saves it in a database. The data can be replayed to reproduce the results of the tests or source it to another system ahead. The data formats available for storing ROS2 bag data are SQLite3 (.db3) or MCAP (.mcap). The MCAP format provides better corruption resilience. The ROS2 bag can be replayed also using Foxglove (San Francisco, California, USA) which is an interactive tool helping developers to record, visualize, and process their ROS2 MCAP file data format.

3.3.4 Radio & Platform Integration using ROS2

After testing the radio for its end-to-end connectivity using network ping tool and file transfer method, it was ready to be integrated with the autonomous rover platform which hosts different subsystems such as navigation, computer vision, and liquid application using ROS2 as shown in Figure 3.10. The ROS2 middleware framework binds all these subsystems together to operate in unison. A ROS2 node for serial communication was developed to subscribe to topics where nodes for different subsystems publish their data. Different subsystems publish data on different topics as they are designed to function independently, especially during the testing phase. Hence, each of the subscriber nodes developed to send data serially to the radio will be fetching information from different topics. There were two ways in which the serial data communication node was tested, 1) Simulating the data transfer behavior using ROS2 bags and 2) Testing the data transfer while operating the system in real time.

Figure 3.10. Radio communication and peripheral connection

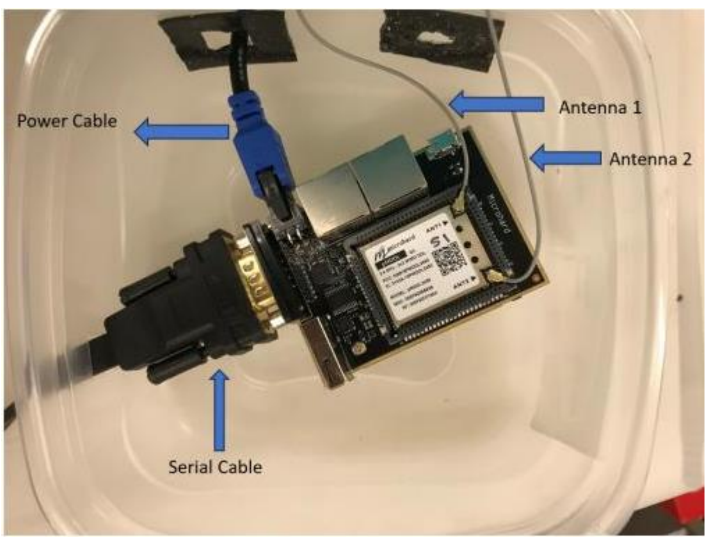

3.3.5 Data packet characteristics

The data packets from each subsystem were selectively collected to prioritize the delivery of essential information. The information from the navigation subsystem included latitude, longitude, and signal fix status to give constant signal estimation shown in Figure 3.12. From the computer vision system, the information about the April tags was gathered such as family of the April tag and its ID conveying detection station. The information from the liquid application system included pressure sensor information to gauge the rise and drop of pressure during operation and the liquid level in the spraying tank shown in Figure 3.11.

Figure 3.11. Example of data packet containing information from spraying system

```
Timestamp1710548084.3097854,Packet Count: 145,Pressure:82.7371463014221
Timestamp:1710548084.331263,Packet Count: 146,Tank_level:75
```

Figure 3.12. Example of data packet containing information from the navigation system

```
Timestamp: 1710550730.7456686, Latitude: 39.186962681666664, Longitude: -96.583894685, Altitude: 288.9189, Status: Fix Stat Based,
Timestamp: 1710550730.8409896, Latitude: 39.186962576666666, Longitude: -96.583895265, Altitude: 288.9905, Status: Fix Stat Based,
```

3.3.6 System Testing

3.3.6.1 Simulation using ROS2 Bags and RQT graph

Deploying the ROS2 nodes for serial communication directly on the autonomous platform for testing can lead to a possibility of breaking the existing functionality and take down the system. Therefore, they were first tested on data collected in the form of ROS2 bags derived by operating the individual subsystems. These ROS2 bags were generated when the system was tested for different features both in lab and field environment.

The ROS2 nodes, designed for serial communication, subscribed to the relevant topics where the data from ROS2 bags was published. Different ROS2 bags consisted of data from different subsystems. The RQT graph tool provided by the ROS2 environment helps in understanding how the communication between two nodes graphically looks like. It shows how nodes publish and subscribe to a particular topic for communicating information. RQT graph helps when the node structure is complicated and difficult to visualize. The ROS2 node dedicated to serial communication extracted latitude, longitude, and satellite fix information from the ROS2 bag sourced of the navigation system, April tag ID details from the computer vision ROS2 bag, and pressure data from the ROS2 bag of the liquid application system. The example in Figure 3.13 shows the RQT graphs of ROS2 bag obtained while testing the spraying system. The 'rosbag2_player' is the ROS2 bag played and the 'at_sprayer' is the subscriber node whereas the '/pressure_sensor0' and '/pressure_senosr1' are the topics to which the 'rosbag2_player' publishes and 'at_sprayer' subscribes to. The messages consist of pressure values that were recorded while testing the liquid application system.

Figure 3.13. Representation of ROS2 node dedicated for serial communication subscribing to a ROS2 bag

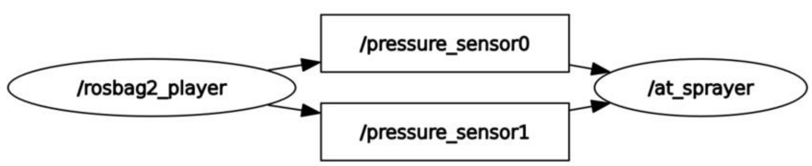

Once the ROS2 node for serial communication was tested for ROS2 bags, they were deployed on the robot for testing the communication in real-time. The node was integrated into the launch file alongside other nodes, and they were launched together when the rover was powered up for the operation.

3.3.6.2 On-ground Testing

The wireless data communication platform was tested in two diverse environments gauging the seamless and real-time information transfer. The two locations included 1) Football Stadium 2) Agricultural Field, both located on Kansas State University campus. The transmitting unit was installed on top of the autonomous rover platform connected with the ORIN using a serial to USB cable and was powered by a 11.1 V battery as shown in Figure 3.14. For the study conducted at the Football stadium, the autonomous rover platform was made to travel on the track thereby covering corners of the ground whereas for the agricultural field, it was made to travel straight, take a turn and comeback thereby traversing on an undulating terrain at a constant speed.

3.3.6.3 Experimental Setup

The following examples in Figure 3.15 shows how the central hub, installation of wireless communication system on the rover and the rover operation was setup on the agricultural field.

Figure 3.14. MIMO radio installed on the Rover Platform

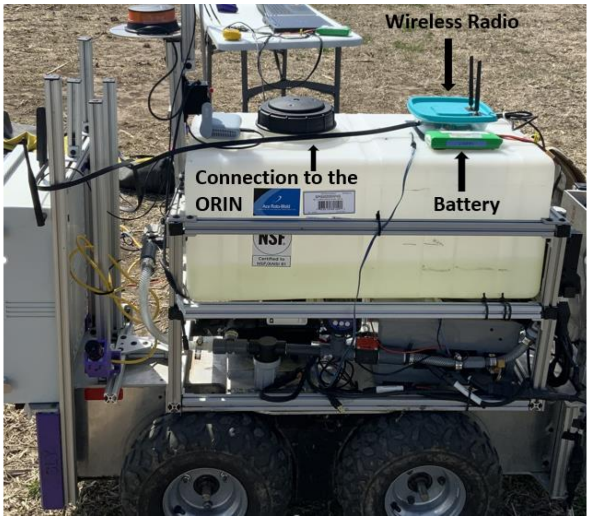

Figure 3.15. Central Hub setup & rover maneuvering in the field

A similar setup was done while testing the system on the football stadium as shown in Figure 3.16. The rover was moving across the edge of the field whereas the base station was setup at a stationary location. The rover maneuvered in a specific path so that it stays in continuous touch with the base station making sure it continuously transmits the information.

Figure 3.16. Rover maneuvering on track of the football stadium

The duration of the experiment for the outdoor tests was 5 Minutes for both the locations. The ROS2 node on the ORIN initiated the data transfer right after it was launched. The master was installed at the central hub which was a stationary location in direct line-of-sight with the autonomous rover platform. It was connected to a laptop which had a Python script running to visualize the incoming data packets and display the final calculations of different packet delivery statistics. There were two types of experiments conducted where it gathered different types of dataset. Firstly, the computer vision system and the liquid application system were tested. While they were operating, the information such as april tag id, pressure of the liquid application system, and tank level was continuously communicated. Secondly, the navigation system was tested and information such as latitude, longitude and type of satellite fix was continuosly communicated to the central hub.

3.4 Results & Discussion

3.4.1 Evaluation Metrics

For calculating the performance in the outdoor tests, three evaluation metrics were selected to gauge the performance of end-to-end data link.

3.4.1.1 Packet Delivery Ratio

The packet delivery ratio (PDR) is the metric to gauge the end-to-end packet delivery. To establish this metric for all the experiments that were carried out, the number of packets transferred and received were calculated. Using the following formula in Equation 3.1, the packet delivery ratio was obtained. The packets were timestamped and tagged with a packet count both upon transmission and reception. A comparison between the transmitted and the received packet number was done to ensure any packet loss.

Equation 3.1. Packet Delivery Ratio

$$Packet\ Delivery\ Ratio = \frac{Number\ of\ packets\ received}{Number\ of\ packets\ transmitted}$$

3.4.1.2 Packet Loss

Packet loss is determined by analyzing the number of packets that failed to reach their destination during transmission. This evaluation involves cross-referencing the transmitted packet count with the received count at the receiving end. An ongoing monitoring of packet numbers facilitates the identification of missing data packets, achieved by comparing counts between transmission and reception. At the end, while calculating the total packet loss, this number is used in Equation 3.2 to calculate the overall loss.

Equation 3.2. Packet loss

$$Packet\ loss = \frac{Number\ of\ packets\ lost}{Number\ of\ packets\ transmitted}$$

3.4.1.3 Latency

Latency refers to the time taken between the transmission of two consecutive data packets. To assess performance and detect discrepancies, this latency calculation is included within the data packet itself and sent alongside the data. At the receiving end, the latency calculation is also performed to evaluate receiver performance. While testing the system, a comparison is made between the latency observed during transmission and reception. This comparison is essential for testing purposes but may be omitted once the systems are confirmed to be synchronized. Equation 3.3. is used to calculate latency at both transmission as well as reception end.

Equation 3.3. Latency of the system

$$\text{Latency} = \text{Timestamp (current packet)} - \text{Timestamp (previous packet)}$$

3.4.2 Experimental Output

3.4.2.1 Football Stadium Experiment

Firstly, the data transmission for the liquid application and the computer vision system was tested for the three different configurations as shown in Table 3.2. The latency observed throughout the system is plotted in Figure 3.17.

Table 3.2. Packet Statistics for liquid application and computer vision system experiment

Configuration	Evaluation Metrics – (Experimental Duration: 5 Minutes)			
	Packet Statistics			Overall Latency (seconds)
	Delivery Ratio	Delivery (%)	Loss (%)	
Default	5468/5468 = 1	100	0	0.1 s
Config 2	6002/6005 = 0.9896	98.96	1.04	0.1 s
Config 3	5770/5771 = 0.9998	99.98	0.02	0.1 s

Figure 3.17. Latency Plots for liquid application and computer vision data collection in various configurations

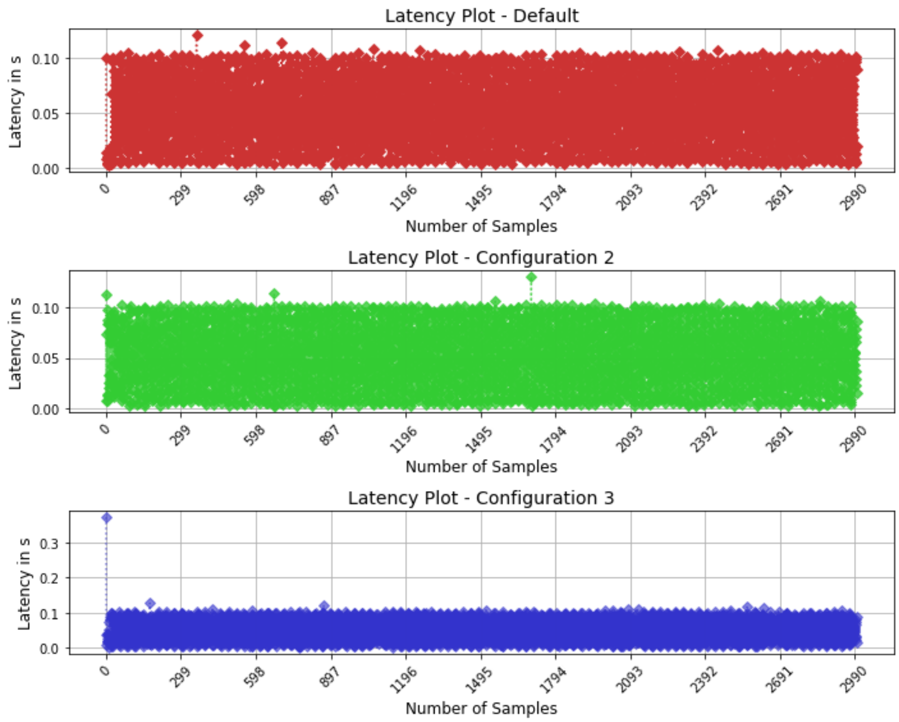

Config 2 gave a loss of 1% of information while testing the computer vision and the liquid application system compared to other configurations which resulted in a negligible loss. The config 2 was the least performing configuration amongst the three configurations, primarily because it had the lowest values selected for different parameters compared to the other two configurations. Config 2 had a channel bandwidth of 4 MHz, whereas the other two configurations had 8 MHz bandwidth. The Tx power was selected to be 10 dBm which was lower compared to the other two configuration and also the least distance of 1000 m was selected. Therefore, it was expected to give substandard performance compared to the rest of the configurations.

Table 3.3 and Figure 3.18 shows the performance of the data communication system and observed latency while testing for the navigation system.

Table 3.3. Packet Statistics for Navigation System experiment

Configuration	Evaluation Metrics – (Experimental Duration: 5 Minutes)			
	Packet Statistics			Overall Latency (seconds)
	Delivery Ratio	Delivery (%)	Loss (%)	
Default	3000/3000 = 1	100	0	0.1 s
Config 2	2528/2909 = 0.8690	86.90	13	0.1 s
Config 3	2948/2997 = 0.9837	98.37	1.63	0.1 s

Figure 3.18. Latency plots for navigation system data collection in various configurations

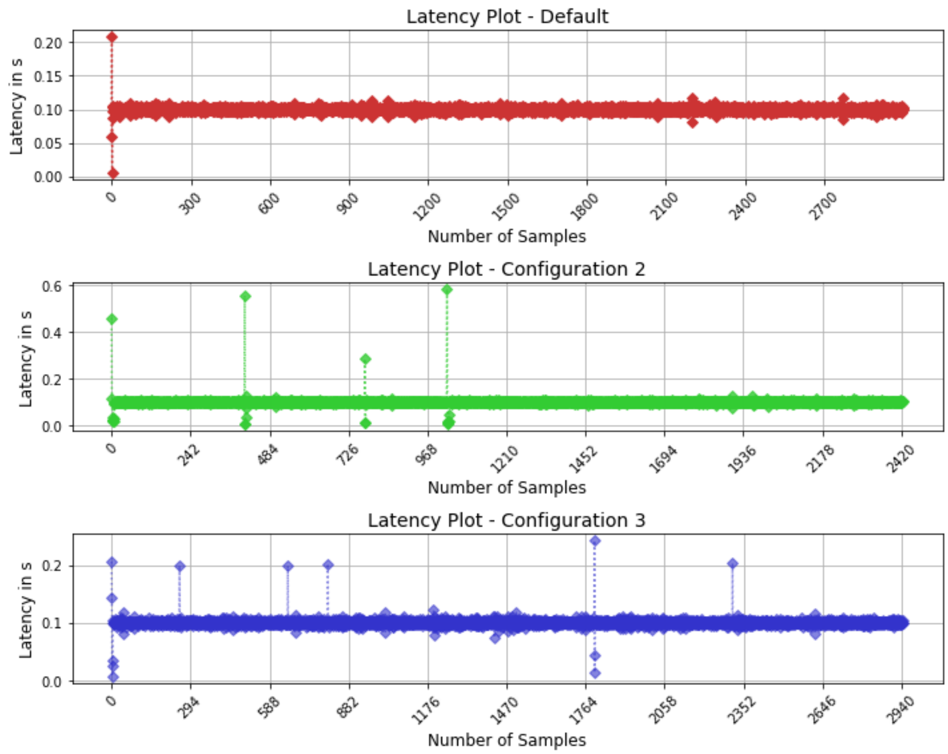

For the navigation system, it is evident that for config 2, the packet delivery is least i.e., 87 % and the packet loss is high i.e., almost 13% compared to the other two configuration.

The default configuration performed well in both the testing scenarios giving the highest packet delivery. For the default configuration, the transmission rate is selected automatically so that the transfer of information will be possible at the highest rate in consideration with the receive signal strength (RSSI). Therefore, for the optimum performance, it is recommended to set the transmission rate to auto. The channel bandwidth was 8 MHz, Tx power was 20 dBm, and wireless distance was 3000 m for the default configuration. For config 3, the performance was closer to the default configuration with channel bandwidth kept same as that of default configuration and the Tx power and wireless distance were 15dBm and 2000 m respectively. Both, the default configuration and configuration 3 produced a packet delivery ratio of 100 % and 98 % respectively with a loss of less than 2 % collectively.

The latency for all the configurations was almost constant during both the experiment trials. Except for the few fluctuations in between, it stayed constant and within the acceptable range of less than 0.1 seconds. The overall latency staying constant throughout ensures the system is unaffected by the unwanted fluctuations making it suitable to perform in dynamic environmental conditions.

3.4.2.2 For the Agricultural Field experiment

This experiment was conducted on an Agricultural Field located at Kansas State University, Animal Science Center. An area of the field was selected and flagged for the rover to maneuver during the experiment. Firstly, the data transmission for the liquid application and the computer vision system was tested for the three different configurations. The following Table 3.4 includes the evaluation metrics collected during the experiment. Also, the latency was calculated during the entire duration of data transmission as shown in Figure 3.19.

Table 3.4. Packet Statistics for the Computer Vision and Spraying System experiment

Configuration	Evaluation Metrics – (Experimental Duration: 5 Minutes)			
	Packet Statistics			Overall Latency (seconds)
	Delivery Ratio	Delivery (%)	Loss (%)	
Default	6038/6038 = 1	100	0	0.1 s
Config 2	5744/6016 = 0.9547	95.47	4.53	0.1 s
Config 3	5980/5981 = 0.9998	99.98	0.02	0.1 s

Figure 3.19. Latency Plots for Computer vision and Liquid application system data collection in various configurations

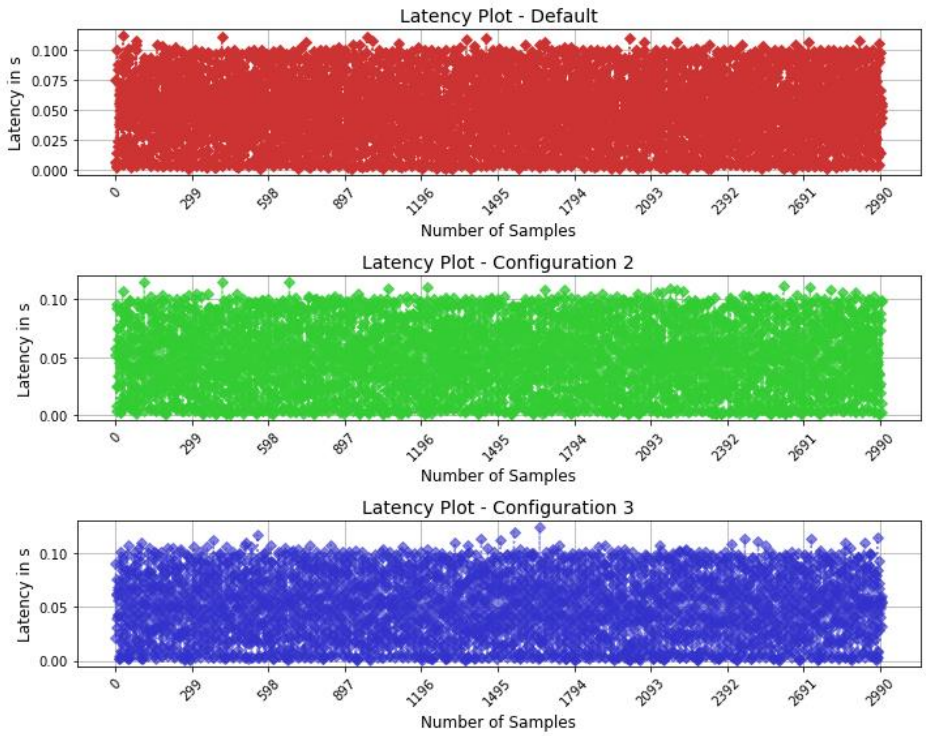

From the table, it is evident that the config 2 performed substandard compared to the default configuration and config 3. The packet delivery ratio for config 2 was 95 % leading to loss of almost 5 %. This is again due to the fact that the parameter values that were selected for configuration 2 were least in comparison to the other two configurations. The default configuration performed well by giving 100 % data transmission whereas configuration 3 gave close to 100 % by just losing a data packet throughout the entire transmission for config 3. The overall latency was constant around 0.1 seconds.

Table 3.5 and Figure 3.20 shows the performance of the data communication system and observed latency while testing for the navigation system in agriculture field environment.

Table 3.5. Packet Statistics for the Navigation System experiment

Configuration	Evaluation Metrics – (Experimental Duration: 5 Minutes)			
	Packet Statistics			Overall Latency (seconds)
	Delivery Ratio	Delivery (%)	Loss (%)	
Default	2608/2608 = 1	100	0	0.3 s
Config 2	2600/2628 = 0.9893	98.93	1.07	0.3 s
Config 3	2471/2472 = 0.9996	99.96	0.05	0.3 s

Figure 3.20. Latency plots for Navigation system data collection in various configurations

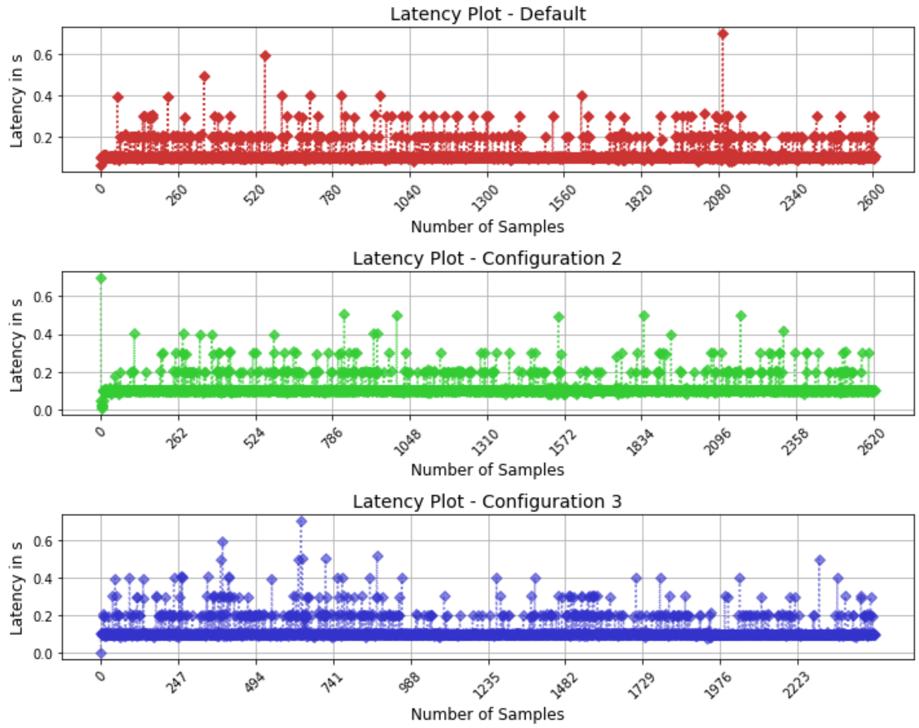

For the navigation experiment, again it was evident that the config 2 lost the most amount of information comparatively, resulting to a data loss of 1 %. The packet delivery for the default configuration and configuration 3 was 100 % only with losing a single data packet for config 3. Therefore, the most suitable configuration that could be opted for is default and configuration 3. The latency throughout all the experiment for all the configuration stayed constant between the range of 0.2 seconds to 0.4 seconds.

3.5 Conclusion & Future Work

In this study it was demonstrated from the experiments conducted and the results obtained that the wireless data communication system was able to provide a seamless data transfer platform for an autonomous farming application that included site-specific liquid application system. Firstly, the end-to-end transmission was tested on bench using the ping test and simple file transfer test. This testified that the radios are able to communicate the information end-to-end for the given configuration.

Further, the data communication system was made compatible with the autonomous platform using ROS2 middleware, which is the backbone for the functioning and operation of different subsystems on the autonomous platform. ROS2 node and topic, which are the building blocks of the middleware, were utilized in seamless and clean interfacing of wireless data communication system with the platform. The ROS2 node for serial communication was first tested with the wireless data transfer platform in a simulated environment using ROS2 bags. This was to ensure that while deploying ROS2 node on the actual platform does not break the existing infrastructure. After successfully testing with the ROS2 bags, the ROS2 node was installed on the platform which was taken outdoor for testing.

The data communication platform was configured for diverse configurations to gauge the overall performance for various factors such as operating frequency, transmission power, channel bandwidth, and operational distance. It underwent comprehensive testing to evaluate its capability in receiving diverse information from various systems, including liquid application, computer vision, and navigation. This included data such as pressure and tank levels, April tag IDs, and location information. Upon testing, the wireless data communication platform performed in line with the specific configuration it was operated under and delivering respective performance.

All the configuration performed well except for config 2 which comparatively gave a substandard performance. For the experiment conducted on the football stadium, it gave a comparatively lower accuracy where it lost a couple of packets while testing the computer vision and the liquid application system operation. Its performance deprecated while testing the navigation system where the packet delivery obtained was 86.90% producing a loss of 13.1%. Whereas, the default and the configuration 3 performed well giving minimum data loss of less than 2% and giving maximum packet delivery of 98% and above for all the subsystem operations. The default configuration can be suggested as the configuration to be selected for implementing the system due to its high packet delivery ratio, low loss, and stable latency. The latency of the data communication platform stayed constant around 0.1 seconds throughout all the configuration except for a few minor fluctuations. This was observed in both while testing the computer-vision and the liquid application system as well as navigation system. Therefore, the system could be deployed in dynamic field conditions with less possibility of being affected by external factors.

For the agricultural field experiment, it was again observed that config 2 comparatively performed inadequate by giving a loss of 4.5 % while testing the computer vision and the liquid application system which is highest amongst all the configurations tested. The packet delivery for the default and config 3 was close to 100 % thereby ensuring end-to-end packet transfer with minimum to no loss throughout testing all the subsystems. Also, the latency of the data communication platform was observed to be stable between 0.2 to 0.4 seconds while testing all the configuration for both the sets of experiments.

This implies the communication platform can sustain in outdoor environment ensuring minimum latency for seamless end-to-end real-time transfer of information. Also, conducting experiments for testing the subsystems in two diverse environments proved the ability of the wireless data communication platform in terms of establishing long range communications and operating in undulated terrain environment testing for its line-of-sight ability. The default configuration and config 3 can be suggested as the configuration to be selected for implementing this system due to its high packet delivery ratio, low loss, and stable latency. Therefore, the system could be successfully deployed in dynamic field conditions for seamless data transfer of the operational and system information from an autonomous farming platform. The substandard performance of the config 2 was due to the parameter values that were selected. Comparatively, the values selected for the channel bandwidth and frequency, TX power, and wireless distance for config 2 were lesser than that of default config and config 3.

Going ahead, the wireless data communication platform would be tested for multiple autonomous system where it would be configured to receive information from more than one autonomous platform. Also, after the planting season starts and the growth of the crops is observed, it would be made to maneuver inside the crop canopy for testing its ability to transfer information through the dense and dynamic environment. There would be changes incurred with respect to the physical and operational aspects such as placement of antennas and alteration in the configurable properties of the data communication platform which would make it robust to overcome challenges the dense environment has to offer while receiving information from multiple platforms.

Chapter 4 - Improving the image triggering and geotagging accuracy using RTK-enabled GNSS solution for UAV remote-sensing applications

4.1 Abstract

Image triggering and geotagging are prominent aspects of Unmanned Aerial Vehicle (UAV) imagery data collection while they are utilized for monitoring and assessing crop health. Typically, Unmanned Aerial Systems (UAS) are equipped with an array of onboard peripheral systems, including image triggering mechanism for activating image sensors collecting imagery data & a geotagging system that couples location information to the imagery data essential for post processing especially during image stitching and photo-merging. These geotagging systems typically incorporate a Global Position System (GPS) module along with the autopilot controller that assists in geotagging positional meta-data to the imagery collected. However, the accuracy of these onboard positioning systems can sometimes be compromised due to reliance on GPS, which provides accuracy in few meters making it unsuitable for specific Precision Agriculture (PA) applications. Moreover, the limited functionality of these different modules may restrict their applicability for multiple tasks, potentially necessitating the addition of more peripherals, thereby increasing the payload of the flight. To address this challenge, a lightweight and platform-independent GNSS solution was developed that facilitates a quick & efficient way of triggering and geotagging images using a fixed-wing UAV flight over cropland. This GNSS solution includes a Printed Circuit Board (PCB) consisting of an optocoupler-based circuit enabling image triggering for any consumer-grade RGB camera installed on the UAV. The image-triggering feature employs a distance-based calculation algorithm executed onboard with the assistance of a dual-frequency

226-channel Global navigation satellite system (GNSS) module. Secondly, the GNSS solution replaces the existing GPS-based geotagging workflow used for Thermal InfraRed (TIR) imagery with a more accurate method, enhancing the precision of geotagging metadata captured alongside the images. Unlike the previous mechanism reliant on National Marine Electronics Association (NMEA) strings generated by the GPS module, the new approach utilizes strings from the GNSS module, offering a higher level of accuracy through Real Time Kinematics (RTK). Test flights were conducted to gauge the image-triggering feature by taking consistent images using the consumer-grade RGB camera. The setup was successfully able to capture images at every 20 and 30 meters of distance traveled by the UAV platform at an altitude of 20 and 30 m respectively. During the 20 m flight, the RTK-enabled imagery closely matched the ground reference points within a range of approximately 0.36 to 3.48 meters, while for the 30 m flight, it ranged in between 0.37 to 3.6 meters with the ground reference points. In both the cases, 80% of the points were successfully RTK-geotagged. Furthermore, a comparative study was conducted to test the thermal imagery geotagging accuracy between the data obtained from standalone and RTK-enabled flights using the GNSS solution and the ground control points. The results indicated that 86% of total points were RTK-geotagged for 50 m flight aligning within a range of 0.7 to 3 meters from the ground reference points while for the 80 m flight, 93 % of the total points were RTK-geotagged within the range of 0.6 to 2.75 from the ground reference points thereby contributing towards precise geotagging and positioning objective.

4.2 Introduction

Remote sensing is one of the most prominent technologies adopted for smart farming and Precision Agriculture (PA) applications given the features that it offers such as non-invasiveness, less labor intensive, and providing spatial variability for conducting intense crop trait analysis (Berger et al., 2020). Different ways of utilizing remote sensing methodologies such as satellites, aircraft, and Unmanned Aerial Vehicles (UAVs) have led to the systematic collection of information at varying degrees depending upon the resolution required as per the user (Khanal, S. et al., 2020, Gadhwal, M. et al., 2023). UAVs are a popular and prominent way of collecting imagery data for conducting crop health monitoring (Gadhwal, M. et al., 2023). It is one of the sought-after choices due to its fast data acquisition and ease of implementation providing high spatial resolution from the flights taken at low altitudes (Tsouros, D. C. et al., 2019). UAVs find their way in different applications, one of which is PA where information is collected using imaging system equipped with different sensors and acquisition units. As the PA applications become more intense, such as managing and collecting minute information at the plant-to-plant level, it is also important for the data acquisition systems on the UAVs to become precise in their abilities to avoid any intricacies in the information gathered. Global Position System (GPS) is the building block technology for UAV navigation and localization as well as geotagging information while they operate in diverse environments. While utilizing Unmanned Aerial Systems (UAS) for collecting imagery data, it is accompanied with an image geotagging mechanism that consists of GPS. The GPS assists the geotagging mechanism to add a geo meta-data as a reference when the imagery information is collected (Lum, C. et al., 2016). The GPS system provides accuracy of information in meters which in case can lead to a sub-standard performance and other problems if used for a specific PA application requiring higher precision. Also, the limited number of satellites available can further affect the PA application giving a lesser precise geo-location estimation information.

A more equipped localization system, Global navigation satellite system (GNSS), includes multiple satellite constellations such as Galileo from the EU, BeiDou from China, GLONASS from Russia, and GPS from North America thereby making it powerful for localization and positioning applications. The positioning accuracy is achieved by using a method called ‘trilateration’ where the location is accurately determined by measuring the distance to four or more satellites (Perez-Ruiz, M. et al., 2021). Using GNSS for precision agriculture is becoming a norm as the requirement for precise information has been growing for zone and plant-level management of the cultivated crop (Hasheminasab, S. M., Zhou et al., 2020). It is more suitable to use a UAV equipped with GNSS to achieve greater precision over the target location to conduct PA applications. To equip the GNSS systems further, Real Time Kinematics (RTK) technology is used to improve the accuracy of the GNSS positioning. While positioning itself, the GNSS receivers measure the time it takes for a signal to travel from the satellite that it communicates with. This signal travels through the atmosphere and other layers leading to slowing down on the way. Using RTK corrections, the accuracy of GNSS can be brought down closer to the centimeter level. There are ways of achieving the RTK correction signal, such as fixed-based station and Networked Transport of RTCM via Internet Protocol (NTRIP). In the case of a fixed base, a base station with known coordinates sends correction signals to the GNSS receiver (Pini, M. et al., 2018) while it continuously communicates with the satellites. Statistical methods are utilized to adjust the phase of the signals and improve the positional accuracy to centimeters. Whereas, NTRIP uses a stable internet connection with the help of a subscription to a local NTRIP service provider that has a fixed base in place for a large network at a regional or national level. The service provider for the NTRIP can then calculate the correction information from the base station and feed it to the GNSS receiver that has a NTRIP receiver. NTRIP is useful since it utilizes already deployed base stations and has no range limits. However, if the network signals are poor or NTRIP service providers are not available, the fixed base station is a must (Ng, K. M. et al., 2018).

Therefore, it is necessary to ensure the imagery data collected using UAS platforms is precisely captured as well as geotagged using location information consisting of maximum accuracy. To do so, a GNSS solution with such capabilities is required to equip the UAS platforms, especially collecting information for diverse remote sensing applications. There are a few examples available that utilizes single-frequency GPS (Daakir, M. et al., 2017, Nikolakopoulos, K. G. et al., 2015) but a compromise in terms of accuracy is made that affects the desired outcome. Some applications use different platforms for different purposes which ultimately leads to an increase in the payload of the unmanned vehicle. This drastically affects the operational time for which the unmanned vehicle operates (Velusamy, P. et al., 2021).

Capturing aerial images and geotagging are the two most important aspects of UAV data collection and should not be compromised to get the best out of the PA applications. Hence the following study targets these two aspects of PA remote sensing applications and exemplifies the ability of a single custom-made GNSS-solution to provide the following features

1. Optocoupler based camera trigger mechanism for consumer-grade RGB camera utilizing distance calculation assisted by RTK-enabled GNSS receiver.
2. Revised image geotagging workflow replacing the conventional GPS based geotagging to an RTK-enabled geotagging for TIR imagery system.

A single, purpose-designed GNSS-solution offers both capabilities, reducing reliance on disparate components for various tasks by providing all necessary features within one integrated system.

4.3 Materials & Methods

4.3.1 System Design

The following block diagram in Figure 4.1 explains how different components are tied together to develop an independent GNSS solution for the 1) Image triggering and 2) Image geotagging objective. Figure 4.2 shows the front and the back side of the PCB of the GNSS solution.

Figure 4.1. Major components present on GNSS solution contributing to serve image triggering and image geotagging mechanism

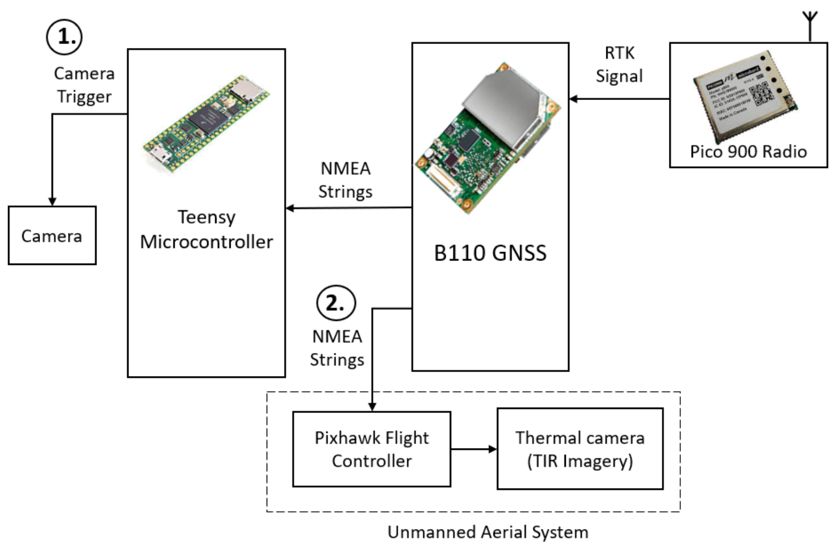

Figure 4.2. GNSS Solution Printed Circuit Board

The GNSS solution developed consists of 3 important components a) A B110 GNSS Board (Topcon, CA, USA), b) A P900 miniature 900 MHz license-free spectrum wireless radio (Microhard, Calgary, Alberta, Canada) c) A Teensy Microcontroller (PJRC, OR USA). The GNSS solution measures 199mm x 194mm x 24mm in dimension, approximately 100 grams in weight and is powered by a 3.3 V Lithium-Ion battery. A lightweight and compact solution which can be easily installed on robust platforms.

4.3.1.1 Topcon B110 GNSS Receiver module

The B110 GNSS receiver module shown in Figure 4.3 provides a sub-meter positioning accuracy while working as a standalone unit whereas if enabled with the RTK, it feeds a centimeter level of positioning accuracy. The ability to receive and process signals from different satellite constellations such as GPS (USA), GLONASS (Russia), and Galileo (Europe) with 224 channels makes the receiver one of the most powerful and sought-after options for positioning and localization applications. The receiver's ability to utilize RTK signals to enhance its accuracy makes it suitable for applications that require zone-level precision such as remote sensing. Studies have shown how using a GNSS receiver for their PA applications has been proven to improve the overall output (Andanaputra, A. B. T. et al., 2020). This will be utilized to generate precise location information for geotagging the images taken by the thermal image sensing system and trigger consumer-grade RGB camera as intended in this study.

Figure 4.3. Topcon B110 GNSS Module

4.3.1.2 Microhard P900 miniature wireless radio

The P900 radio modem shown in Figure 4.4 is used to source the RTK signals to the B110 thereby improving its efficiency to a centimeter level. The radio works in a license-free spectrum band within the 902-928 MHz ISM frequency band. The radio can operate in MESH, point-to-point, and point-to-multipoint topologies. The radio serves an extensive range of 40 miles (approximately 60 Km) line of sight with a maximum data transfer rate of 276 kbps. The radio is available in a small footprint with a power consumption of less than 1 W. The wide range and rugged design of the radio makes it suitable for extensive applications such as precision agriculture.

Figure 4.4. Pico 900 Radio

4.3.1.3 Teensy Microcontroller

Teensy microcontroller is a complete USB-based microcontroller development unit with a small footprint as shown in Figure 4.5 and capable of handling diverse applications. It is a 32-bit controller capable of performing fast operations with multiple input/output making it suitable for integrating into applications catering multiple peripherals. It can be easily configured using Arduino software and libraries with the help of 'Teensyduino' add-on software. It is compatible with the most widely used operating systems available making it ubiquitous and platform agnostic. Due to multiple I/O pins and the functionality of the SD card storage option, it is able to bind multiple independent platforms and provide different functionalities. The camera trigger software functionality would be implemented on the Teensy microcontroller after it receives the precise localization information from the B110 module. Also, the log files generated for the image geotagging process would be saved on the SD card of the microcontroller in a text file format.

Figure 4.5. Teensy 4.1 Microcontroller

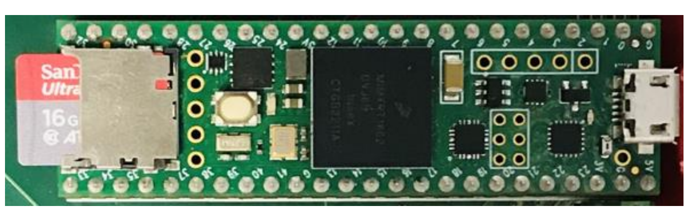

4.3.1.4 RTK Setup

The GNSS solution comprises of a host radio that feeds the onboard GNSS module with the RTK correction signals thereby improving its positional accuracy. In order to achieve this, a setup is used which involves of a base station installed at a stationary location in the desired experimental area as shown in Figure 4.6. This base station (GR5, Topcon, Tokyo, Japan) incorporates a GNSS module through which it communicates with the satellites and obtains its position. The base station is equipped with a serial port and it is configured to output the RTK error-correction signals. This port is connected to an input of a long-range radio in the transmitter configuration. The base station is ready to feed the RTK correction signals to the GNSS module. Next, the radio on the GNSS solution which is in the receiver configuration receives these RTK correction signals and feeds it to the B110 GNSS module for correcting the location information.

Figure 4.6. Base Station & Radio setup for RTK

4.3.1.4.1 Radio Configuration

In order to be able to communicate, the transmitting and the receiving radios are configured in a master and remote configuration fulfilling the requirement for the RTK setup. The radios are configured using AT commands through serial terminal program called HyperTerminal. The radio connected to the base station is in the transmitting mode sending RTK correction signals whereas the radio on the GNSS solution is in the receiving mode. The baud rate is set to 230400 bps and the wireless link rate is 172800 bps. The output power is set to 1 W and the maximum packet size is 256 bytes. The serial channel mode for the both is set to RS232 and the repeat interval is set to 3 to avoid engaging the network for a longer time. The Reed-Solomon forward error correction technique is selected in order to establish long range communication without corrupting the information. Also, other properties like Network ID, Hop Zone, and Hop Pattern are kept same so that the synchronization between the radios holds throughout the communication duration.

4.3.1.5 NMEA Strings

The B110 GNSS module on the GNSS solution generates continuous location information which is corrected by the RTK correction signals fed by the P900 radio. The location information is in the form of National Marine Electronics Association (NMEA) strings/sentences that contain information such as latitude, longitude, and other attributes. For example, the most widely used NMEA string is GPGGA (fixed data providing 3D location and accuracy data). The RTK signal uses Radio Technical Commission for Maritime (RTCM3) type message protocol consisting of differential corrections data for rectifying the location information.

NMEA strings are standard sentences available to interpret the location information. They have been used in all the localization units that are utilized for geolocating any entity on the earth.

The following is an example of a GPGGA NMEA string and its explanation can be found in Table 4.1.

*$GPGGA,211114.90,3911.5194488, N,09634.9578875, W,1,07,4.62,332.3086, M, -28.0701, M, ,*n*

Table 4.1. Description of NMEA Strings

Placeholder	Description
GP	Represents the constellation of the satellite i.e., GPS. It will be GL for GLONASS
211114.90	Time stamp following UTC (Co-ordinated Universal time) in hours, minutes, and seconds.
3911.5194488	Latitude in the DDMM.MMMMM format. Decimal places vary as per requirement.
N	Denotes north latitude
09634.9578875	Longitude in the DDDMM.MMMMM format. Decimal places vary as per requirement.
W	Denotes west longitude.
1	Indicator for the quality of the signal: 1 = Uncorrected coordinate 2 = Differentially correct coordinate (e.g., WAAS, DGPS) 4 = RTK Fix coordinate (centimeter precision) 5 = RTK Float (decimeter precision)
07	Number of satellites used in the coordinate.
4.62	Denotes the HDOP (horizontal dilution of precision).
332.3086	Denotes altitude of the antenna.
M	Denotes units of altitude (i.e., Meters or Feet)
28.0701	Denotes the geoidal separation (subtract this from the altitude of the antenna to arrive at the Height Above Ellipsoid (HAE).
M	Denotes the units used by the geoidal separation.
1.0	Denotes the age of the correction (if any).
0000	Denotes the correction station ID (if any).
*n	Denotes the checksum and is a hexadecimal value.

4.3.2 UAV Platform

A quad-rotor platform (Matrice 100, Shenzhen DJI Sciences and Technologies Ltd.) was selected as a UAV platform on which the GNSS solution was installed as shown in Figure 4.7. Since the GNSS solution is a lightweight platform, it did not affect the operational time and efficiency of the flight during regular operations. The flight planning was done using Mission Planner software where a fixed route of waypoints was designed.

Figure 4.7. Matrice 100 Quad-Rotor Platform

4.3.3 Image Triggering for RGB Camera

4.3.3.1 Image Triggering Unit

A schematic representation of the image triggering unit is shown in Figure 4.8 for better clarity. The output of the image triggering unit implemented on the GNSS solution is routed to a general-purpose 3-pin UART (Universal asynchronous receiver-transmitter) Port called TRIGGERPORT. The trigger signal generated on the Teensy microcontroller is directed to the input of a 4-pin optocoupler unit (part no. PC817X4NSZ1B Transistor Output Optocouplers). The output of the optocoupler unit is then connected to the TX of the TRIGGERPORT whereas the RX and ground are tied together and terminated to the ground.

Figure 4.8. Schematic representation of the image trigger mechanism

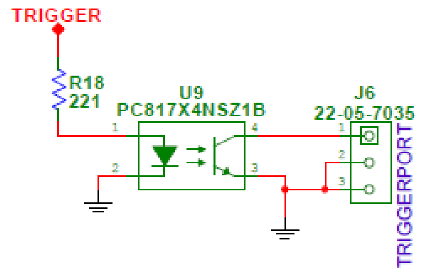

4.3.3.1.1 Distance based image triggering algorithm

The distance-based image triggering algorithm is the backbone of the image triggering mechanism, ensuring timely generation of the TRIGGER signal sent to the image triggering circuit. The algorithm is implemented using a haversine formula which is widely used to calculate the distance between the two points on the earth (Nugroho, A. P. et al., 2019). The formulas shown in Equation 4.1 are collectively used to calculate the distance thereby generating timely trigger signals for the camera to capture images.

Equation 4.1. Calculation of Haversine distance

$$a = \sin^2\left(\frac{\varphi B - \varphi A}{2}\right) + \cos\varphi A * \cos\varphi B * \sin^2\left(\frac{\lambda B - \lambda A}{2}\right) \quad (1)$$

$$c = 2 * \operatorname{atan2}(\sqrt{a}, \sqrt{(1-a)}) \quad (2)$$

$$d = R \cdot c \quad (3)$$

The equation (1) calculating ‘a’ consists of φB and φA which are the latitudes of points B and A respectively whereas λB and λA are the longitudes of points B and A respectively in radians. The half of the difference between the latitude are used with the first sine^2 term whereas the half of the difference between the longitudes are used with the second sine^2 term respectively. Point B and A are the between whom the distance ‘d’ is required to be calculated. Equation (2) consists of calculating ‘tan’ of ‘a’ along with other terms. Lastly, equation (3) uses ‘c’ with the radius of the earth, R = 6371000 meters or 6371 km. The pseudo code calculation of haversine distance is shown in Figure 4.9.

Figure 4.9. Pseudo code for calculating the distance between two points

Algorithm 1 Calculate Distance using Haversine Formula

Inputs: Latitude and longitude of two points, lat_1, lon_1, lat_2, lon_2
Output: Distance d between the two points
$\Delta\phi \leftarrow \frac{\pi}{180} \cdot (lat_2 - lat_1)$
$\Delta\lambda \leftarrow \frac{\pi}{180} \cdot (lon_2 - lon_1)$
$a \leftarrow \sin^2(\Delta\phi/2) + \cos(lat_1) \cdot \cos(lat_2) \cdot \sin^2(\Delta\lambda/2)$
$c \leftarrow 2 \cdot \text{atan2}(\sqrt{a}, \sqrt{1-a})$
$d \leftarrow R \cdot c$, where R is the radius of the Earth
Return d

4.3.3.3 System Integration

The imaging system shown in Figure 4.10 consisted of a Sony α 5100 camera (Sony, Minato City, Tokyo, Japan) that was triggered by the GNSS solution using a UART to USB connector. The UART port has 3 connections out of which signals at pin 2 and 3 are grounded and signal at pin 1 goes to the camera input as a trigger. The GNSS solution enclosed in a 3-D printed case is installed on top of the UAV platform and tightly harnessed. The GNSS solution is powered by a 3.3 V Lithium-Ion battery which serves as a power source.

Figure 4.10. Integration of Sony camera, GNSS solution with the UAV platform

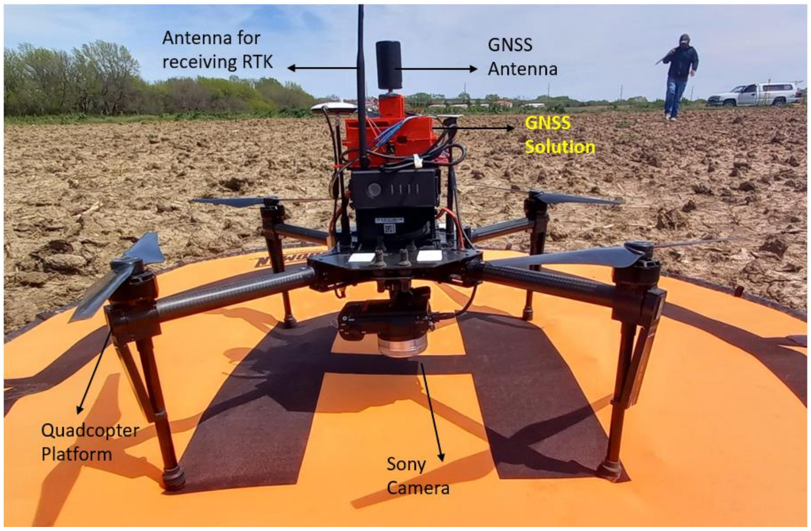

4.3.3.4 Experimental Site & Setup

In order to ensure the functionality of the image triggering mechanism as per the requirement, a preliminary experiment was conducted ensuring the camera captures images at regular distance interval. The experiment was conducted on the Animal Science Farm location on Kansas State University Campus. The experimental setup consisted of an agricultural field where the Ground Control Points (GCP) were placed as a reference points or markers. Figure 4.11 shows the recording of geolocation information and measuring distance in between markers. Initially, for the mission at 20 meters altitude flight, they were positioned 20 meters apart, later adjusted to 30 meters for the 30-meter altitude flight. The precise coordinates of these ground control points were obtained using the GR5, an RTK-enabled GNSS surveying tool, serving as the ground truth during data processing. The image triggering mechanism was set to capture images every time the UAV travels a distance of 20 and 30 meters during the respective flights. The distance trigger information corresponding to the respective trigger events would be stored in a log file to be compared with the ground truth information.

Figure 4.11. Recording geolocation of the GCP and measuring distance between each GCP

The GNSS solution will record the trigger distance of every image captured in a log file. Whenever the distance-based camera trigger mechanism is activated, the distance calculation algorithm will make a note of the distance information of every captured location. Hence, every time an image is recorded, the distance information corresponding to that image will be recorded in a log file. Also, every time a haversine distance is calculated, it was saved in the log file. This functionality will ensure two objectives, 1) A log file containing the distance information of each captured image is utilized for comparison with the surveyed ground locations of the GCP, confirming the successful implementation of the distance-based camera trigger mechanism 2) The haversine distance log will ensure a constant distance trigger mechanism was consistent throughout the process. The experiment was conducted while the GNSS solution is in standalone mode as well as in RTK-enabled mode to gauge how much of a difference does it make with respect to the distance information recorded to be compared with the original ground surveyed points. The details regarding the flight are mentioned in the Table 4.2.

Table 4.2. UAV flight details for image triggering experiment

Date	Number of GCP	Altitude of the Flights	Camera Trigger interval
04/23/24	12 (only for reference)	20 m,30 m	20m, 30 m

The GNSS solution is first operated in RTK enabled mode while it receives the RTK correction signals from the base station setup. After rectifying its position, the camera trigger mechanism calculates the distance travelled and when it meets the distance trigger threshold, the camera is activated to capture the image. While in standalone mode, the GNSS solution is devoid of the RTK correction signals. Here the GNSS solution will generate NMEA strings based on its coverage to the satellites without adding any RTK corrections and utilize it in the distance trigger mechanism to further activate the camera. The following Figure 4.12 shows the status of the GNSS module captured before the both the type flights.

Figure 4.12. Status of GNSS module during the a) RTK-enabled flight b) Standalone flight

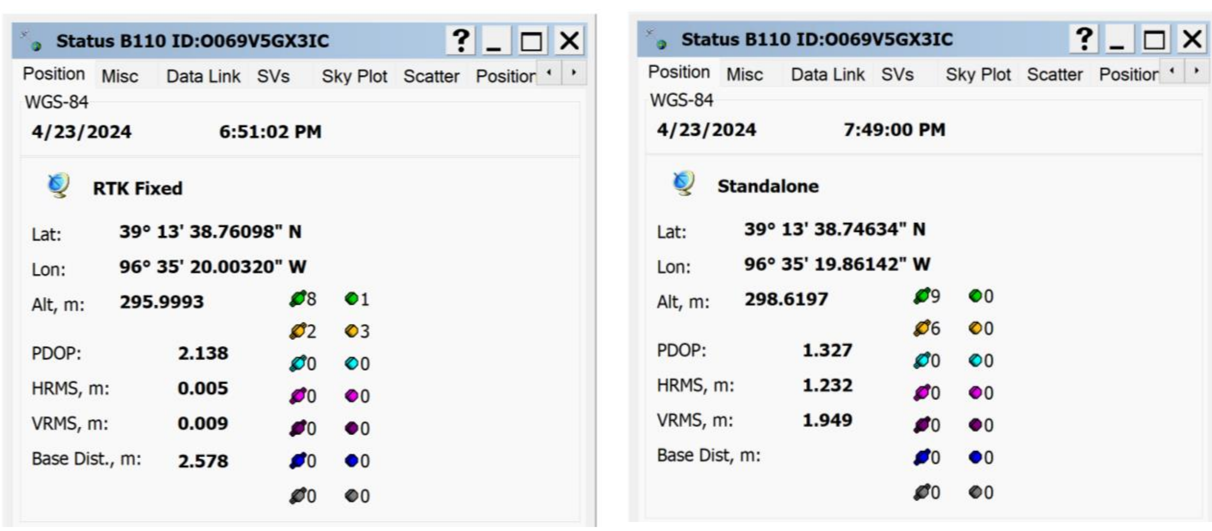

(a) (b)

The goal is to observe whether there is a significant difference in the image triggering events and information gathered while the GNSS solution receives the RTK correction signals and compare it while operating in standalone mode.

4.3.4 Image Geotagging for Thermal Imaging system

The required NMEA strings were initially observed in a lab setting which met the criteria of the flight controller for successfully integrating it with the thermal imagery system as shown in Figure 4.13. The requirement of the flight controller included different types of NMEA strings such as GPGSA (GPS dilution of precision and active satellites), GPGLL (Geographic Latitude and Longitude), GPGGA (Overall Satellite data), GPGSV (Detailed Satellite data), GPRMS (recommended minimum data for GPS), and GPVTG (Vector track and Speed over the Ground) as shown below. Once the required NMEA strings were identified, the B110 GNSS module on the GNSS solution was configured to output those strings.

Figure 4.13. Representation of NMEA Strings

```
14:55:18.773 -> $GPGGA,205520.00,3911.41446,N,09634.96285,W,2,11,0.95,340.3,M,-27.5,M,,0000*69
14:55:18.849 -> $GPGSA,A,3,04,07,08,30,51,14,21,46,09,27,01,,1.86,0.95,1.60*03
14:55:18.932 -> $GPGSV,4,1,13,01,07,144,33,04,11,168,31,07,78,351,44,08,55,063,45*73
14:55:19.015 -> $GPGSV,4,2,13,09,37,194,40,14,30,263,36,21,21,116,38,27,24,044,38*79
14:55:19.100 -> $GPGSV,4,3,13,28,12,255,36,30,52,312,43,46,34,225,40,48,36,221,40*79
14:55:19.141 -> $GPGSV,4,4,13,51,43,197,42*41
14:55:19.179 -> $GPGLL,3911.41446,N,09634.96285,W,205520.00,A,D*7F
14:55:19.656 -> $GPRMC,205521.00,A,3911.41437,N,09634.96292,W,0.056,,260122,,,D*61
14:55:19.742 -> $GPVTG,,T,,M,0.056,N,0.104,K,D*20
```

4.3.3.2 System Integration

The GNSS solution enclosed inside a 3-D printed casing was installed on top of the UAV platform and harnessed tightly. It was made sure that the 3-D printed encloser and the battery for the GNSS solution were safely secured as shown in Figure 4.14 to avoid any disconnection during the flight as the UAV platform travels at a considerable height and speed. A 3.3V Lithium-Ion battery was used to power the GNSS solution. Finally, the output of the GNSS solution was fed to the input of the flight controller. The camera utilized was a FLIR Vue pro thermal camera sensor (FLIR systems, Wilsonville, Oregon, USA). The PixHawk flight controller accepts the NMEA strings from the GNSS solution and converts it into required format feeding it to thermal camera sensor allowing it to geotag the images.

Figure 4.14. GNSS Solution integrated with UAV Platform

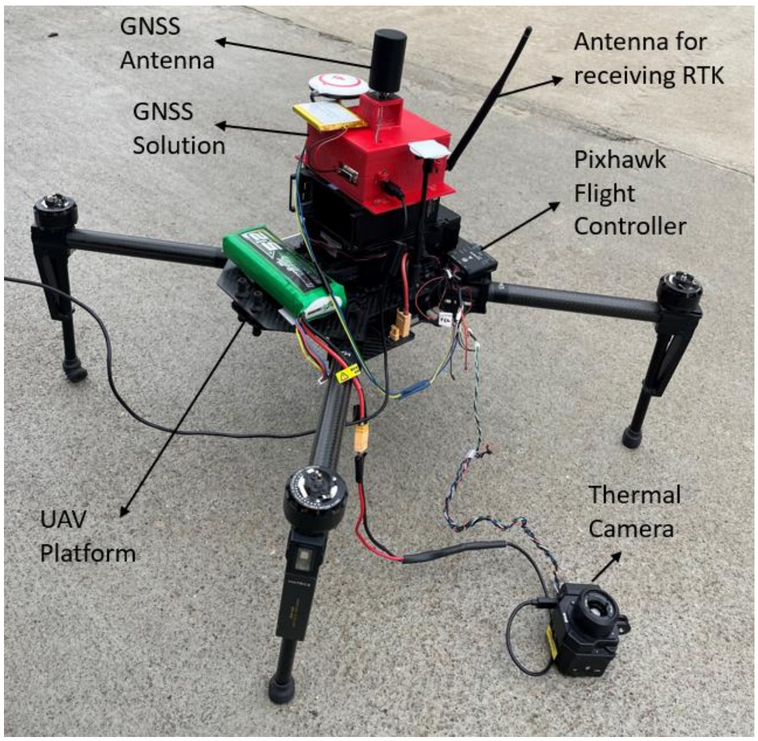

4.3.3.3 Experimental Site and Setup

The Animal Science Farm on the Kansas State University campus was selected to be the location where the experiment was conducted. All the components of the UAS platform (UAV, the flight controller, imaging system) along with the GNSS solution were connected together and prepared for the flight. The experiment consisted of a simple method where the area to be covered during the flight was selected and 15 GCPs were laid geometrically covering the area under the interest which helps for post processing. Also, while laying out the GCPs, their geolocation was also captured using the ground surveying unit as shown in Figure 4.15. This information served as ground truth while comparing the location of the GCP's from the imagery obtained from the RTK-enabled and standalone flights.

Figure 4.15. GCP co-ordinates collection and UAV flight setup

The details regarding the flight are mentioned in the Table 4.3.

Table 4.3. Characteristics of UAV flight for image geotagging

Date	Number of GCP	Altitude of the Flights	Camera Trigger interval
04/04/24	15	50 m,80 m	1 second

Firstly, the GNSS solution operates in RTK enabled mode for which the base station setup that sends the RTK correction signals is utilized as discussed in Section 4.3.1.4. The GNSS solution sends RTK-corrected geolocation information to the on-board flight controller in the form of NMEA strings which further geotags the images taken by the thermal camera connected to it. Next, the GNSS solution operates in standalone mode devoid of the RTK correction signals. Here the GNSS solution will generate NMEA strings based on its coverage to the satellites without adding any RTK corrections and send them to the flight controller that will further geotag the thermal camera images. The following Figure 4.16 shows the status of the GNSS module captured before the both the flights.

Figure 4.16. Status of GNSS module before a) RTK enabled and b) Standalone

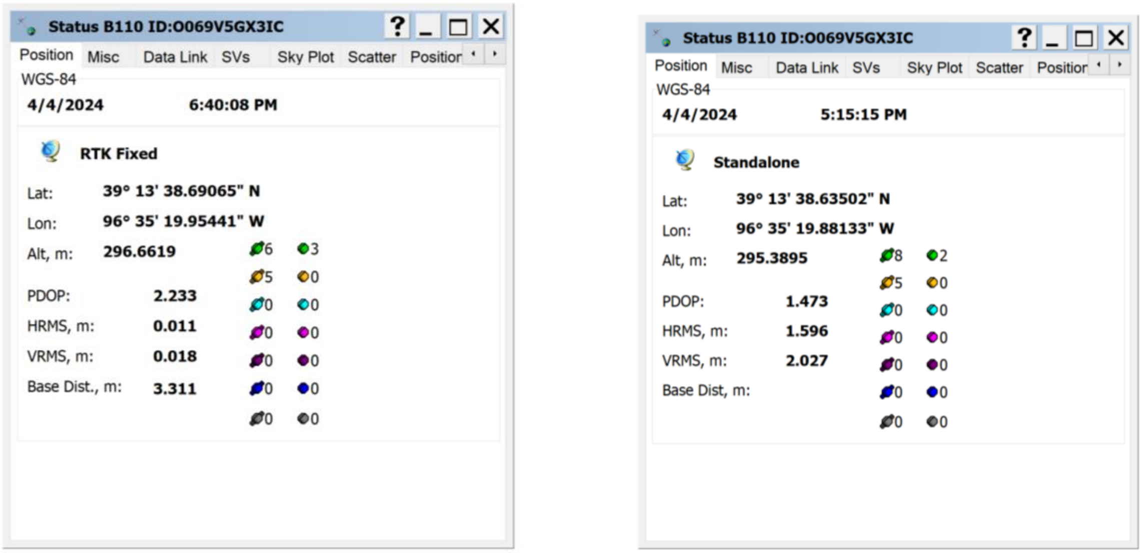

(a) (b)

The goal is to assess whether transmitting the RTK correction signals impacts the geotagging accuracy of the thermal images and compare this accuracy when GNSS operating in a standalone mode.

4.4 Results and Discussion

4.4.1 Image Triggering

The GNSS solution recorded trigger distance information into a file, correlating to the captured images. The GCP marker images, as depicted in Figure 4.17, were obtained using the triggering mechanism designed for RGB camera. It was observed that the captured images were a mixture of disorientation, indistinct, perpendicular point of view, and angled shots. Although the orientation of every image captured should have been in a perpendicular point of view, there were reasons for the disorientations obtained. Since the UAV always flies at an angle, the camera mount which was attached at a fixed perpendicular point of view incurred an additional tilt. Secondly, as the camera was operating in autofocus mode, this led to lose in focus at times as the UAV travels at a considerable speed. Also, while making a turn at corners, the UAV angles & balances itself to steer itself in a particular direction hence the fixed mount captured two corresponding GCP's together at once. Though the objective of the study is not to assess the quality of the images, optimum camera settings, or optimize imaging system, these observations will be useful to utilize the camera with a gimble to maintain a constant camera positioning irrespective of the UAV movements. The 16 mm lens attached to the camera gave an 83° field of view.

Figure 4.17. (a) Perfectly aligned, (b) Angled shot during turns, (c) Indistinct, (d) Dis-oriented

(a)

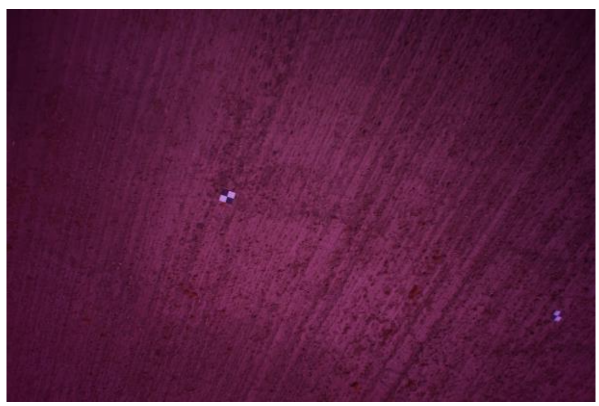

(b)

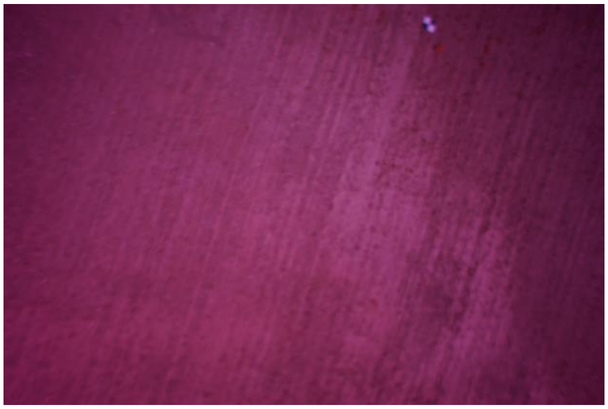

(c)

(d)

The following Tables 4.4 and 4.5 consists of trigger signal activation information gathered in the log file on the GNSS solution during the RTK-enabled and the standalone flight for the 20 m altitude respectively. It also consists of latitude and longitude information of the GCP's which were obtained using the surveying equipment. The variation in trigger signal activation of these two sets of points is made available in the table to observe the difference throughout as shown in Figure 4.18. Also, the corresponding haversine distance is recorded along with the Quality of Status (QOS) to make sure the GNSS solution is in the desired mode of operation with functional image triggering mechanism as shown in Figure 4.19.

Table 4.4. Imagery data flight log in standalone mode for 20 m altitude

GCP	Standalone Data					Difference (m)
	X	Y	QOS	Distance Trigger (On flight) m	Distance Trigger (Calculated) m	
Home Point	-96.589304	39.227651	1	20.045309	19.50	0.54
1	-96.58953	39.227641	1	19.125086	21.23	2.11
2	-96.589775	39.22762	1	19.102744	18.36	0.74
3	-96.589975	39.227677	1	19.627423	24.20	4.57
4	-96.590026	39.227463	1	20.142167	21.85	1.71
5	-96.589773	39.227477	1	20.153781	19.12	1.03
6	-96.589554	39.227449	1	19.632661	16.13	3.5
7	-96.589551	39.227304	1	20.248631	18.19	2.05
8	-96.589762	39.227311	1	19.958431	21.28	1.33
9	-96.590009	39.227307	1	18.892724	16.43	2.46
10	-96.590028	39.22716	1	20.02361	21.18	1.16

11	-96.589785	39.227131	1	-	19.56	-
12	-96.589558	39.227128	-	-	-	-

Table 4.5. Imagery data flight log in RTK-enabled mode for 20 m altitude

GCP	RTK-enabled Data					Difference (m)
	X	Y	QOS	Distance Trigger (On flight) m	Distance Trigger (Calculated) m	
Home Point	-96.589304	39.227651	4	20.142095	19.90	0.24
1	-96.589535	39.227654	5	20.364559	19.56	0.8
2	-96.589762	39.22765	1	20.908385	19.64	1.26
3	-96.58999	39.227654	5	19.881344	19.38	0.5
4	-96.590003	39.22748	4	19.710613	20.09	0.38
5	-96.58977	39.227472	4	19.958318	19.81	0.14
6	-96.58954	39.227475	4	19.907946	19.21	0.69
7	-96.589561	39.227303	5	19.003039	18.86	0.14
8	-96.58978	39.227303	4	20.045371	19.82	0.22
9	-96.59001	39.227309	1	19.018878	19.92	0.91
10	-96.59002	39.22713	4	20.152025	20.41	0.26
11	-96.589783	39.22713	4	-	19.38	-
12	-96.589558	39.227128	-	-	-	-

Figure 4.18. Distance trigger for Standalone and RTK-enabled flight using location information for 20 m altitude

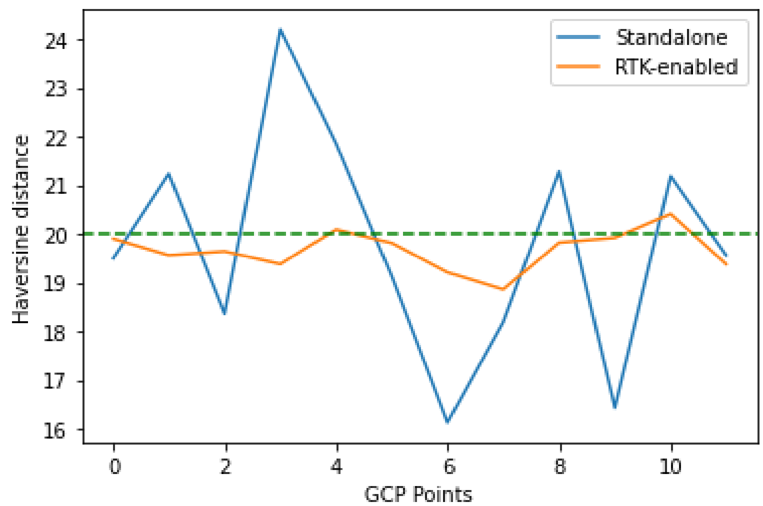

Figure 4.19. Variation in haversine distance for standalone and RTK-enabled flight

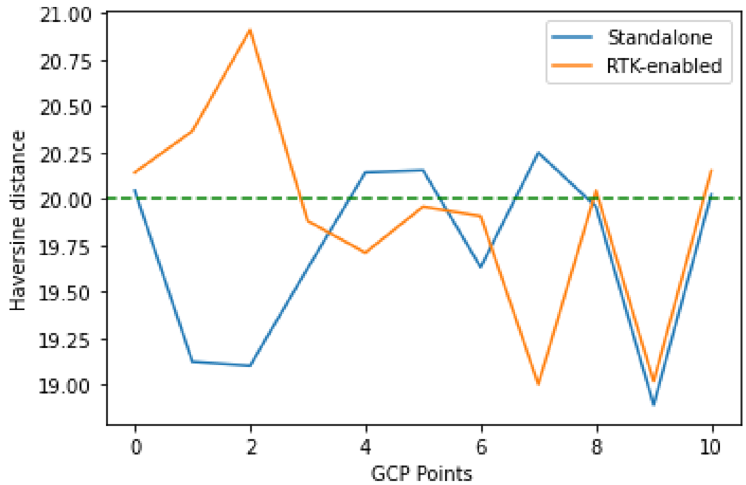

From the graph, it is evident that the trigger points logged by the GNSS solution in RTK-enabled mode performs better than the standalone mode. This helps in understanding that the camera trigger mechanism was implemented closer to the required precision while operating the GNSS solution in the RTK-enabled mode. Also, the haversine distance obtained was consistent and closer to the 20 m as expected establishing the ability of the onboard workflow capturing the location information from the GNSS module and calculating the haversine distance in given amount of time. There were a few points showing a discrepancy for a couple of values recorded but other than that it was found to be fairly constant. While operating in RTK enabled mode, the QOS status of the signal stayed constant in the RTK-enabled mode, switching between fixed and float, making sure the desired mode of operation providing close to cm level of accuracy compared to the standalone mode. The discrepancy found in the values of trigger information in the log file and the variation in the haversine distance could be due to multiple factors such as satellite unavailability to the GNSS module, disconnection with the base transmitting RTK signals, and onboard connections since the UAV travels at a decent altitude & speed. Overall, it ensured that the camera trigger mechanism was practically implemented to serve the need of distance-based triggering. While operating in standalone mode, the triggering mechanism was activated with a margin of error, potentially leading to losing the object of interest that needs to be captured as well as its corresponding trigger information. The haversine distance stayed considerably constant ensuring the triggering mechanism was activated at the points of interest.

In order to test the trigger setup at a different height, another flight at 30 m altitude with the same experiment setup was conducted to gauge the performance of the image triggering mechanism. From the following Table 4.6 and Table 4.7, we could examine the trigger signal activation for the RTK-enabled and standalone points at 30 m altitude respectively. Figure 4.20 displays the variation of trigger signal activation for the standalone flight to be higher than the RTK-enabled flight. Also, the haversine distance recorded for standalone and RTK-enabled flight is shown in Figure 4.21.

Table 4.6. Imagery data flight log in standalone mode for 30 m altitude

GCP	Standalone Data					Difference (m)
	X	Y	QOS	Distance Trigger (On flight)	Distance Trigger (calculated)	
Home Point	-96.589192	39.227653	1	28.343403	27.90	0.44
1	-96.589515	39.227634	1	29.440973	29.20	0.24
2	-96.589854	39.227636	1	29.304808	33.64	4.34
3	-96.59024	39.227682	1	31.242008	26.70	4.54
4	-96.59055	39.22768	1	29.496568	27.99	1.51
5	-96.590575	39.227429	1	31.314372	30.25	1.06
6	-96.590236	39.2275	1	29.292835	31.37	2.08
7	-96.589899	39.227393	1	28.950260	30.59	1.64
8	-96.589545	39.227371	1	30.766825	25.13	5.63
9	-96.589546	39.227145	1	29.074898	29.41	0.34
10	-96.589886	39.227121	1	29.527837	32.23	2.71
11	-96.59026	39.22713	1	-	35.78	-
12	-96.590304	39.22745	-	-	-	-

Table 4.7. Imagery data flight log in RTK-enabled mode for 30 m flight

GCP	RTK-enabled Data					Difference (m)
	X	Y	QOS	Distance Trigger (On flight) m	Distance Trigger (calculated) m	
Home Point	-96.589192	39.227653	5	29.721255	29.12	0.6
1	-96.58953	39.22765	4	29.753596	29.46	0.29
2	-96.589872	39.227655	4	30.022864	29.98	0.04
3	-96.59022	39.22766	4	30.230664	30.12	0.11
4	-96.590569	39.227677	4	30.213107	28.63	1.58
5	-96.590589	39.22742	4	29.327414	29.91	0.59
6	-96.590242	39.22741	1	29.463179	31.54	2.08
7	-96.589879	39.227373	1	31.900957	28.40	3.5
8	-96.58955	39.22739	5	28.098197	29.91	1.82
9	-96.58955	39.227121	4	29.473116	29.39	0.08
10	-96.589891	39.227129	5	30.858206	31.79	0.94
11	-96.59026	39.227133	5	-	29.67	-
12	-96.590604	39.227146	-	-	-	-

Figure 4.20. Distance trigger for Standalone and RTK-enabled flight using location information for 30 m altitude

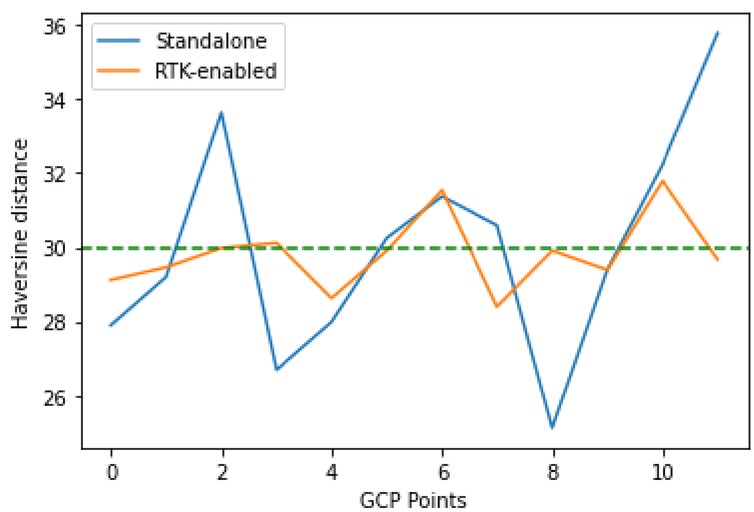

Figure 4.21. Variation of haversine distance for standalone and RTK-enabled flight

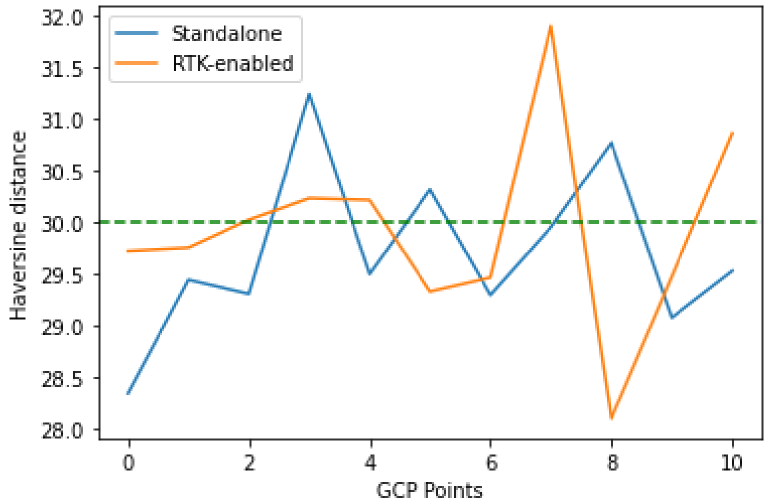

At the 30 m altitude, it was observed that the trigger points generated in RTK-enabled mode were in close proximity with the GCP information confirming the efficacy of the RTK-enabled mode for the GNSS solution. The difference in the points provided a close to cm and sub-meter accuracy except for a couple of points. Also, the QOS status of the signal stayed constant throughout switching between the RTK-float and RTK-fixed status ensuring the required state of operation. The haversine distance trigger points also stayed constant throughout around the 30 m mark. The difference between the majority of standalone data points and the GCP information was higher compared to the difference obtained for RTK-enabled points. There were instances where the RTK-enabled and standalone did not differentiate much and this can be due to various dynamic factors encountered during the flight operations.

Eventually, it is evident that at both the altitudes, RTK-enabled data points provided a closer relevance to the GCP information providing a cm or sub-meter accuracy assisted by the radio communication setup that fed the RTK-corrections from the base station. For both 20 m and 30 m altitude, the RTK-enabled data produced trigger points in close proximity with the GCP's, exhibiting minimum difference in between them. The GNSS module operated in the required mode of operation throughout except for a couple of scenarios. The implementation of the haversine mechanism to trigger the camera based on based on traveling distance criteria also produced desirable results. As the requirement for the precision agriculture application becomes very specific in terms of taking the control at a finer scale, the RTK-enabled applications will contribute more towards developing the respective plans which were evidenced. The distance-based triggering can be readily used for applications across different imaging system where the requirements are based on the amount of distance covered with required overlap providing a dependable option for time-based data collection.

4.4.2 Image Geotagging

The thermal imagery information collected after the experiments were imported into the AgiSoft software (Agisoft LLC, St. Petersburg, Russia) to process the images and extract the geotag information of GCP images which is saved in the form meta-data. The ArcGIS software (Esri, Redlands, California) was used to import & visualize the geolocations of GCP's obtained using surveying equipment as a reference along with the stitched thermal camera images processed using AgiSoft software. Since the experiment was conducted to gauge how RTK-enabled GNSS solution provides location accuracy, the comparison was done between the RTK-enabled and standalone GNSS geotagged meta-data and examine it through visual representation of plotted points.

Following Table 4.8 displays the geotagged information for two flights operating in RTK-enabled and standalone mode for the 50 meters flight that was conducted. During the both flights, the GNSS solution was continuously recording the NMEA strings in the SD card located on the

Teensy microcontroller. This log of information was retrieved to examine the QOS indicator obtained in the NMEA string.

Table 4.8. Geolocation comparison of Standalone and RTK-enabled GNSS data with GCP's for 50 m Flight

GCP	GCP geolocation		Standalone geotag			RTK-enabled geotag			Difference (m)	
	X	Y	X	Y	QOS	X	Y	QOS	Standalone	RTK
1	-96.59069	39.22707	-96.590733	39.227112	1	-96.590685	39.227062	4	6.32	0.78
2	-96.59061	39.22731	-96.590633	39.227339	1	-96.590602	39.227301	4	3.74	1.26
3	-96.59056	39.22750	-96.590578	39.227526	1	-96.590548	39.227491	4	3.13	1.55
4	-96.59053	39.22772	-96.59054	39.227736	1	-96.590511	39.227703	4	2.43	2.02
5	-96.59048	39.22792	-96.590493	39.227931	1	-96.590465	39.227899	1	1.84	2.50
6	-96.59002	39.22711	-96.590049	39.227145	1	-96.590010	39.227103	4	4.77	1.10
7	-96.59001	39.22727	-96.590037	39.227299	1	-96.590000	39.227260	4	4.07	1.44
8	-96.59000	39.22747	-96.590022	39.227498	1	-96.589986	39.227462	5	3.42	1.77
9	-96.58999	39.22771	-96.590004	39.227734	1	-96.589969	39.227699	5	2.59	2.45
10	-96.58998	39.22792	-96.589988	39.227936	1	-96.589956	39.227903	5	1.91	2.80
11	-96.58943	39.22791	-96.589437	39.227922	1	-96.589400	39.227889	1	1.98	3.14
12	-96.58940	39.22771	-96.589413	39.227735	1	-96.589373	39.227700	5	2.70	2.91
13	-96.58938	39.22744	-96.589398	39.227471	1	-96.589356	39.227434	5	3.51	2.41
14	-96.58937	39.22726	-96.589389	39.227294	1	-96.589346	39.227255	4	4.05	2.09
15	-96.58935	39.22708	-96.589371	39.227109	1	-96.589331	39.227072	4	4.15	1.75

The following Figure 4.22 shows how far the RTK-enabled and standalone flight points were from the GCP's original location for 50 m flight.

Figure 4.22. Comparing difference of Standalone and RTK-enabled flight points with GCP's for 50 m flight

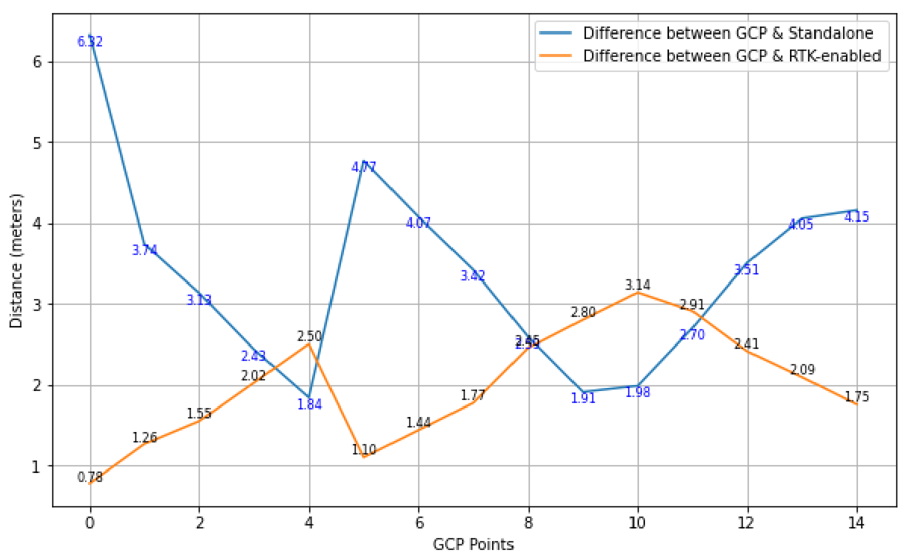

A change in the values can be observed while shifting from standalone geotag to RTK-enabled geotag. This is due to the fact since RTK-enabled geotag is closer to the actual geolocation, thereby giving a high level of accuracy and less difference. The geotagged information attached to the images depends on the exposure of the GNSS module to the number of satellites thereby requiring it to be operating in clear sky condition or else it could lead to poor imagery as well as a compromise in the geotagged information recorded. Except for a couple of points, the RTK-enabled flight was closer to the GCP's geolocation as compared to the standalone flight. The majority of the RTK-enabled flight points were in the range of 0.7 meters to less than 3 m proximity of GCP's geolocation. The difference between the GCP's and the majority of standalone flight points ranged between 2 to 6 m. This exemplifies that the information from the RTK-enabled flight has better geotagging accuracy compared to the standalone flight. This could also be visualized from the images processed for the individual flights where a clear shift noticeable as shown in Figure 4.23. At times, it is visible that the RTK-enabled and standalone GNSS points are not considerably different or the standalone points are closer to the GCP's as compared to the RTK-enabled. The QOS obtained from the NMEA strings in the log file shows that the status of the GNSS solution switches between RTK Fixed to RTK Float. The RTK Float status explains that it is still using the correction information but it is yet to move to the highest precision mode yet. This can be due to various reasons such as poor satellite exposure or RTK correction signal communicated by the base station is not being received seamlessly.

Figure 4.23. Visual representation of (a) Standalone and (b) RTK-enabled points compared with GCP's geolocation for 50 m flight

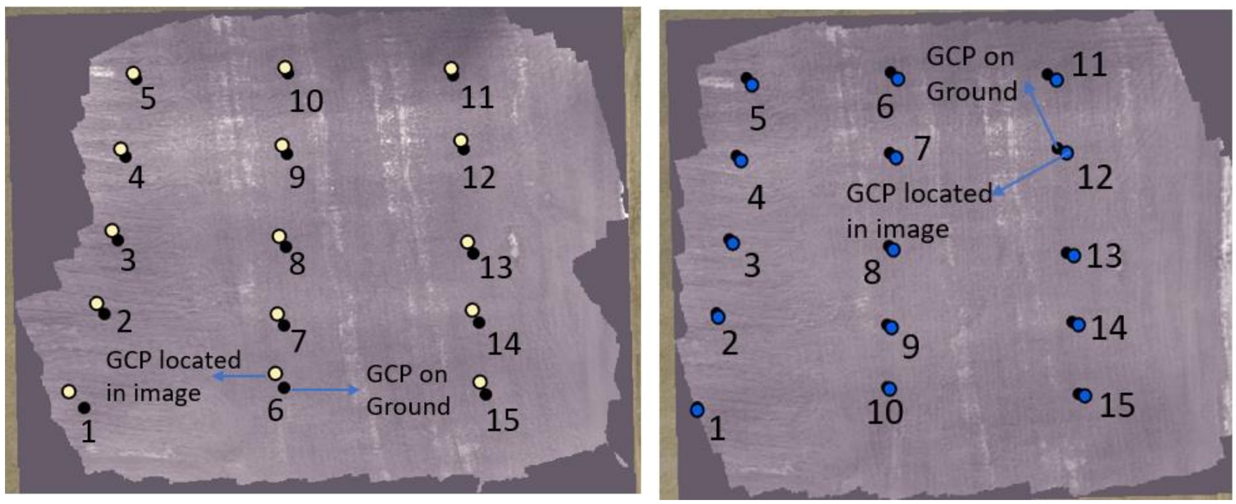

After processing the thermal images along ground data for the 80 m flight, the data obtained is shown in Table 4.9. Again, it shows how the geotag information from the RTK-enabled and standalone flight varies from the GCP geolocation along with the OQS. Followed by the table, a variation of the standalone and RTK-enabled geotag information obtained from the thermal imagery can be visualized in Figure 4.24 when compared with the GCP geolocation as reference.

Table 4.9. Geolocation comparison of Standalone and RTK-enabled GNSS data with GCP's for 80 m Flight

GCP	GCP geolocation		Standalone geotag			RTK-enabled geotag			Difference (m)	
	X	Y	X	Y	QOS	X	Y	QOS	Standalone	RTK
1	-96.59069	39.22707	-96.590712	39.227105	1	-96.590714	39.227047	1	4.63	3.50
2	-96.59061	39.22731	-96.590630	39.227330	1	-96.590632	39.227294	5	2.78	2.74
3	-96.59056	39.22750	-96.590579	39.227506	1	-96.590577	39.227488	5	1.78	2.20
4	-96.59053	39.22772	-96.590541	39.227704	1	-96.590538	39.227707	4	1.94	1.52
5	-96.59048	39.22792	-96.590496	39.227887	1	-96.590493	39.227909	4	3.39	1.10
6	-96.59002	39.22711	-96.590064	39.227151	1	-96.590020	39.227092	4	6.05	1.78
7	-96.59001	39.22727	-96.590053	39.227298	1	-96.590012	39.227255	4	4.81	1.35
8	-96.59000	39.22747	-96.590039	39.227486	1	-96.589999	39.227462	4	3.52	1.06
9	-96.58999	39.22771	-96.590023	39.227708	1	-96.589985	39.227708	4	2.81	0.76
10	-96.58998	39.22792	-96.590008	39.227899	1	-96.589973	39.227917	4	3.36	0.69
11	-96.58943	39.22791	-96.589474	39.227890	1	-96.589402	39.227908	5	4.14	2.43
12	-96.58940	39.22771	-96.589450	39.227714	1	-96.589374	39.227714	5	4.05	2.51
13	-96.58938	39.22744	-96.589434	39.227466	1	-96.589353	39.227441	5	5.21	2.50
14	-96.58937	39.22726	-96.589424	39.227300	1	-96.589339	39.227257	5	6.42	2.62
15	-96.58935	39.22708	-96.589410	39.227124	1	-96.589321	39.227067	5	7.45	2.73

Figure 4.24. Comparing difference of Standalone and RTK-enabled flight points with GCP's for 80 m flight

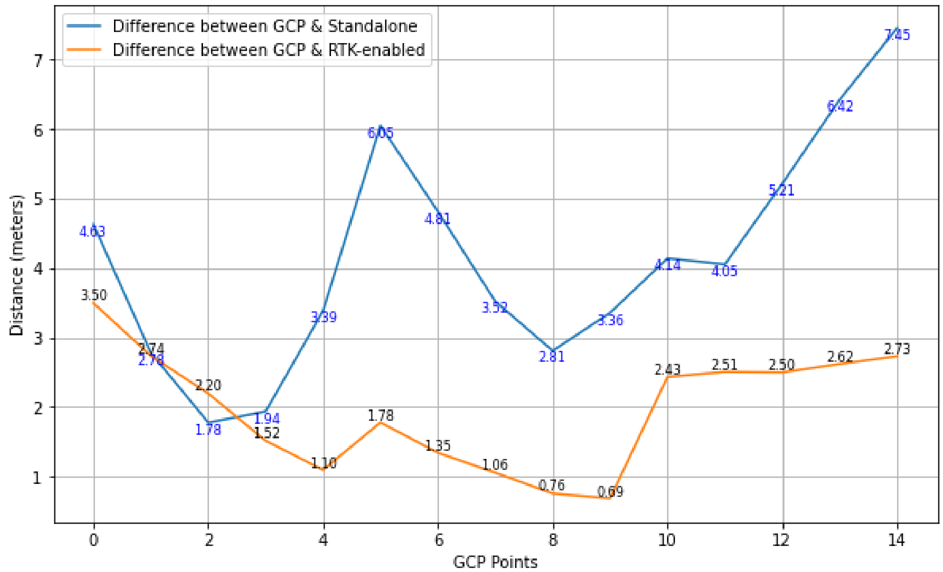

Although flown at a higher altitude, the RTK-enabled geotag produced results closer to the GCP's original geolocations. The range of difference between the RTK enabled and the GCP's geolocation varies between 0.6 meters to 2.75 meters for majority of the points. Also, the QOS status information corresponds that RTK-enabled geotag points were in RTK Float and RTK Fixed status throughout. Except for points a few points, the RTK-enabled flight geotag information was closer to the GCP's geolocation as compared to the standalone flight. The standalone points differed from the GCP's geolocation to a higher degree where difference ranged between 3 to 8 meters. Even at a higher altitude, the RTK-enabled flight has better geotagging accuracy compared to the standalone flight. The communication between the radio transmitting the RTK correction signals and the radio on the GNSS solution was intact and they were able to hold the communication throughout the flight by switching between RTK Float to RTK Fixed status. A visual representation of the GCP's original geolocation compared to the ones obtained from the RTK-enabled and standalone flight can be seen in Figure 4.25. A considerable differentiation can be seen between the standalone flight points and GCP's geolocation whereas the RTK-enabled flight points are sufficiently close to the GCP's geolocation. This is supported by the QOS status obtained from the NMEA strings collected on the log file of the GNSS solution.

Figure 4.25. Visual representation of (a) Standalone and (b) RTK-enabled points compared with GCP's geolocation for 80 m flight

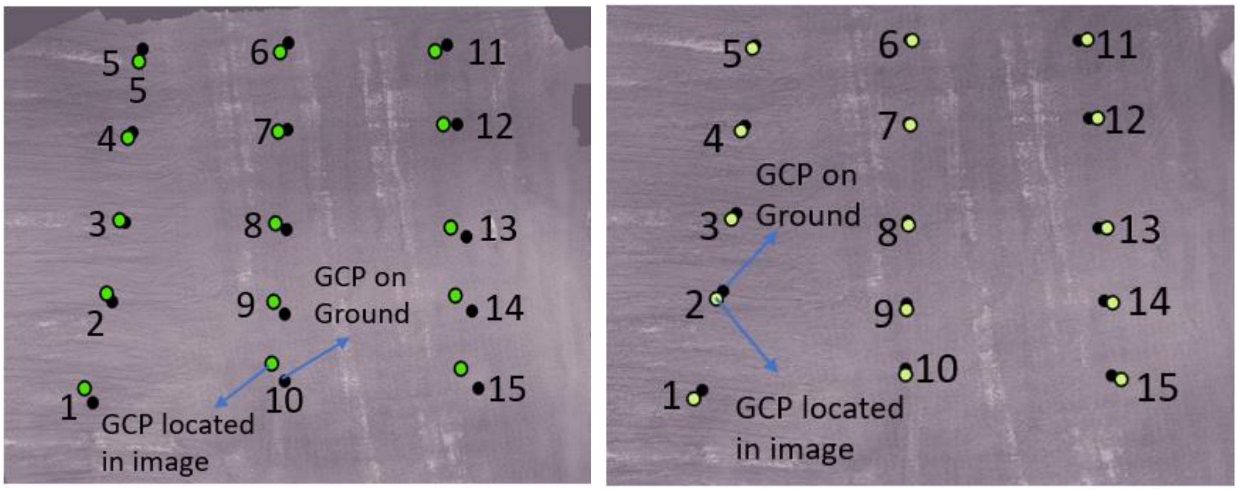

By carefully navigating through the difference between the GCP's original geolocation when compared with the imagery information of RTK-enabled and standalone flight, it is evident that the RTK-enabled mode gives better geolocation accuracy compared to the standalone mode. This was supported by the visual inspection done by plotting the ground truth and the information acquired from the flights. The two altitudes 50 and 80 meters supported the fact that RTK-enabled geotagged information was closer to the GCP's geolocation obtained from the ground surveying. Except for a few points on the 50 m flight, the majority of the RTK-enabled points were closer to the GCP's geolocation and were supported by their corresponding QOS status obtained from the log file. For the 80 m flight, the set of points from the RTK-enabled flight were found closer to the GCP's geolocation compared to the standalone flight. The QOS obtained also supported by maintaining their status between RTK Float & RTK Fixed. When the imagery information was processed and plotted along with the GCP's surveyed geolocation, the visual representation also strengthened the RTK-enabled geolocation to the comparatively closer to the GCP's geolocation. Therefore, the overall aim of the study to show a comparison between the geotagging accuracy of RTK-enabled and standalone flight was met supported by the imagery data processed, visual inspection, ground based information, and the QOS status obtained from the GNSS solution.

4.5 Conclusion and Future Work

4.5.1 Image Triggering

The image triggering mechanism implemented for the RGB camera was realized to target distance-based image triggering and capture. The GNSS solution adapted with RTK corrections served better as compared to the standalone mode. The major outcomes were:

1) The image triggering feature equipped with the haversine distance calculation and optocoupler based hardware provided close to required accuracy triggering based on the threshold distance provided at both 20 and 30 m altitude.
2) The ability of the radio communication setup to continuously feed RTK correction signals to the GNSS solution improved its ability to generate trigger information corresponding to the imagery data precise and closer to the ground surveyed points at 20 m and 30 m altitudes. 80 % of the points were successfully RTK-enabled for both 20 as well as 30 m altitude flights.
3) The image trigger information for the RTK enabled flight had lesser variation compared to the standalone flight. This was primarily because the trigger generated while in RTK enabled mode provides closer to cm level accuracy whereas the standalone mode provides accuracy in meters.

4.5.2 Image Geotagging

The study conducted to assess the image geotagging accuracy aimed at understanding operational ability of the developed GNSS solution in RTK-enabled mode providing better results as compared to standalone mode. The major outcomes included:

1) By cross-referencing the geotag data from thermal camera imagery captured during RTK-enabled flights and standalone flights with the surveyed geolocation of GCPs, it was observed that the geotags from RTK-enabled flights were more closely aligned with the GCPs' geolocation for both 50m and 80m altitude.
2) The difference of RTK-enabled and standalone geotag information when compared with GCP’s geolocation was analyzed and plotted to understand the range of deviation and compare them visually.
3) The deviation of RTK-enabled flight was in the range of 0.7 meters to less than 3 m for 50 meters flight and 0.6 meters to 2.75 meters for the 80 m flight whereas for the standalone flight it was in the range of 2 to 6 m for 50 m flight and 3 to 8 m for the 80 m flight.

Overall, it was noticeable that the RTK-enabled flights performed better compared to the standalone flights. When operating in RTK-enabled mode, the GNSS solution generated RTK-Float and RTK-Fixed points 86% of the time during 50 m flights and 93% of the time during 80 m flights. This helps in understanding the ability of the radios communicating the RTK correction signals and allowing the GNSS to stay in the desired mode of operation. For zone level and plant level management where a precise information is necessary, the UAV geotagging mechanism operated in RTK-enabled mode will give a higher degree of accuracy to the user. It will help in developing and planning detailed operations such as irrigation and nutrient management plans at a granular level, and can be extended to other crop treatment applications.

It was observed that while the GNSS solution was in RTK-enabled mode, there were a few instances where the QOS was not in the desired mode. This can be due to various reasons such as disruption in the communication of the radio which assist in delivering RTK signals. For example, as the UAV changes its orientation while taking turns, it might lead to losing the LOS leading to disconnection. Also, it is important to make sure that the GNSS solution onboarded onto the UAV platform has to be in constant exposure of the satellites or else it might lead to poor geotagging quality of the images that are collected. An efficient positioning of the antennas both for the radios and the GNSS module should be achieved to avoid such issues.

Lastly, flying the UAV platform at different altitudes could also be discovered to gauge the location accuracy to a finer extent. A range of altitudes and their corresponding geotagging accuracy will help the user to choose between the tradeoffs associated. One more factor that could be worth considering is the number of GCP used during the data collection. The number of GCP’s associated could also indirectly play a role especially with respect to gauging the geometric accuracy of the UAV components such as imaging sensors gauging different spectral information. Lastly, NTRIP method of communicating the RTK correction signals can be employed especially in the region with a strong cellular coverage. This will avoid the hassle required to setup an individual base station every time.

Chapter 5 - Conclusion and Future Work

5.1 Conclusion

The research exploring wireless data communication for autonomous farming and precision agriculture application, utilizing license-free spectrum band radios, yielded the following significant outcomes:

1) As the adoption of autonomous farming applications become widespread across their use case scenarios, the data generated by various sensing and actuating subsystems on these platforms need to be catered significantly. They need to be collected and delivered to the desired location in real-time to preserve their relevance and significance which would further assist in making data driven decisions. To address this, a wireless data communication system was developed using a network of 900 MHz radios operating in a license free spectrum band. These radios were configured in distinct configurations: remotes, serving as the data sources; repeaters, extending the network's coverage; and primary, functioning as central hub for aggregating information from the remotes.

   These radios operating in different configuration were deployed in diverse field conditions that constituted undulating terrain and dense crop canopy. The remotes were gauged on their ability to transfer information to the central hub by calculating the packet delivery performance. The network served a packet delivery of 98 % in both field environments with an average power consumption of less than 0.4 watts throughout all the experimental runs. With such robust performance, the wireless data communication platform could be implemented in a plug-and-play mechanism for securely offloading data volumes collected during diverse agricultural operations. This ensures that the information is safely and instantaneously delivered to designated destinations for further analysis.

2) Further, the license free spectrum radio operating in 2.4 GHz frequency was utilized to seamlessly transfer information from an autonomous site-specific liquid application system to a central hub. The transmitting radio was configured and integrated with an autonomous platform built on Robot Operation System 2 (ROS2) middleware. The ability of the ROS2 middleware to bind different subsystem together was extended to incorporate the data communication platform and use serial communication to forward the data packets to radios to be able to send wirelessly to the central hub. Using nodes and topics which are basic building components of the ROS2 framework were utilized to create a seamless interconnection between the central computing platform and the radio communication system. The data communication platform was tested for 3 different configurations namely default, config 2, config 3 in two different field conditions to gauge the long-range communication and line of sight abilities of the radio. The information in the data packets consisted of information from 3 different subsystems namely navigation, computer vision, and liquid application and the performance metrics utilized were packet delivery performance, packet loss, and latency.

While the radio communication system was tested on two different locations, the results gathered depicted that 2 out of 3 configurations produced satisfactory results. In the tests conducted at the football stadium, both the default and config 3 achieved an accuracy of over 99%, with a combined loss of less than 1%. However, config 2 experienced a 2% loss while testing the computer vision and liquid application systems.

Packet delivery was robust for the default and config 3, reaching 98%, whereas config 2 lagged behind at 87%, resulting in a notable 13% data loss for the navigation system test. Shifting to the agricultural field tests, once again, the default setting and config 3 demonstrated strong performance with a 99% packet delivery rate. Conversely, config 2 experienced a 5% data loss for the computer vision and liquid application systems. However, the default and config 3 maintained near-perfect data transfer rates, nearly reaching 100% for the navigation system, while config 2 incurred a 2% loss in information. Also, the overall latency stayed constant at 0.1 seconds for all the configurations and experimental runs at football stadium experiment and in the range of 0.2 to 0.4 s for the agricultural field experiment. Therefore, the default and config 3 can be two sets of recommended configurations that could be utilized for seamless end to end packet delivery for the autonomous liquid application system.

3) The ability of a custom made RTK-enabled GNSS solution for accurate distance-based image triggering and geotagging in UAV applications was tested. The RTK-enabled GNSS solution yielded trigger information closer to the ground truth when triggered a consumer-grade RGB camera and when utilized for geotagging thermal infrared imagery. The information for RTK-enabled and standalone modes were compared with the ground surveyed location of the ground control points. The GNSS solution was RTK-enabled using a license free spectrum band radios operating in 900 MHz frequency band responsible for sending and receiving RTK correction signals.

   To enable triggering a RGB camera, a distance-based camera trigger mechanism was achieved using an optocoupler circuit implemented on the GNSS solution. It was operated by the haversine distance formula wherein it calculates the distance between two points and activates the triggering signal once the threshold is achieved. For the two experiments conducted at 20 m and 30 m altitude, the data points generated by the GNSS solution in RTK-enabled mode when compared to the ground surveyed points showed minimum difference as compared to the points collected in standalone mode. The difference calculated was in the range of cm for RTK-enabled points for both 20 m & 30 m flight. On the contrary, for the points in standalone mode, the difference was in the range of meters, for both 20 & 30 m flight. Also, the QOS status of the signal obtained from the data points displayed that the GNSS solution was successfully RTK-enabled for 80 % of the points for both for 20 and 30 m flight.

While testing for image geotagging, the variation was minimal between the points collected in RTK-enabled mode and those surveyed on the ground. It was in the range of 0.7 meters to less than 3 m for the 50 m flight whereas 0.6 meters to 2.75 meters for the 80 m flight for the geotagging experiment. Whereas for standalone mode, range of 2 to 6 m for 50 m flight and 3 to 8 for the 80 m flight. From the QOS status obtained, the GNSS solution stayed in RTK float and RTK fixed mode for 86% for 50 m flight and 93% for 80 m flight during the geotagging experiment.

In order to obtain optimum accuracy in location information, it is recommended to operate the GNSS solution in RTK-enabled mode. This will assist in performing granular control while developing a zone level and plant level management plans for various agricultural operations such as irrigation, nutrient application, etc.

Overall, the license free spectrum band radios operating in the 900 MHz and 2.4 GHz frequency bands were utilized to serve autonomous farming and precision agriculture applications. Firstly, a data communication platform using the 900 MHz radios were developed and tested independently for performing data communication in undulating terrain and dense crop canopy for different time intervals. Further the 2.4 GHz radios were integrated with an autonomous site-specific liquid application platform to communicate the information gathered from various subsystems and seamlessly deliver it to the destination in real-time. Lastly, the 900 MHz radios were utilized to send and receive RTK correction signals to a GNSS solution in order to improve the location accuracy for thermal imagery geotagging and triggering consumer-grade RGB cameras based on distance calculation mechanism.

5.2 Future work and recommendations

The independent wireless data communication system developed for broad applicability could be instantiated with diverse autonomous platform performing agricultural operations such as planting, spraying, weeding, scouting, etc. It will act as a medium of wirelessly communicating the information to a centralized location at the edge of the farm by seamlessly integrating with the operational platform using a plug and play mechanism. Whereas, the system consisting of MIMO radio integrated with the site-specific liquid application platform could be further implemented in a dense crop canopy to monitor and learn the effects of vegetation on the propagation of the signal. Implementing multiple autonomous platforms equipped with MIMO radio communication systems will assist in addressing challenges associated with data collection from multiple sources, with the potential for streamlined data management through uploading to remote computing platforms. Knowledge graphs could be implemented in understanding the operational ability, performance and prognostics of each of the autonomous platform and successfully convey the underneath semantic for improved decision making. Lastly, the RTK-enabled GNSS solution can be utilized to develop crop treatment plans on small and big holder farms in order to achieve a plant and zone level control delivering precision remote sensing applications. The platform not only replaces various single-functionality modules but also serves as an interface for integrating diverse sensing suites aboard unmanned aerial vehicles.

References

Andanaputra, A. B. T., Ganadhi, E. M., Fakhrezi, M. F., Gunawan, A. A. S., Chowanda, A., Suroso, J. S., ... & Budiharto, W. (2020). GNSS-based navigation systems of autonomous drone for pesticide sprayer in agriculture. ICIC Express Letters, Part B: Applications, 11(12), 1125-1

Atefi, A., Ge, Y., Pitla, S., & Schnable, J. (2021). Robotic technologies for high-throughput plant phenotyping: Contemporary reviews and future perspectives. Frontiers in plant science, 12, 611940.

Atmaja, A. P., El Hakim, A., Wibowo, A. P. A., & Pratama, L. A. (2021). Communication systems of smart agriculture based on wireless sensor networks in IoT. *Journal of Robotics and Control (JRC)*, *2*(4), 297-301.

Bakker, T., Bontsema, J., & Müller, J. (2010). Systematic design of an autonomous platform for robotic weeding. Journal of Terramechanics, 47(2), 63-73.

Bawden, O., Ball, D., Kulk, J., Perez, T., & Russell, R. (2014). A lightweight, modular robotic vehicle for the sustainable intensification of agriculture. In *Proceedings of the 16th Australasian Conference on Robotics and Automation 2014* (pp. 1-9). Australian Robotics and Automation Association (ARAA).

Berger, K., Verrelst, J., Féret, J.-B., Wang, Z., Wocher, M., Strathmann, M., Danner, M., Mauser, W., & Hank, T. (2020). Crop nitrogen monitoring: Recent progress and principal developments in the context of imaging spectroscopy missions. Remote Sensing of Environment, 242, 111758. https://doi.org/10.1016/j.rse.2020.111758

Bogdanoff, M., & Tayeb, S. (2020, September). An ISM-band automated irrigation system for agriculture ioT. In *2020 IEEE International IOT, Electronics and Mechatronics Conference (IEMTRONICS)* (pp. 1-6). IEEE.

Cheng, C., Fu, J., Su, H., & Ren, L. (2023). Recent advancements in agriculture robots: Benefits and challenges. Machines, 11(1), 48.

Conesa-Muñoz, J., Gonzalez-de-Soto, M., Gonzalez-de-Santos, P., & Ribeiro, A. (2015). Distributed multi-level supervision to effectively monitor the operations of a fleet of autonomous vehicles in agricultural tasks. Sensors, 15(3), 5402-5428.

Daakir, M., Pierrot-Deseilligny, M., Bosser, P., Pichard, F., Thom, C., Rabot, Y., & Martin, O. (2017). Lightweight UAV with on-board photogrammetry and single-frequency GPS positioning for metrology applications. ISPRS Journal of Photogrammetry and Remote Sensing, 127, 115-126.

De Alwis, S., Hou, Z., Zhang, Y., Na, M. H., Ofoghi, B., & Sajjanhar, A. (2022). A survey on smart farming data, applications and techniques. Computers in Industry, 138, 103624.Schimmelpfennig, D. (2016). Farm profits and adoption of precision agriculture.

Eissfeller, B., Ameres, G., Kropp, V., & Sanroma, D. (2007, July). Performance of GPS, GLONASS and Galileo. In Photogrammetric week (Vol. 7, pp. 185-199).

Fan, P., Li, W., Cui, X., & Lu, M. (2019). Precise and robust RTK-GNSS positioning in urban environments with dual-antenna configuration. Sensors, 19(16), 3586.

FAO. (2017). The future of food and agriculture– Trends and challenges. Rome.

Feng, X., Yan, F., & Liu, X. (2019). Study of wireless communication technologies on Internet of Things for precision agriculture. Wireless Personal Communications, 108(3), 1785-1802.

Fountas, S., Sorensen, C. G., Tsiropoulos, Z., Cavalaris, C., Liakos, V., & Gemtos, T. (2015). Farm machinery management information system. Computers and electronics in agriculture, 110, 131-138.

Gadhwal, M., & Sharda, A. (2023, June). Feasibility and accuracy assessment of UAV, aircraft, and satellite-based remote sensing for irrigation management using canopy temperature and NDVI. In Autonomous Air and Ground Sensing Systems for Agricultural Optimization and Phenotyping VIII (Vol. 12539, pp. 68-84). SPIE.

Gadhwal, M., Sharda, A., Sangha, H. S., & Van der Merwe, D. (2023). Spatial corn canopy temperature extraction: How focal length and sUAS flying altitude influence thermal infrared sensing accuracy. Computers and Electronics in Agriculture, 209, 107812.

Garcia-Sanchez, A. J., Garcia-Sanchez, F., & Garcia-Haro, J. (2011). Wireless sensor network deployment for integrating video-surveillance and data-monitoring in precision agriculture over distributed crops. Computers and electronics in agriculture, 75(2), 288-303.

Goense, D., & Thelen, J. (2005). Wireless sensor networks for precise Phytophthora decision support. In 2005 ASAE Annual Meeting (p. 1). American Society of Agricultural and Biological Engineers.

Gonzalez-de-Santos, P., Ribeiro, A., Fernandez-Quintanilla, C., Lopez-Granados, F., Brandstoetter, M., Tomic, S., ... & Debilde, B. (2017). Fleets of robots for environmentally-safe pest control in agriculture. Precision Agriculture, 18, 574-614.

Griffin, T. W., Miller, N. J., Bergtold, J., Shanoyan, A., Sharda, A., & Ciampitti, I. A. (2017). Farm's sequence of adoption of information-intensive precision agricultural technology. *Applied Engineering in Agriculture*, *33*(4), 521.

Grijalva, I., Spiesman, B. J., & McCornack, B. (2023). Computer vision model for sorghum aphid detection using deep learning. Journal of Agriculture and Food Research, 13, 100652.

Grijalva, I., Spiesman, B. J., & McCornack, B. (2023). Image classification of sugarcane aphid density using deep convolutional neural networks. Smart Agricultural Technology, 3, 100089.

Gumilar, I., Bramanto, B., Rahman, F. F., & Hermawan, I. M. D. (2019). Variability and performance of short to long-range single baseline RTK GNSS positioning in Indonesia. In E3S Web of Conferences (Vol. 94, p. 01012). EDP Sciences.

Hasheminasab, S. M., Zhou, T., & Habib, A. (2020). GNSS/INS-assisted structure from motion strategies for UAV-based imagery over mechanized agricultural fields. Remote Sensing, 12(3), 351.

Hewage, P., Anderson, M., & Fang, H. (2017, October). An agile farm management information system framework for precision agriculture. In Proceedings of the 9th international conference on information management and engineering (pp. 75-80).

https://www.ros.org/

Kalyani, Y., & Collier, R. (2021). A systematic survey on the role of cloud, fog, and edge computing combination in smart agriculture. Sensors, 21(17), 5922.

Kamilaris, A., Kartakoullis, A., & Prenafeta-Boldú, F. X. (2017). A review on the practice of big data analysis in agriculture. Computers and electronics in agriculture, 143, 23-37.

Kapetanović, N., Nađ, Đ., & Mišković, N. (2021, September). Towards a heterogeneous robotic system for autonomous inspection in mariculture. In OCEANS 2021: San Diego–Porto (pp. 1-6). IEEE.

Khan, A., Aziz, S., Bashir, M., & Khan, M. U. (2020, March). IoT and wireless sensor network based autonomous farming robot. In 2020 international conference on emerging trends in smart technologies (ICETST) (pp. 1-5). IEEE.

Khan, N., Ray, R. L., Sargani, G. R., Ihtisham, M., Khayyam, M., & Ismail, S. (2021). Current progress and future prospects of agriculture technology: Gateway to sustainable agriculture. Sustainability, 13(9), 4883.

Khanal, S., Kc, K., Fulton, J. P., Shearer, S., & Ozkan, E. (2020). Remote sensing in agriculture—accomplishments, limitations, and opportunities. Remote Sensing, 12(22), 3783.

King, C. (2013, April). Fundamentals of wireless communications. In 2013 IEEE Rural Electric Power Conference (REPC) (pp. B6-1). IEEE.

Klimánek, M. (2010). Analysis of the accuracy of GPS Trimble JUNO ST measurement in the conditions of forest canopy. Journal of Forest Science, 56(2), 84-91.

Köksal, Ö., & Tekinerdogan, B. (2019). Architecture design approach for IoT-based farm management information systems. Precision Agriculture, 20, 926-958.

Kukar, M., Vračar, P., Košir, D., Pevec, D., & Bosnić, Z. (2019). AgroDSS: A decision support system for agriculture and farming. Computers and Electronics in Agriculture, 161, 260-271.

Liao, W. T., Rodríguez, L. F., Diesner, J., & Lin, T. (2015). Improving farm management optimization: Application of text data analysis and semantic networks. In 2015 ASABE Annual International Meeting (p. 1). American Society of Agricultural and Biological Engineers.

Lloret, J., Sendra, S., Ardid, M., & Rodrigues, J. J. (2012). Underwater wireless sensor communications in the 2.4 GHz ISM frequency band. Sensors, 12(4), 4237-4264.

Lum, C., Mackenzie, M., Shaw-Feather, C., Luker, E., & Dunbabin, M. (2016, July). Multispectral imaging and elevation mapping from an unmanned aerial system for precision agriculture applications. In Proceedings of the 13th International Conference on Precision Agriculture (Vol. 31, pp. 4-10).

Macenski, S., Foote, T., Gerkey, B., Lalancette, C., & Woodall, W. (2022). Robot operating system 2: Design, architecture, and uses in the wild. Science robotics, 7(66), eabm6074.

Maja, J. M., Polak, M., Burce, M. E., & Barnes, E. (2021). CHAP: cotton-harvesting autonomous platform. AgriEngineering, 3(2), 199-217.

McGlynn, S., & Walters, D. (2019). Agricultural Robots: Future Trends for Autonomous Farming. Int. J. Emerg. Technol. Innov, 6, 944-949.

Miller, N. J., Griffin, T. W., Bergtold, J., Ciampitti, I. A., & Sharda, A. (2017). Farmers' adoption path of precision agriculture technology. Advances in Animal Biosciences, 8(2), 708-712.

Miller, N. J., Griffin, T. W., Ciampitti, I. A., & Sharda, A. (2019). Farm adoption of embodied knowledge and information intensive precision agriculture technology bundles. *Precision Agriculture*, *20*, 348-361.

Motlagh, N. H. (2010). Performance improvement of wireless communications using frequency hopping spread spectrum. *Int J Commun Netw Syst Sci*, *3*(10), 805-810.

Nevalainen, O., Honkavaara, E., Tuominen, S., Viljanen, N., Hakala, T., Yu, X., ... & Tommaselli, A. M. (2017). Individual tree detection and classification with UAV-based photogrammetric point clouds and hyperspectral imaging. Remote sensing, 9(3), 185.

Ng, K. M., Johari, J., Abdullah, S. A. C., Ahmad, A., & Laja, B. N. (2018, October). Performance evaluation of the RTK-GNSS navigating under different landscape. In 2018 18th International Conference on Control, Automation and Systems (ICCAS) (pp. 1424-1428). IEEE.

Nikolakopoulos, K. G., Kavoura, K., Depountis, N., Argyropoulos, N., Koukouvelas, I., & Sabatakakis, N. (2015, October). Active landslide monitoring using remote sensing data, GPS measurements and cameras on board UAV. In Earth Resources and Environmental Remote Sensing/GIS Applications VI (Vol. 9644, pp. 54-62). SPIE.

Nugroho, A. P., Shalih, S. M., Purwantana, B., Sutiarso, L., Markumningsih, S., Masithoh, R. E., ... & Lee, D. G. (2019, November). Development of GPS-based Tracking System to Evaluate the Effectiveness of Tillage using Four-wheel Tractor. In IOP Conference Series: Earth and Environmental Science (Vol. 355, No. 1, p. 012014). IOP Publishing.

Ojha, T., Misra, S., & Raghuwanshi, N. S. (2015). Wireless sensor networks for agriculture: The state-of-the-art in practice and future challenges. Computers and electronics in agriculture, 118, 66-84.

Pak, J., Kim, J., Park, Y., & Son, H. I. (2022). Field evaluation of path-planning algorithms for autonomous mobile robot in smart farms. IEEE Access, 10, 60253-60266.

Perez-Ruiz, M., Martínez-Guanter, J., & Upadhyaya, S. K. (2021). High-precision GNSS for agricultural operations. In GPS and GNSS Technology in Geosciences (pp. 299-335). Elsevier.

Pini, M., Marucco, G., Falco, G., Nicola, M., & De Wilde, W. (2020). Experimental testbed and methodology for the assessment of RTK GNSS receivers used in precision agriculture. IEEE Access, 8, 14690-14703.

R Shamshiri, R., Weltzien, C., Hameed, I. A., J Yule, I., E Grift, T., Balasundram, S. K., ... & Chowdhary, G. (2018). Research and development in agricultural robotics: A perspective of digital farming.

Rahmadian, R., & Widyartono, M. (2020, October). Autonomous robotics in agriculture: a review. In 2020 third international conference on vocational education and electrical engineering (ICVEE) (pp. 1-6). IEEE.

Ray, P.P. (2017). Internet of things for smart agriculture: Technologies, practices and future direction. J. Ambient Intell. Smart Environ., 9, 395-420.

Saiz-Rubio, V., & Rovira-Más, F. (2020). From smart farming towards agriculture 5.0: A review on crop data management. Agronomy, 10(2), 207.

Santhi, P. V., Kapileswar, N., Chenchela, V. K., & Prasad, C. V. S. (2017, August). Sensor and vision based autonomous AGRIBOT for sowing seeds. In 2017 International Conference on Energy, Communication, Data Analytics and Soft Computing (ICECDS) (pp. 242-245). IEEE.

Sørensen, C. G., Pesonen, L., Bochtis, D. D., Vougioukas, S. G., & Suomi, P. (2011). Functional requirements for a future farm management information system. Computers and electronics in agriculture, 76(2), 266-276.

Sowjanya, K. D., Sindhu, R., Parijatham, M., Srikanth, K., & Bhargav, P. (2017, April). Multipurpose autonomous agricultural robot. In 2017 International conference of

Electronics, Communication and Aerospace Technology (ICECA) (Vol. 2, pp. 696-699). IEEE.

Srivastava, V., & Raturi, O. (2022). Implementation of Robotics and Autonomous Systems in Agriculture. In *Recent Advances in Mechanical Engineering: Select Proceedings of CAMSE 2021* (pp. 489-496). Singapore: Springer Nature Singapore.

Steward, B. L., Tang, L., & Han, S. (2015, June). A design framework for off-road equipment automation. In Proceedings of the 2015 Conference on Autonomous and Robotic Construction of Infrastructure (pp. 180-196). Iowa State University, Ames, Iowa.

Tsouros, D. C., Bibi, S., & Sarigiannidis, P. G. (2019). A review on UAV-based applications for precision agriculture. Information, 10(11), 349.

Tylek, P., Szewczyk, G., Kormanek, M., Walczyk, J., Sowa, J. M., Pietrzykowski, M., ... & Szulc, T. (2023). Design of a Planting Module for an Automatic Device for Forest Regeneration. Croatian Journal of Forest Engineering: Journal for Theory and Application of Forestry Engineering, 44(1), 203-215.

UN. (2019). World population prospects

Van Henten, E. J., Hemming, J., Van Tuijl, B. A. J., Kornet, J. G., Meuleman, J., Bontsema, J., & Van Os, E. A. (2002). An autonomous robot for harvesting cucumbers in greenhouses. *Autonomous robots*, *13*(3), 241-258.

Velusamy, P., Rajendran, S., Mahendran, R. K., Naseer, S., Shafiq, M., & Choi, J. G. (2021). Unmanned Aerial Vehicles (UAV) in precision agriculture: Applications and challenges. Energies, 15(1), 217.

Vuran, M. C., Salam, A., Wong, R., & Irmak, S. (2018). Internet of underground things in precision agriculture: Architecture and technology aspects. Ad Hoc Networks, 81, 160-173.

Wang, J., & Olson, E. (2016, October). AprilTag 2: Efficient and robust fiducial detection. In 2016 IEEE/RSJ International Conference on Intelligent Robots and Systems (IROS) (pp. 4193-4198). IEEE.

Xu, R., & Li, C. (2022). A modular agricultural robotic system (MARS) for precision farming: Concept and implementation. Journal of Field Robotics, 39(4), 387-409.

Yahya, A., Sidek, O., & Mohamad-Saleh, J. (2006). Design and Develop Wireless System Using Frequency Hopping Spread Spectrum. *Engineering Letters*, *13*(4).

Zangina, U., Buyamin, S., Aman, M. N., Abidin, M. S. Z., & Mahmud, M. S. A. (2021). Autonomous mobility of a fleet of vehicles for precision pesticide application. Computers and Electronics in Agriculture, 186, 106217.

Zhang, X., Zhang, J., Li, L., Zhang, Y., & Yang, G. (2017). Monitoring Citrus Soil Moisture and Nutrients Using an IoT Based System. Sensors (Basel, Switzerland), 17(3), 447. https://doi.org/10.3390/s17030447

Appendix A - Data Communication, GNSS and Development Platform

Radio Platform: Pico series P900 (900 MHz Spread Spectrum Modem) Specifications

Electrical/General	
Frequency	902 - 928 MHz
Spreading Method	Frequency Hopping
Band Segments	Selectable via Freq. Zones
Error Detection	32 bits of CRC, ARQ
Data Encryption	128, 196 or 256-bit AES Encryption (Requires export permit outside US and Canada.)
Range	40 miles (60km)
Output Power	100mW to 1W (20-30dBm)
Serial Baud Rate	Up to 230.4 kbps asynchronous
Link Rate	Up to 276 kbps

Sensitivity	

Link Rate	10^{-6}BER	10^{-3}BER
57.6 kbps	-111 dBm	-114 dBm
115.2 kbps	-110 dBm	-113 dBm
172 kbps	-108 dBm	-111 dBm
230 kbps	-107 dBm	-110 dBm
276 kbps	-106 dBm	-109 dBm

Environmental	
Operation Temperature:	-40°F(-40°C) to 185°F(85°C)
Humidity	5% to 95% non-condensing
Mechanical	
Dimensions	Approx. 1.05” (26.5mm) X 1.3” (33mm) X 0.13” (3.5mm)
Weight	Approx. 5 grams
Connectors	Antenna: UFL Data: 80 Pin/Pad SMT

Radio Platform: pMDDL2450 2x2 MIMO OEM Wireless Digital Data Link

Electrical/General	
Frequency	2.402 - 2.482 GHz
TX Power	20 dBm - 30 dBm Total (Adjustable)
Channel Bandwidth	4, 8 MHz (Selectable)
Error Detection	CRC, ARQ

Data Encryption *(*Requires Export Permit)*	128-bit AES
Serial Port	300bps to 230kbps - TTL Level RS232
Ethernet	Dual 10/100 BaseT, Auto - MDI/X, IEEE 802.3
USB	2.0
Network Protocols	TCP, UDP, TCP/IP, ARP, ICMP, DHCP, HTTP, HTTPS*, SSH*, SNMP, FTP, DNS, Serial over IP (*May require an export permit)
Operating Modes	Master, Slave/Remote
Management	Local Serial Console, Telnet, WebUI, SNMP, FTP & Wireless Upgrade
Diagnostics	Status LED's, RSSI, remote diagnostics, SNR
Input Voltage	OEM: • Digital Voltage: 3.3 VDC (500mA) • RF Voltage: 5.0 VDC (1.5A)
Environmental	
Operation Temperature:	-40°F(-40°C) to 185°F(85°C)
Humidity	5% to 95% non-condensing
Mechanical	
Dimensions	1.05" (26.5mm) X 1.3" (33mm) X 0.13" (3.5mm)
Weight	Approx. 7 grams
Connectors	Antenna: UFL x2 (ANT1, ANT2) Data: 80 Pin SMT

Power	SMT: 4-Pin Micro MATE-N-LOK AMP 3-794618-4 (Mating Connector: 4-Pin Micro MATE-N-LOK AMP 794617-4)

Topcon B110 GNSS

Electrical/General	
Signal Type	GPS L2C, GLONASS C/A L2, and Galileo E1
RF input frequencies	• GPS: 1575.42 MHz (L1), 1227.60 MHz (L2) • GLONASS: 1598.0625 – 1609.3125 MHz (L1), 1242.9375 – 1251.6875 MHz (L2)
Satellite tracking	Vanguard chip
Channel	224 universal channels, 100 Hz position and measurement updates
Antenna connector	• Hirose HFL straight though hole • 2 connectors
Tracked Signals	• GPS: L1(C/A & P), L2, L2C

	• GLONASS: L1 (C/A & P), L2 (C/A & P)
Serial interfaces	• Two RS-232C • Four LVTTL • CAN • USB 2.0 with 480 Mb/s
Serial data rates	460.8 Kbit/s
Data formats	Proprietary (TPS) data format NMEA 0183 versions 2.1,2.2,2.3, and 3.0,3.1
RTK correction	• RTCM 2.x • RTCM 3.x • TPS • CMR/CMR+
Connector	Master, Slave/Remote
Management	Local Serial Console, Telnet, WebUI, SNMP, FTP & Wireless Upgrade
Diagnostics	Status LED's, RSSI, remote diagnostics, SNR
Power	• Input voltage = +3.4 to +4.5 Vdc • Consumption = 1 W typical, 1.6 W max
Environmental	
Operation Temperature	-40° to +85°C
Storage Temperature	-40° to +85°C
Humidity	95% non-condensing
Vibration	4g Sine Vibe (SAEJ1211) 7.7g Random Vibe (MIL-STD 810F)
Shock	30g (IEC 68-2-27)
Mechanical	

Dimensions	L: 55 mm x W: 40 mm XH: 10 mm (2.17 in x W: 1.57 in x H: 0.30 in)
Weight	0.02 kg (0.04 lbs.)
Connectors	60-pin receptable of DF17 series, Hirose DF17 (3.0)-60DS-0.5V (57)
Mounting	4 holes to install m2 screws

Teensy Micro-Controller

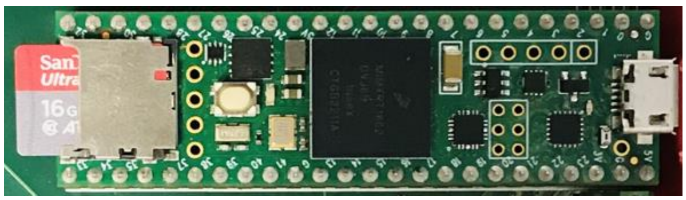

Ethernet	10 / 100 Mbit DP83825 PHY (6 pins)
Processor	ARM Cortex-M7 at 600 MHz
USB Host	5 Pins with power management
SDIO (4-bit data)	Micro SD Socket
PWM Pins	35
Analog Inputs	18
Ports	• 8 serial, • 3 SPI, • 3 I2C ports
Memory	• 7936K Flash, • 1024K RAM (512K tightly coupled), • 4K EEPROM (emulated)
Breadboard I/O	42
Bottom SMT Pads	7
Total I/O Pins	55
Software	Arduino IDE + Teensyduino add-on

Power	3.3 V (voltage regulator which reduces the 5V VUSB / VIN power to 3.3V)
Dimension	61 inches x 18 inches